

**Thermodynamics and Structure of Peptide-
Aggregates at Membrane Surfaces**

INAUGURALDISSERTATION

zur

Erlangung der Würde eines Doktors der Philosophie

vorgelegt der

Philosophischen-Naturwissenschaftlichen Fakultät

der Universität Basel

von

Matthias Meier

aus

Hamburg, Deutschland

Basel 2006

Genehmigt von der Philosophischen-Naturwissenschaftlichen Fakultät auf Antrag von

Prof. Dr. Joachim Seelig

Prof. Dr. Dagmar Klostermeier

Basel, den 7.11.06

Prof. Dr. Hans-Peter Hauri
(Dekan)

Table of Contents

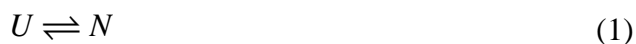
1. Introduction	1
1.1 – Thermodynamics of Protein Aggregation	1
1.2 – Formation of Protein Aggregates	3
1.3 – Protein Aggregation at Lipid Membrane Surfaces	5
1.4 – Diseases caused by Protein Aggregation	8
1.5 – The Amyloid Peptide: A Paradigm for Peptide Aggregation	9
1.6 – The KIGAKI Peptide as Model System of Protein Aggregation	12
1.7 – Literature	14
2. Aims of Research	21
3. Interaction of Verapamil with Lipid Membranes and P-glycoprotein: Connecting Thermodynamics and Membrane Structure with Functional Activity	23
3.1 – Summary	24
3.2 – Published Article	26
3.3 – Appendix	39
4. Thermodynamics of the Coil \rightleftharpoons β -sheet Transition in a Membrane Environment	45
4.1 – Summary	46
4.2 – Published Article	47
5. Length dependence of the Coil \rightleftharpoons β -sheet Transition in a Membrane Environment	61
5.1 – Summary	62
5.2 – Manuscript	63
6. Structure Analysis of Encapsulated Peptide-Aggregates in Reverse Micelles	97
6.1 – Summary	98
6.2 – Manuscript	99
7. Interaction between Xenon and Phospholipid Membranes studied by $^{129}\text{Xe}/^2\text{H}$ -NMR	117
7.1 – Summary	118
7.2 – Manuscript	119
8. Summary	144
9. Acknowledgement	146
10. Curriculum Vitae	147
11. Declaration	149

1. Introduction

1.1 - Thermodynamics of Protein Aggregation

Proteins are unbranched heteropolymers formed from different naturally occurring α -L-amino acids connected by amide bonds. In order to perform their biological function, almost all proteins adopt a three dimensional structure, which is determined by the primary amino acid sequence and the local environment¹. Despite the large configurational space available, proteins show a remarkable propensity to adopt unique, well-defined conformation. Many small proteins fold into their native stable ordered forms readily in solution, but it is also true that under some conditions proteins can interconvert among various ordered states, as well as between ordered and random forms. Such conformational changes generally occur in response to variations in an external parameter such as temperature, pH or solvent.

The conformational stability of a protein is generally defined as the free energy change (ΔG^0) for the reaction between the folded or native (N) and unfolded or denatured (U) state of the protein^{2,3}



in an aqueous solution at ambient temperature and pressure. For the characterization of folding thermodynamics and thus the structural stability it is sufficient to characterize the folded and unfolded states under different conditions, as the free energy difference between them determines the macroscopic state observed at equilibrium. The analysis of the folding and unfolding reactions of various proteins by spectroscopic and calorimetric techniques⁴ has shown that a multitude of noncovalent intramolecular interactions as well as intermolecular protein-solvent contacts stabilize the protein structure. Specific electrostatic interactions, hydrogen bonds and van-der-Waals forces contributing to protein stability⁵, but the major driving force of protein folding is thought to result from the hydrophobic effect or hydrophobic free energy⁶. At ambient temperature the hydrophobic free energy is mainly entropic and can be explained by ordering of the solvent molecules around the protein surface, which is accompanied by the loss of orientational freedom. Thus, the hydrophobic effect favors the burial of protein surface in

order to minimize the solvent accessible surface area. Multiple interactions between protein residues well separated in primary structure cause the overall compaction and defined fold of the native protein⁷.

The fact that the native protein structure is thermodynamically stable does not necessarily imply that there is no other conformation, which exhibits a lower free energy state than the native state^{8,9}. In many cases, only small variations in an external variable are required to disturb the natural folding equilibrium and as a consequence protein misfolding and finally aggregation can be observed. Furthermore, the formation of proteins in an aggregated state, A, is today considered as a process that compete with the natural folding reaction¹⁰.



Through environmental changes, e.g. pH or temperature^{11, 12}, proteins can sacrifice stabilizing intrachain contacts in favor of configurations that promote intermolecular interactions leading to the formation of aggregates. These aggregates range from amorphous structures without order to highly structured fibrils, each arising by distinct aggregation pathways. In a globular protein, for example, the polypeptide main chain and the hydrophobic side chains are largely buried within the folded structure. Therefore proteins have to unfold at least partially to expose hydrophobic patches¹³. In contrast to native proteins relative little is known about interactions, which stabilize protein aggregates. Direct comparison of the native state, with the aggregated state is impossible due to insolubility, heterogeneity, and high degree of polymerization of the protein aggregates. Quite often, the aggregated states of a protein are not in equilibrium with the unfolded state, which further complicates the analysis. On the other hand, the high resistance of the aggregated form to denaturation by detergents and to thermal and solvent-induced denaturations serves as an illustration of the extremely high thermodynamic stability compared to the metastability of the native state of proteins¹⁴. From these considerations the question arises, why the protein aggregation pathway is generally not accessible during folding under native condition? It has been argued that the rate of protein aggregation is slower by several orders of magnitude than the rate of folding into the native protein conformation^{13,15}.

1.2 - Formation of Protein Aggregates

The formation of aggregates with similar structural features by proteins and peptides of unrelated primary sequence, suggests a generic mechanism governing the process^{13, 16}. Proteins can aggregate either in an unordered or highly ordered fashion but relatively little is known about the conditions that favor one aggregation pathway over the other. Generally, both aggregation types are rich in extended β -sheet structures^{17, 18}. Nevertheless, the typical phenotype of ordered protein aggregation is the protein fibril. Protein fibrils are straight, unbranched fibers, 7-12 nm in diameter and of indeterminate length¹⁹. X-ray diffraction and solid state NMR spectroscopy studies²⁰⁻²² revealed a repeating core structure for so called amyloid fibrils (see below). This structure consists predominantly of β -sheets, which is orientated perpendicular to the fiber axis. The β -sheet structure within the amyloid fibrils are stabilized by backbone hydrogen bonding and hydrophobic interactions, rather than through specific interactions of different side chains²³. The fact that unordered protein aggregates are often found next to *in vitro* synthesized ordered aggregates, suggests that an interconversion between both types can take place²⁴⁻²⁶. Structural information of amorphous protein aggregates is rare because of their heterogeneity.

Several models have been proposed to quantitatively describe protein fibrillization^{16, 27-29}. Generally, the nucleation dependent polymerization model can describe the experimentally observed kinetics of fibrillogenesis³⁰. This process is characterized by (a) a slow nucleation phase, in which the protein undergoes a series of unfavorable association steps to form a partially ordered oligomeric nucleus, (b) a growth phase, in which the nucleus rapidly grows to form larger polymers, and (c) a steady state phase, in which the ordered aggregate and the monomer appear to be at equilibrium (see Figure 1)^{30, 31}. In a typical nucleation-dependent polymerization, polymers are not observed until the monomer concentration exceeds a certain level known as the critical concentration. Below this critical concentration the monomer is the predominant species. Raising the monomer concentration above the critical concentration leads to formation of polymer but the monomer concentration remains the same. Fibril nucleation is slow and as consequence supersaturated peptide solutions are metastable, or kinetically soluble³⁰. However, the kinetically soluble monomer is time dependent. The length of time during which a

supersaturated solution remains kinetically soluble before fibril formation occurs is called the lag time. During the lag time prenuclei are sequentially formed in a dynamic equilibrium. The length of the lag time can be extremely sensitive to protein concentration, depending on the oligomer size of the nucleus³².

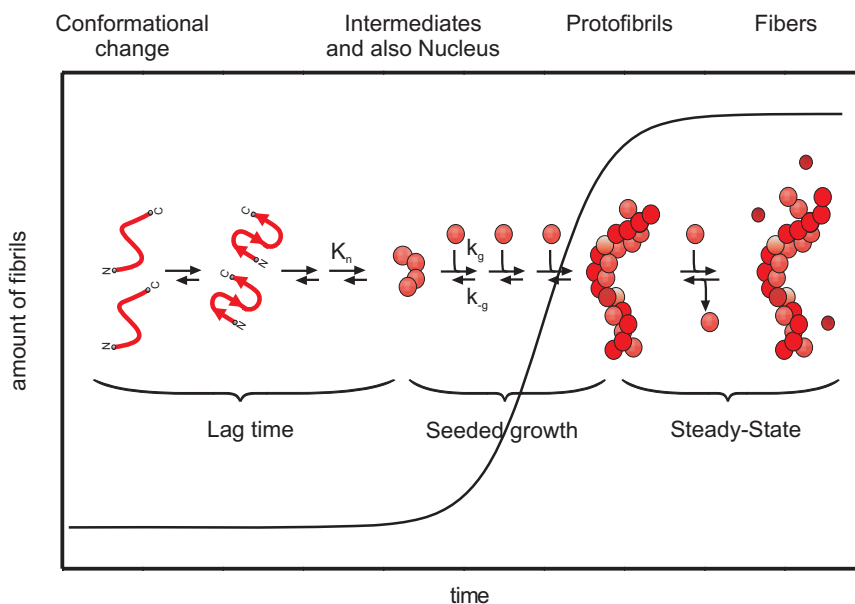


Figure 1. The nucleation-dependent mechanism of fibril formation shows a series of unfavourable peptide-peptide association equilibria (K_n) accompanied by a structural transition for the peptide monomers, followed by a series of favourable equilibria (k_g) that lead to fibril formation. The critical concentration phenomenon results from a shift from unfavourable to favourable equilibria.

This is in line with the findings that the nucleation process exhibits an apparent reaction order ≥ 2 , whereas the folding reaction of a protein into its native structure is generally a first-order reaction^{4, 33}. The slow nucleation step can be bypassed by introduction of exogenous nucleus or seeds^{31, 34, 35}, thus eliminating the lag time. Aggregation seeds for fibrils are also considered as modulators³⁶. A vast variety of modulators of fibril formation is known to date, for example: lipids³⁷, carbohydrates³⁸, and metal ions³⁹. Once a nucleus is formed, it elongates via end growth. Monomer addition to the fiber ends coincides with a conformational rearrangement. Theoretically this process lasts until a steady-state-equilibrium between monomer and a precursor of the fibrils is reached. The precursors leading to mature fibrils are named protofibrils^{15, 40}. The conversion of protofibrils to fibrils involves inter- and intrafibrillar changes^{15, 41}. In particular, end-to-end annealing

and lateral association mechanisms are thought to take place during the maturation of fibrils⁴².

Even though a simple nucleation dependent polymerization model can describe the overall process of fibril assembling, most of the sub-processes are not understood at the molecular level. The key for a better understanding of fibril formation is the identification and characterization of the slowest, or rate-limiting step in the overall process. As discussed above, the rate of nucleus formation is slow, owing primarily to the unfavorable association equilibria rather than to the intrinsically slow association rates⁴³. It is therefore critical to distinguish thermodynamic effects (structure, stability, solubility) from kinetic effects. Nucleus formation has to overcome two great entropy barriers, namely the protein conformation and association.

1.3 - Protein Aggregation at Lipid Membrane surfaces

Most proteins are surface active molecules, a property that is demonstrated by the spontaneous accumulation or adsorption of proteins at interfaces^{44,45}. This property results from the amphiphilic amino acid composition of proteins. Many theoretical approaches of protein adsorption from aqueous solution to solid-liquid interfaces have been described^{46,47}, still this process is poorly understood.

Lipid membranes constitute a biological interface and therefore lipid-protein interactions are of special interest. The adsorption of protein to membranes involves electrostatic and hydrophobic interactions, protonation reactions and dehydration effects. Minimization of the free energy of a protein-interface-system can lead to a shift in the folding equilibrium, i.e. surfaces can promote folding or unfolding of proteins⁴⁸⁻⁵². Perturbation of the folding equilibrium has inevitable consequences on the protein aggregation reaction. Indeed protein aggregation is frequently observed upon membrane binding. The mechanism of membrane-induced aggregation differs from that occurring in bulk solution because of the restrictions imposed by (a) the physicochemical and dynamic properties of the lipid membrane surface, (b) concentration differences due to accumulation of proteins at the lipid-water interface^{37 53 54}, and (c) dimensional restrictions and orientation effects of the membrane^{55 56}.

Aggregation of proteins at the membrane surface is frequently but not always initialized by electrostatic attraction between the protein and the membrane^{53, 57-60}. Negatively and

positively charged lipids produce an electrostatic potential in the aqueous phase, immediately adjacent to the membrane, which leads to the repulsion or attraction of the proteins and ions. Electrostatic membrane potentials are also found at neutral membrane surfaces, due to preferential absorption of ions⁶¹. Such a membrane potential can be described quantitatively as diffuse double layer by the Gouy-Chapman theory^{62, 63}. For a lipid membrane with surface potential of -60 mV the theory with physiological boundary conditions predicts that the concentration of monovalent ions or proteins at the lipid membrane surface is one order of magnitude higher than their bulk concentrations⁶⁴. In parallel, the local pH will be one unit lower than in the bulk. The effect of ion accumulation at the membrane surface due to a membrane potential is illustrated in figure. 2.

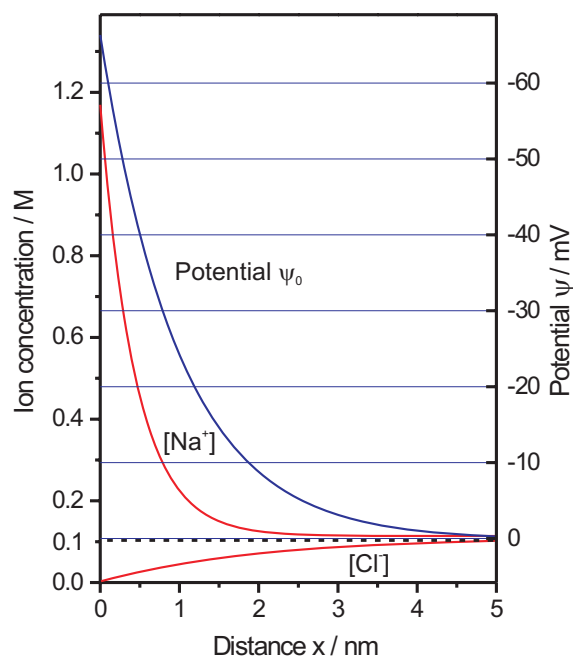


Figure 2. (A) Surface membrane potential and ionic density profiles for a 0.1 M monovalent electrolyte near a membrane surface of charge density, $\sigma = -0.0621 \text{ Cm}^{-2}$ (1 electronic charge per 2.6 nm^2). The profiles were calculated from the Gouy-Chapman theory with a $\psi_0 = -60 \text{ mV}$.

These surface effects are able to induce conformational transitions of proteins at the membrane surface. The higher charge state of the protein at lower pH may enhance side chain repulsion on the protein surface and thereby support aggregation. On the other hand screening of protein charges through lipid molecules or ions in the close vicinity of the membrane can lower repulsion forces between adsorbed proteins⁶⁵. An important conclusion is that accumulation of proteins at the membrane surface can cause fibril

nucleation, when the local protein concentration exceeds the critical concentration. A number of studies have provided experimental evidence for this mechanism. It was concluded further that the lipid membrane lowers the energy barriers of nucleus formation (see Chapter 1.2)^{60, 65-68}. It should be mentioned that fibril formation in aqueous solution is diffusion controlled. Membrane adsorbed proteins, however, are not freely diffusing and thus the dynamics of fibril formation at the membrane surface is changed compared to bulk dynamics.

Because membranes can induce folding or unfolding upon adsorption of the protein, the resulting protein structure often differs from that in aqueous solution. The hierarchy of stabilizing interactions, which govern the folding reaction in aqueous solution, is changed due to the apolar properties of the membrane surface. For example hydrogen bonds take on a much greater significance in a hydrophobic milieu than in water, since the lipid solvent is unable to compete with intramolecular H-bonds. Thus hydrogen bonds between amino acid side chains and peptide backbone interactions are thought to dominate protein stabilization in the membrane surface environment^{69, 70}. It is also obvious that lipid membrane surfaces can compete for the same hydrophobic interactions, which stabilize the native protein structure in aqueous solution⁴⁷. Further, the transfer of nonpolar amino acid side chains from the polar water phase to the apolar membrane interface phase results in a free energy gain^{71, 72}. This free energy of transfer is thought to be the major driving force for folding of membrane protein.

After nucleus formation ordered or unordered aggregates are assembled. In contrast to this process occurs at the lipid-water interface. This means the association of monomers to the protein oligomers differs in the translational degree of freedom compared to the bulk aggregation process^{73 56}. In addition, the grow axis of the fibril is restricted by the membrane surface⁵⁵. The role of lipids is more versatile in terms of protein aggregation than it has been depicted in this introduction. Further effects include the lateral packing density, thickness and composition of the lipid membrane. Although, these effects might play an important role in protein aggregation, they are protein dependent (see examples in chapter 1.5).

1.4 - Diseases caused by Protein Aggregation

The failure of a protein to fold correctly leads to a functional deficit, which can have serious consequences for cells. Therefore eukaryotic and prokaryotic cells have developed complex protein machineries for assisting protein folding^{74, 75}, but also for recognition and degradation of misfolded proteins⁷⁶. Nevertheless protein misfolding and finally aggregation occurs and has been connected to various diseases. Considerable attention is presently focused on a group of protein folding diseases known as amyloidoses. The amyloidoses have traditionally been defined as diseases in which normally soluble proteins accumulate in the extracellular space of various tissues as insoluble deposits of fibrils that are rich in β -sheet structure and have characteristic dye-binding properties⁷⁷. The fibril deposits were discovered first by Virchow in 1854⁷⁸. He described the deposits as connote waxy, eosinophilic tissue and coined it in analogy to the comparable carbohydrate structure 'amyloid'. The term amyloid persists up to the present day despite the fact that Friedrich and Kekulé found already in 1859, that amyloid deposits were formed from proteins⁷⁹. Another general feature of these protein-folding disorders is the prolonged period before clinical manifestations appear. During the prolonged preclinical phase proteins misfold, build up and progressively compromise cellular and tissue function. About 30 diseases are known today which comply the typical characteristics of an amyloidoses (for a review see⁸⁰). The most prominent diseases among of them are the Alzheimer's-, Huntington's-, and Creutzfeld-Jakob's disease^{81, 82}. In some aggressive amyloidoses protein-folding disorders can occur in young and early middle-aged individuals. In such cases, time still has a role but the fibrillogenic process requires less time overall because particular biochemical circumstances promote accelerated nucleation. The Down's syndrome is one example for the early onset of an amyloidosis. How protein aggregates emerge and are involved in the progress of the disease is shown in a case example in the next paragraph for the Alzheimer's disease.

1.5 - The Amyloid Peptide: A Paradigm for Peptide Aggregation

The Alzheimer disease is today explained on a molecular level by the "amyloid hypothesis", which states that the disease is initiated by the production, aggregation and deposition of the amyloid β -peptide ($A\beta$). $A\beta$ peptide is derived from the 170 kDa amyloid peptide precursor protein (APP), as a natural cleavage product^{83, 84}. It is generated by cleavage of APP at two locations by proteases denoted as the β - and γ -secretases. The initial proteolysis by the β -secretase results in a residual C-terminal fragment containing the transmembrane and cytoplasmic domains of APP, which undergoes an additional, intramembranous cleavage by a γ -secretase to release $A\beta$. The γ -secretase cleavage site is heterogeneous and produces $A\beta$ fragments that can vary in length from 39-42 residues^{85, 86}. However, the two predominant species are peptides 1-40 ($A\beta_{40}$) and 1-42 ($A\beta_{42}$). Figure 3 shows the sequence of $A\beta_{40}$ and $A\beta_{42}$ and their amphipathic character.



Figure 3 Amino acid sequences of $A\beta_{40}$ and $A\beta_{42}$ in one letter code. Yellow and red marked amino acids denote positively and negatively charged residues, respectively under physiological conditions. Amino acids labelled in grey at the C-terminus indicate the former membrane domain of the $A\beta$ peptides.

The peptide $A\beta$ fragments are found to circulate in nanomolar concentration in the blood and cerebrospinal fluid of AD patients but also in unaffected individuals^{87, 88}. The soluble monomeric form of both peptides are generally considered to be non-toxic⁸⁹. The hallmark of the Alzheimer's disease is however the formation of $A\beta$ fibrils. $A\beta$ fibrils are visible in large plaques in the extracellular matrix of the neuronal tissue⁸⁹. Therefore the prevailing explanation for the toxicity involves association of $A\beta$ peptides and a structural transition of the polypeptide chain from the native to misfolded conformation. Several lines of evidence have converged recently to demonstrate that soluble oligomers of β -sheet aggregated $A\beta$, may be responsible for synaptic dysfunction in the brains of AD patients. Metastable intermediates in the formation of fibrils by synthetic $A\beta$, referred to as AD

diffusible ligands (ADDLs) or protofibrils⁹⁰, also cause injury to cultured neurons. But the most conspicuous form of the A β peptides is the mature amyloid fibril⁹¹.

The amyloid hypothesis remains nevertheless controversial because a specific neurotoxic species of A β and the nature of its effects on neural function have not been defined *in vivo*. To shed light on the toxicity of A β , research focused on *in vitro* experiments to characterize the self-aggregation process of A β . Unfortunately, the attempt to quantify the self-aggregation process and the accompanied conformational change of A β were confounded by the range of apparently conflicted behaviors observed. A β peptides are polymorphic and the structure of these peptides are highly depending on the environmental conditions, such as pH, salt concentration, temperature or pressure⁹²⁻⁹⁵. While the natural conformation of A β within the APP is believed to be α -helical⁹⁶, the monomeric soluble form of A β adopts a random coil structure. In water/alcohol mixtures or in micellar solution, which are used as membrane mimics, A β adopts an α -helical conformation⁹⁷. The position and length of the helical segments varies according to the media applied^{98, 99}. A random coil conformation is observed in aqueous solution^{100, 101}. However, structural studies of protofibrils have shown that the prevailing structural element in these precursors of fibrils and matured fibrils is the β -sheet (see chapter 1.2).

Apart from the structural changes of A β , the discrepancy between the experimentally defined critical concentration of fibril formation (in the micromolar range in pure water)^{28, 53} and the A β concentration in the blood and cerebrospinal fluid of AD patients (in the nanomolar range)^{87, 88} are thought to be a key hint for the understanding of A β aggregation. In order for A β amyloid formation to occur in the brain, a process must exist whereby a local A β concentration is created, which exceeds the naturally occurring concentration by three orders of magnitude. A simple way to explain the concentration difference is to assume that an endogenous substance could lower the *in vivo* critical concentration. This theory is supported by the finding that amyloid plaques consist not only of A β fibrils but contain also of non-fibrillar components including glycosaminoglycans^{102 103}, apolipoprotein E¹⁰⁴, metal ions^{39, 105} and serum amyloid P component (SAP)¹⁰⁶. Most of these substances accelerate fibril formation in AD but not all of them promote ordered aggregation *in vitro*. Another mechanism for achieving a high

local A β concentration is the binding of A β to proteoglycans or directly to the cell membrane surface (see also chapter 1.3).

The cell membrane surface is of special interest not only due to its capability to assist fibril formation but also because it is the target of A β mediated cell death¹⁰⁷. Oligomers, which are formed in the close vicinity of the membrane, are suspected to alter the membrane structure, which then leads to cell death. Several experiments give rise to speculations how A β is influencing the lipid membranes. For example, the possibilities of membrane channel formation¹⁰⁸ and the disruption¹⁰⁹ of neuronal cell membrane by A β have been pointed out. In both cases partitioning of the peptide into the cell membrane is stipulated. On the other hand, A β can cause changes of the lipid membrane mobility, integrity or simply insulation by absorption to lipid membrane surface^{110, 111}.

Specific interaction of A β with gangliosides¹¹², a major lipid component in neural cell membranes, with cholesterol^{113, 114} or with phosphatidylinositol¹¹⁵ have been proposed. A more general mechanism for the binding of A β to lipid membranes is described by electrostatic interactions A β to negatively charged phospholipids membranes (containing phosphatidylserin or phosphatidylglycerol)⁵³. Interaction of A β with membrane surfaces promotes a conformational transition in favor of the β -sheet structure at low lipid to peptide ratio, but at high lipid peptide ratios also the α -helical structure is observed⁵³. Deuterium NMR studies have shown that interactions of A β with the lipid membrane are exclusively localized to the membrane surface, with no significant insertion of the peptide into the lipid bilayer¹⁰¹. Similar, studies of lipid monolayers found insertion of A β only at lateral pressure below those found in lipid bilayers¹⁰¹. In contrast, a number of studies has demonstrated a disruption of membrane integrity caused by A β which presumably implies the penetration of the peptide into the hydrophobic core of the bilayer^{109, 116}. All of the studies worked with the hypothesis that A β peptides might stay in the lipid membrane upon its cleavage from the amyloid precursor protein. However, to observe insertion of A β into lipid membranes the peptides has to be co-solubilized with lipids in organic solvents, before both components are transferred to aqueous solution¹¹⁷⁻¹¹⁹. The anchored form of A β has been shown to alter the fluidity of phospholipid membranes. All of these studies have not yet led to a comprehensive understanding of the structural detail of the A β interaction with the lipid membrane.

1.6 - The KIGAKI Peptide as Model System of Protein Aggregation

The previous sections have demonstrated the complexity of protein aggregation. The studies of A β or other amyloid forming peptides suffer from a major experimental problem: the lack of a method to quantify aggregation. The drawbacks of using naturally derived proteins or peptides as model systems for aggregation and β -sheet formation are mainly low solubility, structural polymorphism, and strong environmental dependencies i.e. pH, temperature and salt conditions of the aggregation and conformational folding process. Additionally, synthesis of insoluble peptides, such as A β variants, is extremely difficult¹²⁰. Impurities arising from the synthesis have significant effect on the aggregation thermodynamics and kinetics³⁰.

A designed model system for peptide aggregation in a membrane environment, should resemble the natural amyloid forming proteins and peptides in their common characteristics: (a) strong electrostatic binding of the protein or peptide to negatively charged lipid membranes, (b) random coil-to- β -sheet transition upon binding to the lipid membrane followed by (c) association and formation of oligomers and larger aggregates. The peptide with the sequence of (KIGAKI)₃ complies with these basic requirements¹²¹. Moreover, due to its net positive charge of its lysine residues the peptide is well soluble (>2 mM) and self-aggregation in aqueous solution at a pH lower than 9 could not be observed. Although, the (KIGAKI)₃ peptide sequence has been designed, its sequence pattern of polar and unpolar amino acids is also found in natural derived amyloid peptides, like within the polyglutamine repeats of the exon-1 peptide, which is related to the Huntington's disease¹⁷.

In contrast to the A β peptides, which forms helix and β -sheet structures, the (KIGAKI)₃ peptide can only form β -sheet structures at the membrane surface, which simplifies the investigation of conformational changes (see figure 3). In addition, the chemical synthesis of (KIGAKI)₃ is much simpler than that of A β , due to the shorter chain length and higher polarity.

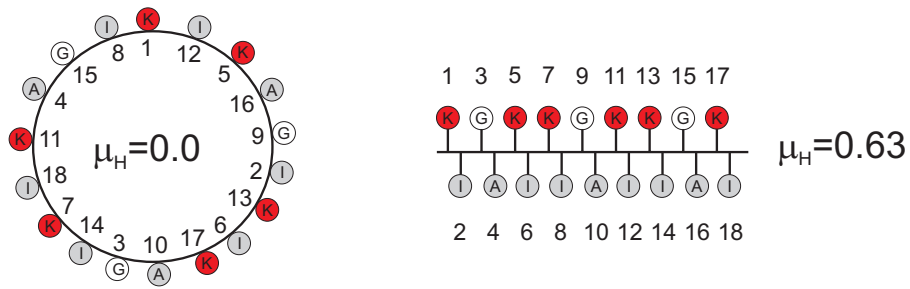


Figure 3. Helical wheel (left) and β -sheet diagram (right) showing the distribution of amino acids (red = positively charged lysine, grey = hydrophobic amino acids, white = glycine). The hydrophobic moment (μ_H) is calculated by using the consensus hydrophobicity scale and is denoted for both conformations¹²². The picture is taken from reference¹²¹.

1.7 - Literature

1. Anfinsen, C. B. Principles that govern the folding of protein chains. *Science* 181, 223-30 (1973).
2. Anson, M. L. & Mirsky, A. E. The reversibility of protein coagulation. *J Phys Chem* 35, 185-193 (1936).
3. Mirsky, A. E. & Pauling, L. On the Structure of Native, Denatured, and Coagulated Proteins. *Proc Natl Acad Sci U S A* 22, 439-47 (1936).
4. Buchner, J. & Kiefhaber, T. *Protein Folding Handbook* (Wiley-VCH, 2005).
5. Israelachvili, J. N. *Intermolecular surface forces* (Academic Press, London, 1991).
6. Kauzmann, W. Some factors in the interpretation of protein denaturation. *Adv Protein Chem* 14, 1-63 (1959).
7. Creighton, T. E. *Proteins: structures and molecular properties* (W. H. Freeman, New York, 1993).
8. Hammarstrom, P., Wiseman, R. L., Powers, E. T. & Kelly, J. W. Prevention of transthyretin amyloid disease by changing protein misfolding energetics. *Science* 299, 713-6 (2003).
9. Baskakov, I. V., Legname, G., Baldwin, M. A., Prusiner, S. B. & Cohen, F. E. Pathway complexity of prion protein assembly into amyloid. *J Biol Chem* 277, 21140-8 (2002).
10. Kiefhaber, T., Rudolph, R., Kohler, H. H. & Buchner, J. Protein aggregation in vitro and in vivo: a quantitative model of the kinetic competition between folding and aggregation. *Biotechnology (N Y)* 9, 825-9 (1991).
11. Dong, A., Prestrelski, S. J., Allison, S. D. & Carpenter, J. F. Infrared spectroscopic studies of lyophilization- and temperature-induced protein aggregation. *J Pharm Sci* 84, 415-24 (1995).
12. Yang, W. Y., Larios, E. & Gruebele, M. On the extended beta-conformation propensity of polypeptides at high temperature. *J Am Chem Soc* 125, 16220-7 (2003).
13. Dobson, C. M. Protein folding and misfolding. *Nature* 426, 884-90 (2003).
14. Meersman, F. & Dobson, C. M. Probing the pressure-temperature stability of amyloid fibrils provides new insights into their molecular properties. *Biochim Biophys Acta* 1764, 452-60 (2006).
15. Harper, J. D., Wong, S. S., Lieber, C. M. & Lansbury, P. T. Observation of metastable A β amyloid protofibrils by atomic force microscopy. *Chem Biol* 4, 119-25 (1997).
16. Kelly, J. W. Mechanisms of amyloidogenesis. *Nat Struct Biol* 7, 824-6 (2000).
17. Perutz, M. F., Pope, B. J., Owen, D., Wanker, E. E. & Scherzinger, E. Aggregation of proteins with expanded glutamine and alanine repeats of the glutamine-rich and asparagine-rich domains of Sup35 and of the amyloid beta-peptide of amyloid plaques. *Proc Natl Acad Sci U S A* 99, 5596-600 (2002).
18. Tycko, R. Molecular structure of amyloid fibrils: insights from solid-state NMR. *Q Rev Biophys* 39, 1-55 (2006).
19. Shirahama, T. & Cohen, A. S. High-resolution electron microscopic analysis of the amyloid fibril. *J Cell Biol* 33, 679-708 (1967).
20. Sunde, M. & Blake, C. C. From the globular to the fibrous state: protein structure and structural conversion in amyloid formation. *Q Rev Biophys* 31, 1-39 (1998).

21. Serpell, L. C. & Smith, J. M. Direct visualisation of the beta-sheet structure of synthetic Alzheimer's amyloid. *J Mol Biol* 299, 225-31 (2000).
22. Oyler, N. A. & Tycko, R. Absolute structural constraints on amyloid fibrils from solid-state NMR spectroscopy of partially oriented samples. *J Am Chem Soc* 126, 4478-9 (2004).
23. Chiti, F. et al. Designing conditions for in vitro formation of amyloid protofilaments and fibrils. *Proc Natl Acad Sci U S A* 96, 3590-4 (1999).
24. Snyder, S. W. et al. Amyloid-beta aggregation: selective inhibition of aggregation in mixtures of amyloid with different chain lengths. *Biophys J* 67, 1216-28 (1994).
25. Caughey, B. & Lansbury, P. T. Protofibrils, pores, fibrils, and neurodegeneration: separating the responsible protein aggregates from the innocent bystanders. *Annu Rev Neurosci* 26, 267-98 (2003).
26. Petty, S. A. & Decatur, S. M. Intersheet rearrangement of polypeptides during nucleation of {beta}-sheet aggregates. *Proc Natl Acad Sci U S A* 102, 14272-7 (2005).
27. Come, J. H., Fraser, P. E. & Lansbury, P. T., Jr. A kinetic model for amyloid formation in the prion diseases: importance of seeding. *Proc Natl Acad Sci U S A* 90, 5959-63 (1993).
28. Lomakin, A., Chung, D. S., Benedek, G. B., Kirschner, D. A. & Teplow, D. B. On the nucleation and growth of amyloid beta-protein fibrils: detection of nuclei and quantitation of rate constants. *Proc Natl Acad Sci U S A* 93, 1125-9 (1996).
29. Pallitto, M. M. & Murphy, R. M. A mathematical model of the kinetics of beta-amyloid fibril growth from the denatured state. *Biophys J* 81, 1805-22 (2001).
30. Jarrett, J. T. & Lansbury, P. T., Jr. Seeding "one-dimensional crystallization" of amyloid: a pathogenic mechanism in Alzheimer's disease and scrapie? *Cell* 73, 1055-8 (1993).
31. Andreu, J. M. & Timasheff, S. N. The measurement of cooperative protein self-assembly by turbidity and other techniques. *Methods Enzymol* 130, 47-59 (1986).
32. Tomski, S. J. & Murphy, R. M. Kinetics of aggregation of synthetic beta-amyloid peptide. *Arch Biochem Biophys* 294, 630-8 (1992).
33. Zettlmeissl, G., Rudolph, R. & Jaenicke, R. Reconstitution of lactic dehydrogenase. Noncovalent aggregation vs. reactivation. 1. Physical properties and kinetics of aggregation. *Biochemistry* 18, 5567-71 (1979).
34. Jarrett, J. T., Berger, E. P. & Lansbury, P. T., Jr. The carboxy terminus of the beta amyloid protein is critical for the seeding of amyloid formation: implications for the pathogenesis of Alzheimer's disease. *Biochemistry* 32, 4693-7 (1993).
35. Eaton, W. A. & Hofrichter, J. The biophysics of sickle cell hydroxyurea therapy. *Science* 268, 1142-3 (1995).
36. McLaurin, J., Yang, D., Yip, C. M. & Fraser, P. E. Review: modulating factors in amyloid-beta fibril formation. *J Struct Biol* 130, 259-70 (2000).
37. Terzi, E., Holzemann, G. & Seelig, J. Reversible random coil-beta-sheet transition of the Alzheimer beta-amyloid fragment (25-35). *Biochemistry* 33, 1345-50 (1994).
38. Snow, A. D. et al. The presence of heparan sulfate proteoglycans in the neuritic plaques and congophilic angiopathy in Alzheimer's disease. *Am J Pathol* 133, 456-63 (1988).
39. Bush, A. I. et al. Rapid induction of Alzheimer A beta amyloid formation by zinc. *Science* 265, 1464-7 (1994).
40. Stine, W. B., Jr. et al. The nanometer-scale structure of amyloid-beta visualized by atomic force microscopy. *J Protein Chem* 15, 193-203 (1996).

41. Walsh, D. M., Lomakin, A., Benedek, G. B., Condron, M. M. & Teplow, D. B. Amyloid beta-protein fibrillogenesis. Detection of a protofibrillar intermediate. *J Biol Chem* 272, 22364-72 (1997).
42. Aggeli, A. et al. Hierarchical self-assembly of chiral rod-like molecules as a model for peptide beta -sheet tapes, ribbons, fibrils, and fibers. *Proc Natl Acad Sci U S A* 98, 11857-62 (2001).
43. Harper, J. D. & Lansbury, P. T., Jr. Models of amyloid seeding in Alzheimer's disease and scrapie: mechanistic truths and physiological consequences of the time-dependent solubility of amyloid proteins. *Annu Rev Biochem* 66, 385-407 (1997).
44. Andrade, J. D. *Surface and Interfacial Aspects of Biomedical Polymers. 2. Protein Adsorption* (ed. Andrade, J. D.) (Plenum Press, New York, 1985).
45. Malmsten, M. e. *Biopolymer at Interfaces* (ed. Malmsten, M.) (Dekker, New York, 1998).
46. Norde, W. Adsorption of proteins from solution at the solid-liquid interface. *Advances in Colloid and Interface Science* 25, 267-340 (1986).
47. Haynes, C. A. & Norde, W. Structures and Stabilities of Adsorbed Proteins. *Journal of Colloid and Interface Science* 169, 313-328 (1995).
48. Buijs, J. & Hlady, V. Adsorption Kinetics, Conformation, and Mobility of the Growth Hormone and Lysozyme on Solid Surfaces, Studied with TIRF. *Journal of Colloid and Interface Science* 190, 171-181 (1997).
49. White, S. H. & Wimley, W. C. Hydrophobic interactions of peptides with membrane interfaces. *Biochim Biophys Acta* 1376, 339-52 (1998).
50. Ladokhin, A. S. & White, S. H. Interfacial folding and membrane insertion of a designed helical peptide. *Biochemistry* 43, 5782-91 (2004).
51. Wieprecht, T., Apostolov, O., Beyermann, M. & Seelig, J. Thermodynamics of the alpha-helix-coil transition of amphipathic peptides in a membrane environment: implications for the peptide-membrane binding equilibrium. *J Mol Biol* 294, 785-94 (1999).
52. Clayton, A. H., Vultureanu, A. G. & Sawyer, W. H. Unfolding of class A amphipathic peptides on a lipid surface. *Biochemistry* 42, 1747-53 (2003).
53. Terzi, E., Holzemann, G. & Seelig, J. Self-association of beta-amyloid peptide (1-40) in solution and binding to lipid membranes. *J Mol Biol* 252, 633-42 (1995).
54. Zhu, M., Souillac, P. O., Ionescu-Zanetti, C., Carter, S. A. & Fink, A. L. Surface-catalyzed amyloid fibril formation. *J Biol Chem* 277, 50914-22 (2002).
55. van Klompenburg, W., Nilsson, I., von Heijne, G. & de Kruijff, B. Anionic phospholipids are determinants of membrane protein topology. *Embo J* 16, 4261-6 (1997).
56. Knight, J. D. & Miranker, A. D. Phospholipid catalysis of diabetic amyloid assembly. *J Mol Biol* 341, 1175-87 (2004).
57. Andreola, A. et al. Conformational switching and fibrillogenesis in the amyloidogenic fragment of apolipoprotein a-I. *J Biol Chem* 278, 2444-51 (2003).
58. Zhao, H., Tuominen, E. K. & Kinnunen, P. K. Formation of amyloid fibers triggered by phosphatidylserine-containing membranes. *Biochemistry* 43, 10302-7 (2004).
59. Zhu, M. & Fink, A. L. Lipid binding inhibits alpha-synuclein fibril formation. *J Biol Chem* 278, 16873-7 (2003).
60. Ege, C. & Lee, K. Y. Insertion of Alzheimer's A beta 40 peptide into lipid monolayers. *Biophys J* 87, 1732-40 (2004).

61. McLaughlin, A., Grathwohl, C. & McLaughlin, S. The adsorption of divalent cations to phosphatidylcholine bilayer membranes. *Biochim Biophys Acta* 513, 338-57 (1978).
62. Gouy, G. *Journal of Physics*, 457 (1910).
63. Chapman, D. L. *Phil.Mag.* 6, 475 (1913).
64. McLaughlin, S. Electrostatic potentials at membrane-solution interfaces. *Curr Top Membr Transp* 9, 71-144 (1977).
65. Chiti, F., Stefani, M., Taddei, N., Ramponi, G. & Dobson, C. M. Rationalization of the effects of mutations on peptide and protein aggregation rates. *Nature* 424, 805-8 (2003).
66. Wilson, D. M. & Binder, L. I. Free fatty acids stimulate the polymerization of tau and amyloid beta peptides. In vitro evidence for a common effector of pathogenesis in Alzheimer's disease. *Am J Pathol* 150, 2181-95 (1997).
67. King, M. E., Ahuja, V., Binder, L. I. & Kuret, J. Ligand-dependent tau filament formation: implications for Alzheimer's disease progression. *Biochemistry* 38, 14851-9 (1999).
68. Lee, H. J., Choi, C. & Lee, S. J. Membrane-bound alpha-synuclein has a high aggregation propensity and the ability to seed the aggregation of the cytosolic form. *J Biol Chem* 277, 671-8 (2002).
69. Popot, J. L. & Engelman, D. M. Membrane protein folding and oligomerization: the two-stage model. *Biochemistry* 29, 4031-7 (1990).
70. Popot, J. L. & Engelman, D. M. Helical membrane protein folding, stability, and evolution. *Annu Rev Biochem* 69, 881-922 (2000).
71. Wimley, W. C. & White, S. H. Experimentally determined hydrophobicity scale for proteins at membrane interfaces. *Nat Struct Biol* 3, 842-8 (1996).
72. Wimley, W. C., Creamer, T. P. & White, S. H. Solvation energies of amino acid side chains and backbone in a family of host-guest pentapeptides. *Biochemistry* 35, 5109-24 (1996).
73. Renault, A. et al. Surface-induced polymerization of actin. *Biophys J* 76, 1580-90 (1999).
74. Lang, K., Schmid, F. X. & Fischer, G. Catalysis of protein folding by prolyl isomerase. *Nature* 329, 268-70 (1987).
75. Walter, S. & Buchner, J. Molecular chaperones--cellular machines for protein folding. *Angew Chem Int Ed Engl* 41, 1098-113 (2002).
76. Patil, C. & Walter, P. Intracellular signaling from the endoplasmic reticulum to the nucleus: the unfolded protein response in yeast and mammals. *Curr Opin Cell Biol* 13, 349-55 (2001).
77. Selkoe, D. J. Folding proteins in fatal ways. *Nature* 426, 900-4 (2003).
78. Virchow, R. *Virchows Arch. Pathol. Anat.* 6, 135-137 (1854).
79. Friedrich, N. & Kekulé, A. *Arch Pathol Anat Physiol Klin Med* 16, 50-55 (1859).
80. Bucciantini, M. et al. Inherent toxicity of aggregates implies a common mechanism for protein misfolding diseases. *Nature* 416, 507-11 (2002).
81. Dobson, C. M. Protein aggregation and its consequences for human disease. *Protein Pept Lett* 13, 219-27 (2006).
82. Koo, E. H., Lansbury, P. T., Jr. & Kelly, J. W. Amyloid diseases: abnormal protein aggregation in neurodegeneration. *Proc Natl Acad Sci U S A* 96, 9989-90 (1999).
83. Esch, F. S. et al. Cleavage of amyloid beta peptide during constitutive processing of its precursor. *Science* 248, 1122-4 (1990).
84. Haass, C. et al. Amyloid beta-peptide is produced by cultured cells during normal metabolism. *Nature* 359, 322-5 (1992).

85. Suzuki, N. et al. An increased percentage of long amyloid beta protein secreted by familial amyloid beta protein precursor (beta APP717) mutants. *Science* 264, 1336-40 (1994).
86. Cai, X. D., Golde, T. E. & Younkin, S. G. Release of excess amyloid beta protein from a mutant amyloid beta protein precursor. *Science* 259, 514-6 (1993).
87. Nitsch, R. M. et al. Cerebrospinal fluid levels of amyloid beta-protein in Alzheimer's disease: inverse correlation with severity of dementia and effect of apolipoprotein E genotype. *Ann Neurol* 37, 512-8 (1995).
88. van Gool, W. A., Kuiper, M. A., Walstra, G. J., Wolters, E. C. & Bolhuis, P. A. Concentrations of amyloid beta protein in cerebrospinal fluid of patients with Alzheimer's disease. *Ann Neurol* 37, 277-9 (1995).
89. Lorenzo, A. & Yankner, B. A. Beta-amyloid neurotoxicity requires fibril formation and is inhibited by congo red. *Proc Natl Acad Sci U S A* 91, 12243-7 (1994).
90. Lambert, M. P. et al. Diffusible, nonfibrillar ligands derived from Abeta1-42 are potent central nervous system neurotoxins. *Proc Natl Acad Sci U S A* 95, 6448-53 (1998).
91. Pike, C. J., Walencewicz, A. J., Glabe, C. G. & Cotman, C. W. In vitro aging of beta-amyloid protein causes peptide aggregation and neurotoxicity. *Brain Res* 563, 311-4 (1991).
92. Shen, C. L., Fitzgerald, M. C. & Murphy, R. M. Effect of acid predissolution on fibril size and fibril flexibility of synthetic beta-amyloid peptide. *Biophys J* 67, 1238-46 (1994).
93. Narayanan, S. & Reif, B. Characterization of chemical exchange between soluble and aggregated states of beta-amyloid by solution-state NMR upon variation of salt conditions. *Biochemistry* 44, 1444-52 (2005).
94. Torrent, J., Balny, C. & Lange, R. High pressure modulates amyloid formation. *Protein Pept Lett* 13, 271-7 (2006).
95. Srinivasan, R. et al. pH-dependent amyloid and protofibril formation by the ABri peptide of familial British dementia. *J Mol Biol* 333, 1003-23 (2003).
96. Ortega-Aznar, A., de la Torre, J. & Castellvi, J. [The CNS amyloid]. *Rev Neurol* 30, 1175-80 (2000).
97. Serpell, L. C. Alzheimer's amyloid fibrils: structure and assembly. *Biochim Biophys Acta* 1502, 16-30 (2000).
98. Sticht, H. et al. Structure of amyloid A4-(1-40)-peptide of Alzheimer's disease. *Eur J Biochem* 233, 293-8 (1995).
99. Crescenzi, O. et al. Solution structure of the Alzheimer amyloid beta-peptide (1-42) in an apolar microenvironment. Similarity with a virus fusion domain. *Eur J Biochem* 269, 5642-8 (2002).
100. Riek, R., Guntert, P., Dobeli, H., Wipf, B. & Wuthrich, K. NMR studies in aqueous solution fail to identify significant conformational differences between the monomeric forms of two Alzheimer peptides with widely different plaque-competence, A beta(1-40)(ox) and A beta(1-42)(ox). *Eur J Biochem* 268, 5930-6 (2001).
101. Terzi, E., Holzemann, G. & Seelig, J. Interaction of Alzheimer beta-amyloid peptide(1-40) with lipid membranes. *Biochemistry* 36, 14845-52 (1997).
102. Brunden, K. R., Richter-Cook, N. J., Chaturvedi, N. & Frederickson, R. C. pH-dependent binding of synthetic beta-amyloid peptides to glycosaminoglycans. *J Neurochem* 61, 2147-54 (1993).

103. McLaurin, J., Franklin, T., Zhang, X., Deng, J. & Fraser, P. E. Interactions of Alzheimer amyloid-beta peptides with glycosaminoglycans effects on fibril nucleation and growth. *Eur J Biochem* 266, 1101-10 (1999).
104. Corder, E. H. et al. Gene dose of apolipoprotein E type 4 allele and the risk of Alzheimer's disease in late onset families. *Science* 261, 921-3 (1993).
105. Atwood, C. S. et al. Characterization of copper interactions with alzheimer amyloid beta peptides: identification of an attomolar-affinity copper binding site on amyloid beta1-42. *J Neurochem* 75, 1219-33 (2000).
106. Hamazaki, H. Ca(2+)-dependent binding of human serum amyloid P component to Alzheimer's beta-amyloid peptide. *J Biol Chem* 270, 10392-4 (1995).
107. Torp, R. et al. Ultrastructural evidence of fibrillar beta-amyloid associated with neuronal membranes in behaviorally characterized aged dog brains. *Neuroscience* 96, 495-506 (2000).
108. Arispe, N., Rojas, E. & Pollard, H. B. Alzheimer disease amyloid beta protein forms calcium channels in bilayer membranes: blockade by tromethamine and aluminum. *Proc Natl Acad Sci U S A* 90, 567-71 (1993).
109. McLaurin, J. & Chakrabarty, A. Membrane disruption by Alzheimer beta-amyloid peptides mediated through specific binding to either phospholipids or gangliosides. Implications for neurotoxicity. *J Biol Chem* 271, 26482-9 (1996).
110. Eckert, G. P., Wood, W. G. & Muller, W. E. Effects of aging and beta-amyloid on the properties of brain synaptic and mitochondrial membranes. *J Neural Transm* 108, 1051-64 (2001).
111. Pouny, Y., Rapaport, D., Mor, A., Nicolas, P. & Shai, Y. Interaction of antimicrobial dermaseptin and its fluorescently labeled analogues with phospholipid membranes. *Biochemistry* 31, 12416-23 (1992).
112. Yanagisawa, K., Odaka, A., Suzuki, N. & Ihara, Y. GM1 ganglioside-bound amyloid beta-protein (A beta): a possible form of preamyloid in Alzheimer's disease. *Nat Med* 1, 1062-6 (1995).
113. Simons, M. et al. Cholesterol depletion inhibits the generation of beta-amyloid in hippocampal neurons. *Proc Natl Acad Sci U S A* 95, 6460-4 (1998).
114. Yip, C. M., Elton, E. A., Darabie, A. A., Morrison, M. R. & McLaurin, J. Cholesterol, a modulator of membrane-associated Abeta-fibrillogenesis and neurotoxicity. *J Mol Biol* 311, 723-34 (2001).
115. McLaurin, J., Franklin, T., Chakrabarty, A. & Fraser, P. E. Phosphatidylinositol and inositol involvement in Alzheimer amyloid-beta fibril growth and arrest. *J Mol Biol* 278, 183-94 (1998).
116. Arispe, N., Pollard, H. B. & Rojas, E. Giant multilevel cation channels formed by Alzheimer disease amyloid beta-protein [A beta P-(1-40)] in bilayer membranes. *Proc Natl Acad Sci U S A* 90, 10573-7 (1993).
117. Muller, W. E. et al. Effects of beta-amyloid peptides on the fluidity of membranes from frontal and parietal lobes of human brain. High potencies of A beta 1-42 and A beta 1-43. *Amyloid* 5, 10-5 (1998).
118. Kremer, J. J., Sklansky, D. J. & Murphy, R. M. Profile of changes in lipid bilayer structure caused by beta-amyloid peptide. *Biochemistry* 40, 8563-71 (2001).
119. Bokvist, M., Lindstrom, F., Watts, A. & Grobner, G. Two types of Alzheimer's beta-amyloid (1-40) peptide membrane interactions: aggregation preventing transmembrane anchoring versus accelerated surface fibril formation. *J Mol Biol* 335, 1039-49 (2004).
120. Hendrix, J. C., Halverson, K. J. & Lansbury, P. T. A convergent synthesis of the amyloid protein of Alzheimer's disease. *J Am Chem Soc*, 7930-7931 (1992).

121. Blazyk, J. et al. A novel linear amphipathic beta-sheet cationic antimicrobial peptide with enhanced selectivity for bacterial lipids. *J Biol Chem* 276, 27899-906 (2001).
122. Eisenberg, D., Weiss, R. M. & Terwilliger, T. C. The hydrophobic moment detects periodicity in protein hydrophobicity. *Proc Natl Acad Sci U S A* 81, 140-4 (1984).

2. Aims of research

The formation of aggregates with similar structures by proteins of unrelated primary sequence suggests a generic mechanism governing the process. A full understanding of the protein aggregation mechanism requires the knowledge of the thermodynamic and conformational changes occurring during the protein transition from a native to an aggregated state. The study of the thermodynamic driving forces and structural changes of an aggregation process is the main goal of this thesis.

The most abundant structural element in protein aggregates is the β -sheet. It has been proposed that intermolecular β -sheet formation is the initial molecular event in the protein aggregation pathway, especially in the case of amyloid formation. For this purpose we attempted to develop a well-defined model system for a random coil \rightleftharpoons β -sheet transition, which allows drawing general conclusions about the structural and thermodynamic properties of protein aggregation.

A promising model peptide to study the random coil \rightleftharpoons β -sheet transition is the (KIGAKI)₃ peptide. The benefit of the KIGAKI₃ peptide is that the structural transition of interest can be induced upon binding to anionic lipid vesicles. To understand membrane induced β -sheet folding for the (KIGAKI)₃ peptide, we first have to understand peptide binding to the membrane surface. Therefore, the first part of this thesis (Chapter 3) derives and evaluates a general binding model for charged molecules to lipid membranes. The binding model is in particular suitable for data evaluation of isothermal titration calorimetry (ITC) experiments. ITC is the most direct technique to measure thermodynamic parameters and thus it will serve to identify the driving forces of the random coil \rightleftharpoons β -sheet folding reaction in a membrane environment (Chapter 4).

A further aim is to investigate the difference between the β -sheet folding reaction in a native and aggregated protein (Chapter 5). Current models of extended β -sheets, like in amyloid fibrils, indicate that β -sheet folds in aggregates tend to be distinctively longer (about 10 residues) than in native proteins (2 to 6 residues). Therefore the length dependence of the random coil \rightleftharpoons β -sheet folding reaction is studied for a set of peptides with the repeating sequence of KIGAKI to reveal differences in the folding reaction.

In order to obtain information about the structure and dynamics of the (KIGAKI)₃ peptides at the membrane surface, we employ circular dichroism (CD) and nuclear magnetic resonance spectroscopy (NMR) (Chapter 4 and 5). An experimental strategy was developed to gradually disrupt the extended β -sheet structure of (KIGAKI)₃ at the membrane surface. Spectroscopic results were correlated with the thermodynamic observations of the β -sheet folding reaction. In addition, we focused on gaining information about the size and mobility of extended β -sheet structure at the membrane surface. With respect to medical implications we are also interested to investigate the integrity of the lipid membrane upon binding and formation of β -sheet aggregates.

In chapter 6 we provide a new approach to determine high-resolution structures of peptide aggregates at lipid membrane surfaces. For this purpose we encapsulate the (KIGAKI)₃ peptide in reverse micelles. The surfactant interface of the reverse micelles is thought to mimic the biological membrane environment while fast correlation of reverse micelles in a low viscosity solvent enhances spectroscopic resolution.

In a further part of the thesis we study partitioning of xenon atoms into lipid bilayers by ¹²⁹Xe- and ²H-NMR (Chapter 7). Xenon membrane partitioning is of special interest due to the ability of xenon to induce general anesthesia. The participation of lipid molecules in mediating the anesthetic effect has been a long lasting question. We have probed lipid molecule and xenon atoms upon partitioning by NMR in order to shed light on this question. Because of profound differences of xenon compared to other common anesthetic components we expect to obtain new information on the mechanism of the anesthetic effect.

3. Interaction of Verapamil with Lipid Membranes and P-glycoprotein: Connecting Thermodynamics and Membrane Structure with Functional Activity

M. Meier, X. Li Blatter, A. Seelig and J. Seelig

Department of Biophysical Chemistry, Biozentrum, University of Basel,

Klingelbergstrasse 50/70, CH-4056 Basel, Switzerland

Tel: +41-61-267 2190, Fax: +41-61-267 2189, e-mail: joachim.seelig@unibas.ch

3.1 – Summary: Interaction of Verapamil with Lipid Membranes and P-glycoprotein: Connecting Thermodynamics and Membrane Structure with Functional Activity

The first part of the thesis is a general thermodynamic binding study of a model drug component to the membrane protein P-glycoprotein (Pgp), an ABC transporter that binds its substrates generally from the inner leaflet of the lipid membrane. This work is directly linked to the overall topic of peptide aggregation at membrane surfaces due to the fact that binding of charged molecules, like drug components or peptides, to lipid membranes obey the same thermodynamic rules. We therefore derived a binding model with the Gouy-Chapman theory, which takes electrostatic attraction and repulsion between charged molecules and lipid membranes to consideration. The binding theory does not differentiate between incorporation and adsorption of charged molecule to the lipid membrane. In order to evaluate and test the binding model, we studied binding of a well behaving drug component, verapamil, to lipid membranes under different electrostatic conditions by isothermal titration calorimetry. Within the presented work we evidence that the derived Gouy-Chapman binding model is valid for binding of charged molecules to positively, neutral and negatively charged lipid membranes under a variety of conditions. It is thus the framework for the following peptide binding studies.

Concomitantly, we correlated the determined lipid binding parameters of verapamil with functional activity measurements of Pgp, to answer biologically relevant questions of drug membrane and protein interactions. Accordingly, verapamil is a substrate of P-glycoprotein. Pgp binds drugs from the cytosolic leaflet of the cell membrane and exports them to the extracellular environment. As a consequence, Pgp may cause multidrug resistance if overexpressed upon a prolonged exposure of biological cells to such drugs. In this view, it is a long-lasting question, how Pgp recognize its various substrates. Most theoretical predictions of substrate binding to Pgp failed simply due to unknown or inconsistent experimental binding data. The major drawback in studying substrate binding to Pgp is that the drug first has to partition into the membrane. Binding data of substrates to Pgp hitherto published are binding constants, which include the membrane partition coefficients of the drugs. Here, strong binding constants reflect mostly the hydrophobicity of the drug ("membrane partitioning") and not the intrinsic binding to Pgp. Conclusions

from such binding constants about the molecular interactions between drugs and to Pgp are thus misleading.

We therefore revealed for the first time direct drug-Pgp binding constants within the lipid bilayer by dissecting the binding process into two steps, namely into a partitioning step of the drug from the aqueous phase into the lipid membrane, and a binding step of the drug to the Pgp active site in the membrane. The resulting binding constant of verapamil to Pgp revealed that the effective free energy of binding is only about -4.7 kcal/mol, which explains the low specificity of Pgp for its substrates. For two other drugs of the same family (Calcium antagonists) we found comparable values for the free energy of binding. Using a novel hypothesis for substrate recognition of Pgp via well-defined hydrogen bond acceptor groups, we calculated an average free energy of hydrogen bond formation of -0.95 kcal/mol between Pgp and verapamil. Finally, alteration of lipid conformation upon membrane-insertion of verapamil and thus possible changes of the activity on Pgp could be excluded by deuterium nuclear magnetic resonance spectroscopy.

3.2 – Published Article

Biophysical Journal Volume 91 October 2006 2943–2955

2943

Interaction of Verapamil with Lipid Membranes and P-Glycoprotein: Connecting Thermodynamics and Membrane Structure with Functional Activity

M. Meier, X. Li Blatter, A. Seelig, and J. Seelig

Department of Biophysical Chemistry, Biozentrum, University of Basel, Basel, Switzerland

ABSTRACT Verapamil and amlodipine are calcium ion influx inhibitors of wide clinical use. They are partially charged at neutral pH and exhibit amphiphilic properties. The noncharged species can easily cross the lipid membrane. We have measured with solid-state NMR the structural changes induced by verapamil upon incorporation into phospholipid bilayers and have compared them with earlier data on amlodipine and nimodipine. Verapamil and amlodipine produce a rotation of the phosphocholine headgroup away from the membrane surface and a disordering of the fatty acid chains. We have determined the thermodynamics of verapamil partitioning into neutral and negatively charged membranes with isothermal titration calorimetry. Verapamil undergoes a pK_a-shift of $\Delta pK_a = 1.2$ units in neutral lipid membranes and the percentage of the noncharged species increases from 5% to 45%. Verapamil partitioning is increased for negatively charged membranes and the binding isotherms are strongly affected by the salt concentration. The electrostatic screening can be explained with the Gouy-Chapman theory. Using a functional phosphate assay we have measured the affinity of verapamil, amlodipine, and nimodipine for P-glycoprotein, and have calculated the free energy of drug binding from the aqueous phase to the active center of P-glycoprotein in the lipid phase. By combining the latter results with the lipid partitioning data it was possible, for the first time, to determine the true affinity of the three drugs for the P-glycoprotein active center if the reaction takes place exclusively in the lipid matrix.

INTRODUCTION

Broad-spectrum resistance to chemotherapeutic agents has been termed multidrug resistance (MDR). Although several mechanisms may contribute to MDR in mammalian cells, the best characterized is the efflux or flippase activity of the 170 kDa plasma membrane protein P-glycoprotein (Pgp, MDR1, or ABCB1). Pgp binds its substrates in the cytosolic leaflet of the lipid membrane and flips them to the extracellular leaflet or exports them to the extracellular environment (for review see (2)). Substrate binding to Pgp is best described by a two-step mechanism consisting of 1), a lipid-water partitioning step followed by 2), a binding to the transporter in the lipid phase (*l*) (3,4). The overall binding constant K_{tw} for the binding from the aqueous phase (*w*) to the transporter (*t*) can thus be expressed as product of the lipid-water partition coefficient, K_{lw} , and the transporter binding constant in the lipid phase, K_{tl} (5). We measured the transporter-water binding constant, K_{tw} , and the lipid-water partition coefficient, K_{lw} , for several structurally different drugs and derived the corresponding free energies of binding ΔG_{tw}^0 and ΔG_{lw}^0 . The free energy of substrate binding to Pgp in the lipid membrane, ΔG_{tl}^0 , cannot be measured directly but was determined as the difference $\Delta G_{tl}^0 = \Delta G_{tw}^0 - \Delta G_{lw}^0$ (6). The value ΔG_{tl}^0 can be rationalized with a modular binding concept based on hydrogen-bond formation (6–8).

The quantitative understanding of the two-step Pgp binding mechanism is of importance for efficient pharmacotherapy as

well as for drug design. We therefore have selected three calcium channel blockers (verapamil, amlodipine, and nimodipine) of chemically different structure but similar numbers of hydrogen-bond modules (Fig. 1) for a detailed thermodynamic and functional study. Verapamil (pK_a 8.9 (9)) and amlodipine (pK_a 8.6 (10)) are positively charged at pH 7.4 whereas nimodipine is electrically neutral. Using thermodynamic and spectroscopic techniques we examine the partitioning of verapamil into phospholipid membranes and compare it to previous studies on amlodipine and nimodipine (11). The structure of the lipid membrane at different concentrations of verapamil was elucidated with solid-state NMR methods using selectively deuterated lipids. The influence of verapamil on the order of the lipid membrane is of special interest since it was claimed that a decrease in membrane order would reduce the activity of Pgp (for review, see (12,13)). The thermodynamic results are correlated with a functional assay for the binding of the three calcium-channel antagonists to Pgp in inside-out vesicles of MDR1-transfected mouse embryo fibroblasts (NIH-MDR1-G185) (14,15) and compared to extracellular acidification rate measurements performed with living cells (6,16,17).

MATERIALS AND METHODS

Materials

Verapamil hydrochloride was purchased from Fluka Biochemika (Buchs, Switzerland), amlodipine maleate from Sequoia Research Products (Pangbourne, United Kingdom), and nimodipine from Sigma-Aldrich (Sternheim, Germany). 1-palmitoyl-2-oleoyl-*sn*-glycero-3-phosphocholine

Submitted May 23, 2006, and accepted for publication July 17, 2006.

Address reprint requests to J. Seelig, Tel: 41-61-267 2190; E-mail: joachim.seelig@unibas.ch.

© 2006 by the Biophysical Society

0006-3495/06/10/2943/13 \$2.00

doi: 10.1529/biophysj.106.089581

2944

Meier et al.

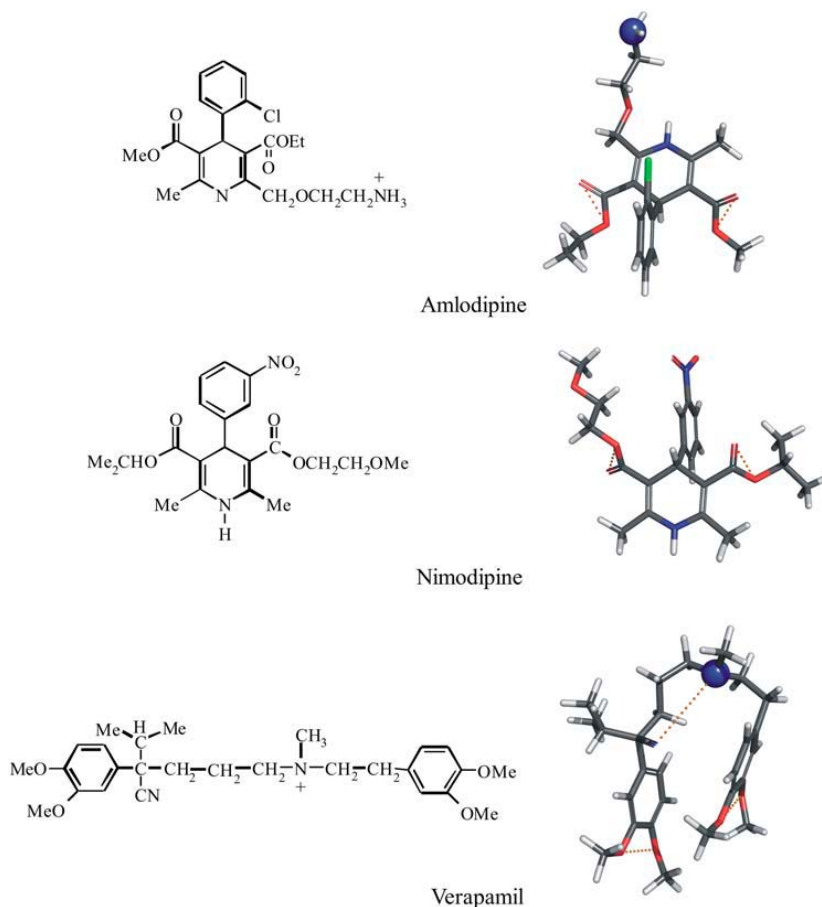


FIGURE 1 Chemical structures and conformational models of three calcium channel antagonists: verapamil, nimodipine, and amlodipine. The three-dimensional structures were obtained by searching the most amphiphilic, energy-minimized conformation with the minimal cross-sectional area, A_p . Oxygen and nitrogen molecules are shown in red and blue, respectively. Hydrogen-bond acceptors, constituting the binding modules for P-glycoprotein, are connected with dotted yellow lines. Pgp does not accept secondary amino groups ($-NHR$) or $-NO_2$ groups (for details, see (7)).

(POPC), 1,2-dioleoyl-trimethylammonium-propane (DOTAP), and 1-palmitoyl-2-oleoyl-*sn*-glycero-3-phosphoglycerol (POPG) were from Avanti Polar Lipids (Alabaster, AL). All other chemicals were purchased at highest purity from commercial sources.

Preparation of lipid vesicles

Small unilamellar vesicles (SUVs) of ~ 30 nm diameter were prepared as follows. Defined amounts of lipid were dissolved in chloroform and were dried first with a stream of N_2 and then overnight under high vacuum. For binary lipid mixtures the second lipid was added in chloroform solution to the dried film of the first lipid and treated as before. Subsequently, buffer solution (typically 50 mM HEPES, pH 7.4, plus various NaCl concentrations) was added to the lipid film and the mixture was vortexed extensively. Next, the lipid dispersion was sonicated under a nitrogen atmosphere for 10–25 min (at $10^\circ C$) until a clear solution was obtained. Metal debris from the titanium tip was removed by centrifugation at 14,000 g for 10 min.

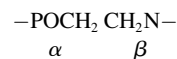
Cell lines and cell culture

The mouse embryo fibroblast cell lines NIH3T3 and NIH3T3 transfected with the human *MDR1* gene, NIH-MDR-G185, were generously provided by Dr. M. M. Gottesman, National Institutes of Health, Bethesda, MD. Cells

were maintained as described earlier (16,17). From these cells crude membranes were prepared as described elsewhere (17,18).

NMR measurements

POPC was deuterated either at the α - or β -position of the choline headgroup or at the *cis*-double bond of the oleic acyl chain (carbon atoms C-9', C-10') (19,20),



A defined amount of deuterated lipid was transferred into a NMR sample tube (typically 10–20 mg lipid) and drug/buffer solution was added to achieve a predefined drug/lipid ratio. For all NMR samples we used 25 mM MES, pH 5.5, and 100 mM NaCl as buffer. The concentration of verapamil was determined before mixing by UV spectroscopy at $\lambda = 277$ nm ($\epsilon = 5818.8 \text{ M}^{-1} \text{ cm}^{-1}$). To achieve a homogeneous suspension, the sample was extensively vortexed at room temperature with several freeze-thaw cycles in-between. Centrifugation at 30,000 g for 60 min at room temperature led to a clear supernatant. To calculate the molar amount of verapamil bound per mol of POPC, X_b (mol/mol), the verapamil concentration in the supernatant was determined again. A flat baseline above 380 nm was used as a criterion

Verapamil and P-Glycoprotein

2945

for complete lipid removal. All ^2H -NMR experiments were performed on a Bruker Avance 400 MHz spectrometer (Bruker AXS, Berlin, Germany). ^2H -NMR spectra were recorded at 64 MHz with the quadrupole echo technique. The lipid pellets were used without further manipulations. ^2H -NMR spectra simulation was done with the NMR WebLab V.4.0 program (21). ^{31}P -NMR spectra were recorded at 161 MHz using a Hahn echo sequence with broadband proton decoupling (WALTZ-16) and a recycle delay of 6 s. The chemical shielding anisotropy, $\Delta\sigma$, was measured as full width at 10% maximum intensity.

Isothermal titration calorimetry

Isothermal titration calorimetry was performed with a VP ITC instrument (Microcal, Northampton, MA). Unless noted otherwise, measurements were made at 37°C. Appropriate buffer solutions were freshly prepared and the pH was properly adjusted when the temperature was changed. The sample cell contained the verapamil solution at a concentration of typically 100 μM . Lipid vesicles suspended in the same buffer as verapamil (lipid concentration of ~25–30 mM) were placed in a 300 μL syringe. Five microliter injections were made every 5 min. As a control, lipid vesicles were injected into the calorimeter cell containing buffer without verapamil.

Analysis of the ITC data

The classical way to describe drug partitioning into the lipid phase is to use the bulk concentration, $C_{\text{D,eq}}$. Here $C_{\text{D,eq}}$ is the equilibrium drug concentration far from the membrane surface. The amount of bound drug, $X_{\text{b}} = n_{\text{D}}/n_{\text{L}}^0$, is then given by

$$X_{\text{b}} = KC_{\text{D,eq}} \quad (1)$$

Here n_{D} is the molar amount of bound drug and n_{L}^0 is the total lipid available for binding (for charged drugs that cannot permeate the lipid membrane, n_{L}^0 is the lipid on the outer vesicle surface). This simple partitioning law is valid for neutral drug molecules such as nimodipine. A more complex situation is encountered for charged drugs as the adsorption of the cationic amphiphiles leads to a positive surface potential ψ , repelling ions of like charge. Alternatively, the membrane may contain negatively charged lipids, producing a negative surface potential. Under these conditions, drug binding is increased because of electrostatic attraction. In both cases, the drug concentration at the plane of binding, $C_{\text{D,M}}$, is not identical to the bulk concentration, $C_{\text{D,eq}}$, but is given by

$$C_{\text{D,M}} = C_{\text{D,eq}} e^{-z_{\text{D}}F_0\psi/RT}, \quad (2)$$

where $z_{\text{D}}F_0$ is the molar electric charge, and RT is the thermal energy. The partition equilibrium Eq. 1 can then be modified as

$$X_{\text{b}} = K_{\text{p}}C_{\text{D,M}} \quad (3)$$

Electrostatic attraction/repulsion effects are thus explicitly taken into account. Equation 3 predicts a linear relationship between the extent of membrane-bound drug and the drug surface concentration. Comparison with Eq. 1 demonstrates that K is not constant for charged drugs but depends on the surface potential and the effective charge according to $K = K_{\text{p}}e^{-z_{\text{D}}F_0\psi/RT}$. Consequently, K varies with the drug and salt concentration. For a monovalent drug such as verapamil and anionic POPC/POPG (75:25 mol/mol) membranes in 0.1 M NaCl, K is typically 5–10 times larger than K_{p} (verapamil concentration is in the mM-range). The surface potential, ψ , can be evaluated with the Gouy-Chapman theory (22,23) and the details of this analysis have been described previously (11,24). The analysis includes the binding of Na^+ ions to phosphatidylglycerol using the Langmuir adsorption isotherm with a Na^+ binding constant of 0.6 M^{-1} . In this evaluation the HEPES buffer was counted as a 1:1 salt. The sulfonic acid has a $\text{pK}_{\text{a}} \sim 3.6$ (25) and is fully charged; the counterion is Na^+ . The piperazin ring is 50% charged. This latter effect was not included.

Surface activity measurements

Surface activity measurements were performed at ambient temperature and pH 7.4 (50 mM Tris buffer, 114 mM NaCl) (26,27). Due to the low solubility of amlodipine and nimodipine in water, stock solutions were prepared in methanol. The total concentration of methanol in the Langmuir trough was, however, <5% v/v. The surface activity was corrected for the effect of methanol. Despite this correction, the surface activity of charged drugs dissolved in methanol tends to be slightly higher than that of drugs dissolved in water due to a small pK_{a} shift. To obtain comparable experimental conditions, verapamil was also injected as methanolic stock solution, despite its better water solubility.

Pgp-ATPase activation assay

The P-glycoprotein associated ATPase activity was measured according to Litman et al. (15) in a 96-well microtiter plate. The ATPase assay buffer contained 25 mM Tris-HCl, 50 mM KCl, 3 mM ATP, 2.5 mM MgSO_4 , 3 mM DTT, 0.5 mM EGTA, 2 mM ouabain, and 3 mM sodium azide, where the latter three compounds were used to inhibit the Ca-, the Na/K-, and the mitochondrial ATPase, respectively. The assay buffer was adjusted to pH 7.4 at 37°C. Membrane vesicles were diluted to a protein concentration of 0.1 mg/ml in ice-cold ATPase assay buffer. Each series of experiments contained 5 μg protein in a total assay volume of 60 μL . Incubation with the various drugs was started by transferring the plate from ice to a water bath, where it was kept 1 h at 37°C. The reaction was terminated by rapidly cooling the plate on ice. The released inorganic phosphate was determined by adding to each well an ice-cold stopping medium (200 μL) containing the color reagent (sulfuric acid 1.43% v/v; and SDS, 0.9% w/v), ammonium molybdate (0.2% (w/v)), and freshly prepared ascorbic acid (1% (w/v)). After incubation at room temperature for 30 min, the released phosphate was quantified calorimetrically at 820 nm using a microplate reader Spectramax M2 (Molecular Devices, Sunnyvale, CA). To determine the vanadate-sensitive Pgp ATPase activity, control samples were incubated in parallel with 500 μM vanadate and the values were subtracted from the values of the Pgp ATPase activation measurements. For stock solutions, drugs were dissolved in DMSO. The DMSO content of the sample was 1.67% (v/v). The data were analyzed according to the model proposed by Litman et al. (15),

$$V_{\text{sw}} = \frac{K_1K_2V_{\text{bas}} + K_2V_1C_{\text{sw}} + V_2C_{\text{sw}}^2}{K_1K_2 + K_2C_{\text{sw}} + C_{\text{sw}}^2}, \quad (4)$$

where V_{sw} is the rate of P_1 release as a function of C_{sw} , the substrate concentration in aqueous solution; V_{bas} is the basal activity of Pgp in the absence of drug; V_1 is the maximum transporter activity (if only activation occurred); and V_2 is the minimum activity at infinite substrate concentration. At a substrate concentration, $C_{\text{sw}} = K_1$, half-maximum binding of the activating binding region is reached and at a substrate concentration, $C_{\text{sw}} = K_2$, half-maximum binding of the inhibitory binding region is reached.

RESULTS

Verapamil-induced structural changes of the lipid bilayer

Fig. 2 shows ^2H -NMR spectra obtained with coarse liposomes composed of POPC, deuterated at the α -segment of the choline moiety ($-\text{POCD}_2\text{CH}_2\text{N}-$) and measured in buffer at pH 5.5. Under these conditions, verapamil carries a charge of $z = +1$ ($\text{pK}_{\text{a}} 8.9$, at 25°C (9)).

All spectra are characteristic of liquid crystalline bilayers with a single quadrupole splitting seen at all drug concentrations. A single, time-averaged quadrupole splitting is also

2946

Meier et al.

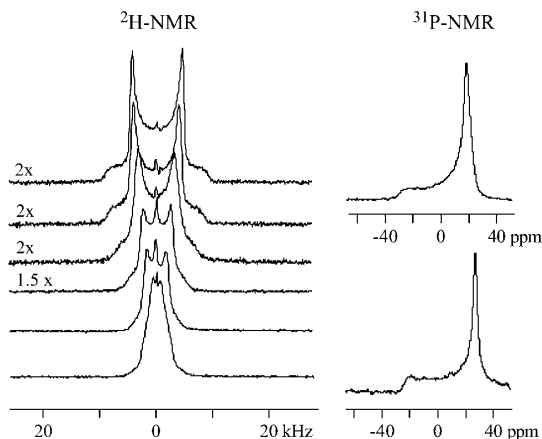


FIGURE 2 Deuterium and phosphorus-31 NMR spectra of POPC liposomes deuterated at the α -position of the choline headgroup ($-\text{POCD}_2\text{CH}_2\text{N}^+$). Approximately twenty-five milligrams of POPC was suspended in 50 μL buffer (25 mM, MES 0.1 M NaCl, pH 5.5, deuterium-depleted water) containing different concentrations of verapamil. The two top spectra correspond to pure POPC membranes without verapamil. The spectra below are characterized by increasing drug concentrations. The verapamil/POPC molar ratio from top to bottom is: 0, 0.02, 0.04, 0.07, 0.11, and 0.14. Virtually all verapamil is incorporated into the membrane. (Number of FIDs: ^2H NMR spectra 8 K, ^{31}P NMR 2 K.)

found for the β -segment of the choline headgroup and the *cis*-double bond of the oleic acyl chain (carbon atoms C-9', C-10'). Apparently, the mobility of verapamil in the lipid membrane is fast enough so that the presence of the drug is sensed by all lipids in the bilayer within 10^{-5} s even at low drug concentration. The quadrupole splitting, $\Delta\nu_Q$, which is defined as the separation of the two most intense peaks in the deuterium NMR spectrum, is gradually changed as the molar verapamil/POPC ratio increases. The quadrupole splittings of the labeled carbon atoms are plotted in Fig. 3 as a function of bound drug, X_b (mol drug bound per mol lipid), revealing a linear relationship between the two parameters. For the two headgroup segments, linear regression analysis yields

$$\Delta\nu_Q(\alpha) = 6.45 - 46.14 X_b \text{ (kHz)} \quad (5)$$

and

$$\Delta\nu_Q(\beta) = 5.5 + 15.3 X_b \text{ (kHz)}. \quad (6)$$

Fig. 2 also demonstrates that the quadrupole splitting of the α -segment collapses to a single line at a mole fraction of $\sim X_b \sim 0.14$. The bilayer structure remains, however, unchanged as evidenced by the phosphorus-31 NMR spectra shown next to the corresponding deuterium NMR spectra. The phosphorus-31 NMR spectra with and without verapamil are very similar and exhibit the typical signature of the bilayer phase (28). The chemical shielding anisotropy is $\Delta\sigma = -47.9$ ppm and remains approximately constant in the concentration range investigated. From the shape of the phosphorus-31 NMR

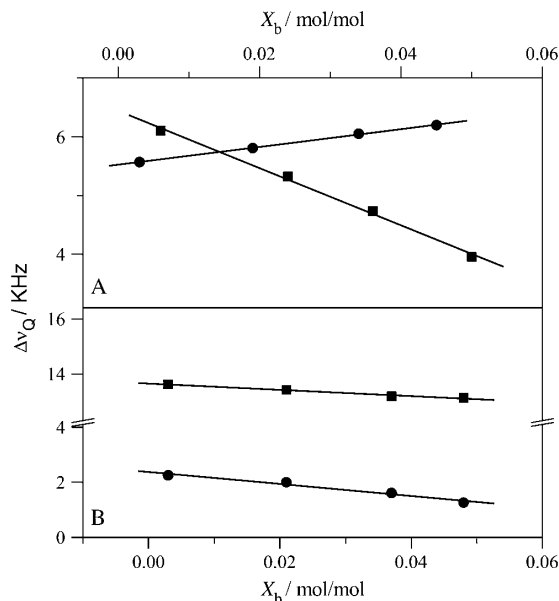


FIGURE 3 Variation of the deuterium NMR quadrupole splittings of POPC membranes with the verapamil/lipid molar ratio. (A) Phosphocholine headgroup segments: (■) α -CD₂ POPC ($-\text{POCD}_2\text{CH}_2\text{N}^+$); (●) β -CD₂-POPC ($-\text{POCH}_2\text{CD}_2\text{N}^+$). (B) POPC deuterated at the *cis*-double bond of the oleic acyl chain: (■) C-9' deuterium, (●) C-10' deuterium. Measurements at 22°C in buffer (MES 25 mM + 0.1 M NaCl, pH 5.5).

spectra it can be concluded that the long-range structure of the bilayer remains unaltered. The deuterium NMR spectra, on the other hand, provide evidence for a change in the orientation of the choline dipole.

The verapamil-induced orientational change of the phosphocholine headgroup can be specified in more detail. Binding of the cationic verapamil to neutral POPC membranes imparts a positive electric charge onto the membrane surface. The orientation of choline headgroup P-N⁺ vector with respect to the membrane surface is, however, dependent on the membrane surface charge density (29). In particular, a positive surface charge moves the N⁺ end of the P-N⁺ dipole toward the water phase. This change in orientation entails a counter-directional response of the quadrupole splittings of the α - and β -segment such that $\Delta\nu_Q(\alpha)$ decreases and $\Delta\nu_Q(\beta)$ increases. Indeed, this counterdirectional change of the quadrupole splitting of the two choline segments is also observed for verapamil (Fig. 3). The extent of the out-of-plane rotation cannot yet be quantitated but exceeds that induced by amlodipine (11) or other monovalent hydrophobic drugs when applied at a similar membrane concentration (30).

The influence of verapamil on the hydrophobic part of the bilayer membrane was also examined with deuterium NMR. The deuterium labels were attached to the *cis*-double bond (C-9' and C-10' segment) of the *sn*-2 oleic acyl chain of POPC.

The two deuterons give rise to two separate quadrupole splittings with separations of 13.5 (C-9') and 2.3 kHz (C-10'), even though they are connected to the same rigid structure (see Fig. 4). The molecular origin of this effect is a

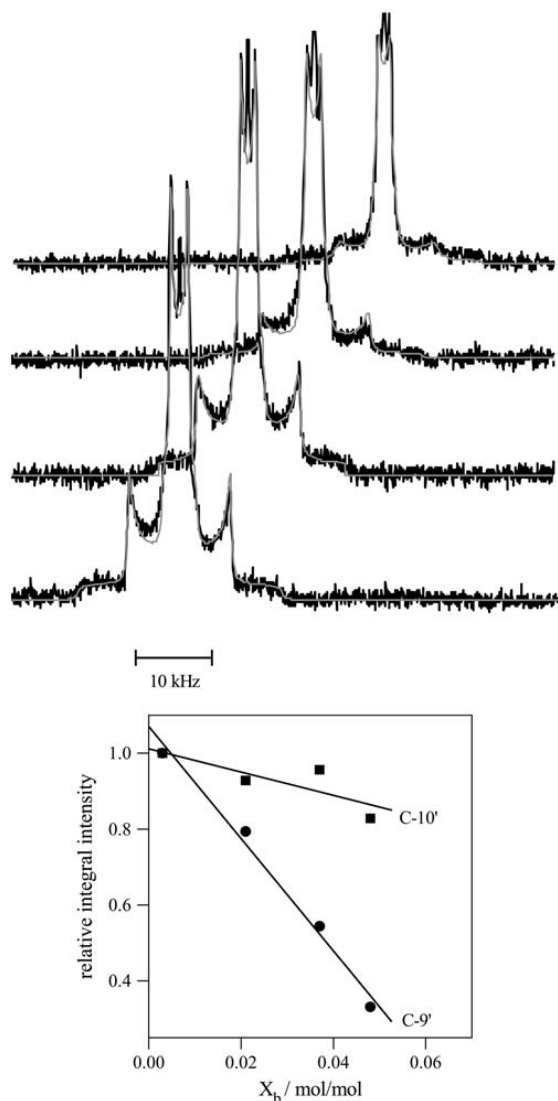


FIGURE 4 ^2H -NMR spectra of POPC membranes deuterated at the *cis*-double bond of the *sn*-2-oleic acyl chain and suspended in buffer with various verapamil concentrations. Approximately twenty-five milligrams of lipid suspended in 50 μL buffer (MES 25 mM + 0.1 M NaCl, pH 5.5) were used. The verapamil/lipid molar ratios from bottom-to-top are 0.003, 0.021, 0.037, and 0.048. The smooth lines are the simulated deuterium NMR spectra. The lower panel shows the loss in signal intensity of the C-9' and C-10' deuteron as a function of the verapamil/lipid molar ratio referenced to the pure POPC spectrum. The C-9' deuteron with a 13 kHz splitting shows a much steeper intensity loss than the C-10' deuteron with a 2 kHz splitting. (4 K free induction decays for all spectra.)

tilting of the *cis*-double bond with respect to the bilayer normal (20).

The variation of these quadrupole splittings with the mole fraction of bound verapamil is included in Fig. 3. The quadrupole splittings of both deuterons are moderately decreased upon increasing the verapamil concentration, according to

$$\Delta\nu_Q(\text{C-9}') = -11.5 X_b + 13.65 \text{ (kHz)} \quad (7)$$

and

$$\Delta\nu_Q(\text{C-10}') = -21.9 X_b + 2.3 \text{ (kHz)}. \quad (8)$$

The fact that both quadrupole splittings decrease simultaneously suggests a disordering of the hydrophobic core upon verapamil intercalation, that is, a more random motion of the *cis*-double bond. This is quite different from amlodipine and nimodipine, which induce a small increase in the C-9' and C-10' quadrupole splittings (11).

Fig. 4 illustrates a second effect induced by the incorporation of verapamil into the lipid bilayer but limited to the hydrophobic region. All spectra in Fig. 4 were measured under identical conditions, in particular, the same number of free induction decays. Inspection of Fig. 4 nevertheless reveals a loss in signal intensity with increasing amount of verapamil in the membrane, which can be quantified by spectral simulation (*smooth lines* in Fig. 4). The spectrum with the lowest verapamil concentration serves as a reference spectrum and the areas under the two quadrupole splittings of this spectrum are identical (1:1 intensity ratio, Fig. 4, *lower panel*). At the highest verapamil concentration ($X_b = 0.43$) the intensity of the C-10' deuteron is still 83% of the initial intensity; that of the C-9' deuteron, however, is reduced to 33%. The most likely explanation of this effect is a reduction in the rate of motion of the *cis*-double bond caused by a weak complex formation with the aromatic ring system of verapamil. The reduced rate of motion makes the refocusing of the quadrupole echo more difficult, particularly for large quadrupole splittings. Similar effects have been observed for amlodipine in POPC membranes (11) and for reconstituted lipid-protein systems such as sarcoplasmic reticulum membranes, cytochrome c-oxidase, and rhodopsin (31–33). No intensity losses are observed for the α - and β -segments of the choline headgroup, indicating that the dynamics of the headgroup is not affected by the presence of verapamil.

Verapamil binding to lipid bilayers: variation of salt concentration and membrane charge

The adsorption of charged, amphipathic molecules to membranes involves electrostatic and hydrophobic interactions, protonation reactions, and dehydration effects. They contribute, to differing extent, to the heat measured in an isothermal titration calorimetry (ITC) experiment. As an example, Fig. 5 shows the titration of a 100 μM verapamil solution in buffer (50 mM HEPES, 50 mM NaCl, pH 7.4) with sonicated lipid

2948

Meier et al.

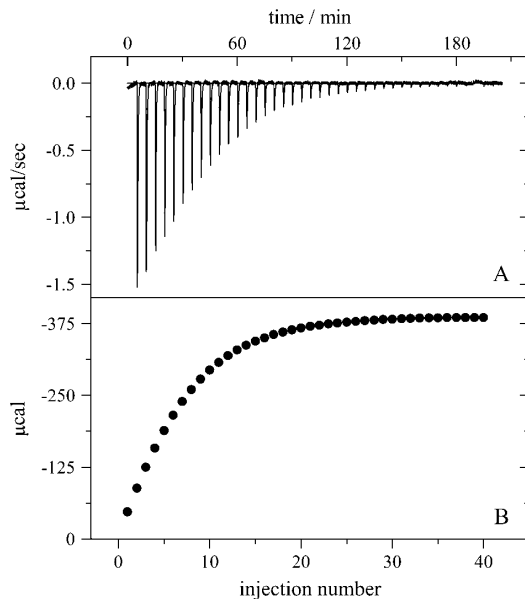


FIGURE 5 Titration of a 100 μM verapamil solution in 50 mM HEPES, pH 7.4 with 30 nm unilamellar lipid vesicles in the same buffer. Lipid composition is POPC/POPG (75:25 mol/mol). The injection of the lipid vesicles was in 5 μL steps. Measuring temperature 37°C. (A) Heat flow and (B) cumulative heat of reaction as a function of injection number.

vesicles composed of POPC/POPG (75/25 mol/mol). Verapamil is contained in the calorimeter cell ($V_{\text{cell}} = 1.4037$ mL) while the lipid suspension is injected at 5 μL aliquots. The total lipid concentration is 25 mM. Each lipid injection causes an exothermic binding reaction as revealed by the heat flow in Fig. 5 A. The size of the titration peak becomes smaller with increasing number of injections as less and less verapamil is available for binding. The integration of the heat flow peaks yield the heats of reaction, h_i , and Fig. 5 B displays the cumulative heat of reaction, $\sum h_i$, as a function of the injection number i .

Fig. 5 further demonstrates that the reaction comes to completion after $n \sim 30$ injections. The molar binding enthalpy, ΔH_{D}^0 , can then be calculated according to

$$\Delta H_{\text{D}}^0 = \sum_{i=1}^n h_i / n_{\text{D}}^0, \quad (9)$$

where n_{D}^0 is the total molar amount of verapamil in the calorimeter cell. Fig. 6 and Table 1 summarize the binding enthalpies, ΔH_{D}^0 , of verapamil binding to POPC/POPG, POPC, and POPC/DOTAP membranes, as a function of total salt concentration (at 37°C). HEPES buffer was treated as a monovalent salt.

For negatively charged POPC/POPG vesicles the binding enthalpy is almost independent of the salt concentration and averages to $\Delta H_{\text{D}}^0 = -2.8 \pm 0.5$ kcal/mol. Neutral POPC and cationic POPC/DOTAP vesicles have ΔH_{D}^0 values in the

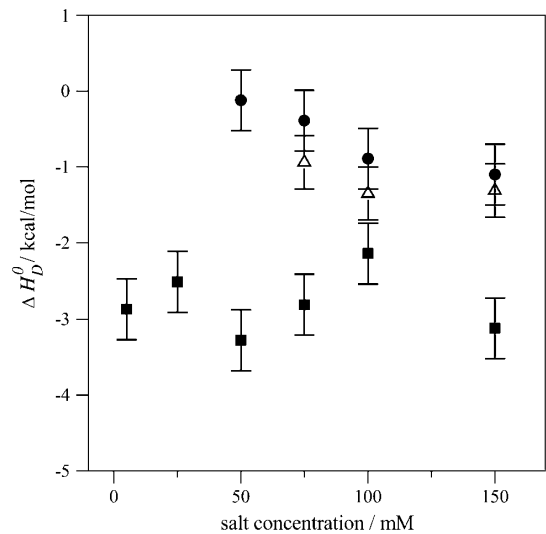


FIGURE 6 Reaction enthalpies of verapamil binding to phospholipid vesicles (30 nm) of different lipid composition. Variation of the binding enthalpy, ΔH_{D}^0 , with the salt concentration. (■) POPC/POPG 75:25 mol/mol, (●) pure POPC, and (△) POPC/DOTAP 95:5 mol/mol.

range of -0.4 to -1.1 kcal/mol, which decrease with increasing salt concentration. At salt concentrations < 50 mM for POPC and < 75 mM for POPC/DOTAP (95:5 mol/mol), no heat of reaction could be observed. Also, no drug binding could be measured when the DOTAP molar percentage was raised above 10 mol %.

It is possible to deduce the amount of bound drug directly from the calorimetric titration according to

$$n_{\text{D, bound}}^{(i)} = \sum_{k=1}^i h_k / (\Delta H_{\text{D}}^0 V_{\text{cell}} C_{\text{D}}^0), \quad (10)$$

where $n_{\text{D, bound}}^{(i)}$ is the molar amount of bound drug after i injections, $\sum_{k=1}^i h_k$ is the cumulative heat of the first i injections, V_{cell} is the volume of drug solution in the calorimeter cell, and C_{D}^0 is the total drug concentration. The amount of free drug is then given from mass conservation as

$$n_{\text{D, free}}^{(i)} = n_{\text{D}}^0 - n_{\text{D, bound}}^{(i)}. \quad (11)$$

The degree of binding was defined above as

$$X_{\text{b}}^{(i)} = n_{\text{D, bound}}^{(i)} / \gamma n_{\text{L}}^0, \quad (12)$$

where n_{L}^0 is the total molar amount of lipid and γn_{L}^0 is the fraction of lipid accessible to the drug. It is hence possible to deduce the complete binding isotherm $X_{\text{b}} = f(c_{\text{eq}})$ from the calorimetric titration without invoking a specific binding model.

For POPC/POPG vesicles at pH 5.5, n_{L}^0 is only 60% of the total lipid ($\gamma = 0.6$), since the drug is fully charged and cannot translocate across the membrane. For all other measurements

TABLE 1 Thermodynamics of verapamil binding to phospholipids bilayer vesicles of different charge and size

SUV 30 nm	POPC mol %	POPG mol %	HEPES mM	NaCl	Drug electric charge near membrane surface (\bar{z})	ΔH_D^0 kcal/mol	K_p M ⁻¹	ΔG_D^0 kcal/mol
	75	25	50	100	0.84–0.89	–3.2	520	–3.84
	75	25	50	50	0.87–0.93	–2.1	400	–3.75
	75	25	50	25	0.88–0.94	–2.8	450	–3.75
	75	25	50	0	0.91–0.96	–3.3	300	–3.50
	80	20	25	0	0.91–0.97	–2.5	380	–3.65
	80	20	5	0	0.96–0.99	–2.9	330	–3.56
	100		50	100	0.57–0.63	–1.1	900	–4.18
	100		50	50	0.57–0.62	–0.9	800	–4.1
	100		50	25	0.53–0.61	–0.4	1200	–4.35
			TRIS					
	100		50	100	0.59–0.64	–3.1	900	–4.18
			PO ₄ ⁻					
	100		50	100	0.59–0.64	+1.4	750	–4.06
		DOTAP	HEPES					
	94.2	5.8	50	100	0.49–0.51	–1.1	500	–3.81
LUV 100 nm	100		50	100	0.61–0.64	–1.0	470	–3.78
	100		50	50	0.61–0.63	–1.1	400	–3.68
	100		50	25	0.59–0.63	–0.6	500	–3.81

Note that all measurements are at 37°C, pH 7.4.

described in this study, a rapid translocation of verapamil across the membrane was assumed ($\gamma = 1$). For example, POPC/POPG vesicles at 150 mM salt and pH 7.4 exhibit a surface potential of ~ -30 mV, which reduces the pH near the membrane surface to pH 6.8. At this pH, the neutral form of verapamil accounts for only 1% of the total drug concentration. However, upon entering the membrane, verapamil experiences a pK_a shift by 1.2 units (see below). Both effects together are sufficient to establish a rapid *trans*-membrane equilibrium.

Fig. 7 then displays ITC-derived binding isotherms for POPC/POPG bilayers at various salt concentrations. The strongest binding is observed for the lowest salt concentration where the electrostatic attraction between the anionic membrane and the cationic drug is maximal. All binding isotherms have a curved appearance and the binding constant defined according to Eq. 1 varies with the verapamil and salt concentration. At a verapamil concentration of $C_{D,eq} = 10 \mu\text{M}$, apparent binding constants are $K \sim 4 \times 10^3 \text{ M}^{-1}$. In contrast, the solid lines in Fig. 7 were calculated with the Gouy-Chapman theory and a common binding constant $K_p = 410 \pm 30 \text{ M}^{-1}$ describes all three binding isotherms over the whole concentration range. The value K_p refers to the binding of the charged form of verapamil. Table 1 summarizes the K_p values for the different systems investigated. The value K_p is distinctly smaller than the apparent binding constant K , since the electrostatic attraction is not included.

For neutral POPC and cationic POPC/DOTAP vesicles at pH 7.4, the pH increases near the membrane surface and the fraction of the neutral form also increases. Membrane translocation of the drug is thus easily possible. Fig. 8 shows binding isotherms for POPC SUVs (three different salt concentrations) and for POPC/DOTAP SUVs. The extent of

drug binding to POPC and POPC/DOTAP SUVs is clearly smaller than that observed for POPC/POPG SUVs at the same salt concentration. Electrostatic attraction/repulsion is the dominant factor for verapamil binding to charged membranes. For anionic POPC/POPG membranes the electrostatic

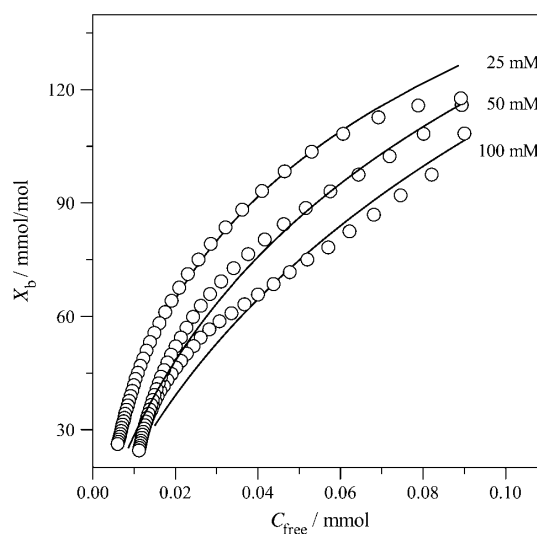


FIGURE 7 Verapamil binding isotherms for POPC/POPG membranes (75:25 mol/mol) at three different salt concentrations. All measurements made at pH 7.4 and 37°C. 50 mM HEPES + 50 mM NaCl; 50 mM HEPES; and 25 mM HEPES. The solid lines were calculated with the partition constants, K_p , given in Table 1 and the Gouy-Chapman theory. A rapid translocation of the neutral form of verapamil across the membrane was assumed.

2950

Meier et al.

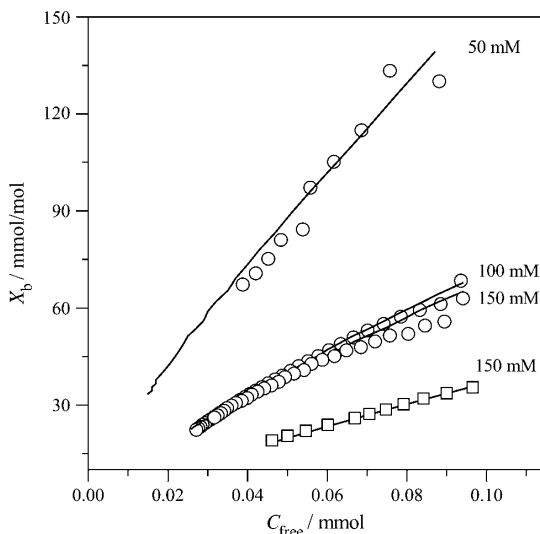


FIGURE 8 Binding of verapamil to POPC SUVs and mixed POPC/DOTAP (94.2:15.8 mol/mol) SUVs at various salt concentrations. (○) Pure POPC SUVs; (□) POPC/DOTAP SUVs. All measurements in 50 mM Tris or HEPES buffer + various concentrations of NaCl at 37°C: The solid lines are theoretical binding isotherms calculated with the partition coefficients listed in Table 1.

interaction is favorable, for cationic POPC/DOTAP membranes it is repulsive. However, even for neutral membranes, electrostatics is important since the membrane surface becomes positively charged as soon as the first cationic drug molecule is incorporated into the membrane. Further binding of drug molecules thus becomes increasingly more difficult. The solid lines in Fig. 8 were again calculated with the Gouy-Chapman theory.

The results described above were obtained with vesicles prepared by sonication, having an average diameter of ~ 30 nm (SUV). Verapamil binding to POPC membranes was also studied with unilamellar vesicles of 100 nm diameter (LUVs) prepared by extrusion through polycarbonate filters. LUVs exhibit a tighter lipid packing than SUVs and resemble more closely planar lipid bilayers. The ITC data were analyzed with the same model as described for SUVs. Again fast translocation of the drug (in its uncharged form) across the membrane was assumed. The experimental results are included in Table 1. The reaction enthalpy at 37°C is $\Delta H_D^0 = -1.1$ kcal/mol for SUVs and $\Delta H_D^0 \approx -1.0$ kcal/mol for LUVs. The binding constants, again deduced with the Gouy-Chapman theory, are somewhat smaller than those of SUVs (see Table 1).

Membrane-induced pK_a shift of verapamil

The ionization constant of verapamil in aqueous solution at 25°C is pK_a 8.9 (9). It is temperature-dependent and decreases

with increasing temperature (see below). A decrease in pK_a can also be expected for verapamil entering the lipid membrane, because the neutral form is favored in the nonpolar environment. The pK_a shift was quantified by measuring the binding reaction in buffers of different dissociation enthalpies, since the reaction enthalpy is the sum of the verapamil deprotonation and the buffer protonation. Verapamil binding to POPC vesicles yields $\Delta H_D^0 = -3.0$ kcal/mol in 50 mM Tris buffer, $\Delta H_D^0 = -1.1$ kcal/mol in 50 mM HEPES buffer, and $\Delta H_D^0 = +1.4$ kcal/mol in phosphate buffer (all measurements at 100 mM NaCl, pH 7.4). This provides evidence for a deprotonation reaction (34–36) of verapamil as it enters the membrane. Fig. 9 shows a plot of the binding enthalpy, ΔH_D^0 , versus the buffer dissociation enthalpy, ΔH_{buffer} , yielding

$$\Delta H_D^0 = -0.41 \Delta H_{\text{buffer}} + 1.5. \quad (13)$$

From the slope it can be deduced that 0.41 H^+ dissociate upon verapamil insertion into the neutral POPC membrane. While the average charge of verapamil in solution at pH 7.4 is $\langle z_D \rangle = 0.97$ e.u., the membrane-bound drug carries an average charge of $\langle z_D \rangle \approx 0.56$ e.u. The reduction by $\delta z = 0.41$ e.u. can be traced back to two sources. Upon binding to the membrane, verapamil repels H^+ ions from the membrane surface. At 150 mM salt and 0.1 mM verapamil, the pH at the membrane surface increases to \sim pH 7.6 and the electric charge of verapamil decreases concomitantly to $z = 0.95$ e.u. ($\delta z = 0.02$ e.u.). However, from the buffer dependence one deduces a much larger change of $\delta z = 0.41$ e.u., attesting to a

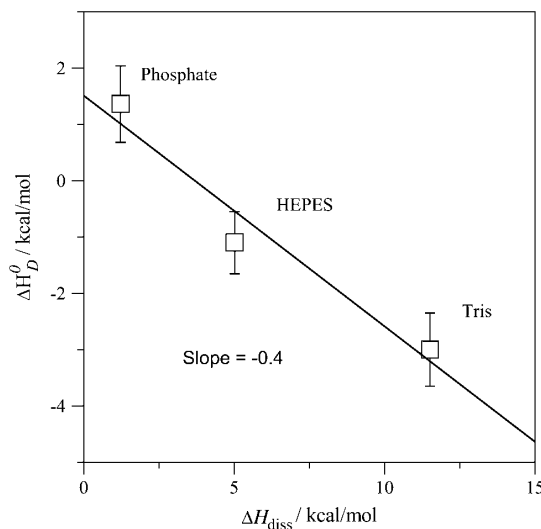


FIGURE 9 Variation of the verapamil binding enthalpies with the buffer dissociation enthalpies. POPC vesicles with 30 nm diameter. Measurements made in Tris ($\Delta H_{\text{Diss}} = 11.51$ kcal/mol), HEPES ($\Delta H_{\text{Diss}} = 4.9$ kcal/mol), and phosphate ($\Delta H_{\text{Diss}} = 1.22$ kcal/mol) at 37°C (36).

pK_a shift as the drug enters the hydrophobic environment. At pH 7.6, a pK_a shift from pK_a ~ 8.9 to pK_a ~ 7.7 reduces the charge from $\langle z \rangle = 0.95$ to $z = 0.56$ ($\delta z = 0.39$). The two effects together (pH change plus pK_a shift) then explain the experimental data. Based on chemical equilibria considerations it can be calculated that the uncharged drug has a $10^{\Delta pK_a} \sim 16$ -times higher partition-coefficient for the lipid membrane than the protonated species. The binding constant of uncharged verapamil is thus $K_p = 6.5 \times 10^3 \text{ M}^{-1}$ for POPC/POPG membranes and $K_p \sim 1.6 \times 10^4 \text{ M}^{-1}$ for POPC vesicles (at pH 7.4 and 37°C).

For membranes composed of diphytanoyl PC, a dissociation constant for uncharged verapamil was estimated as $K_d = 0.061 \pm 0.01 \text{ mM}$ at pH 10.5 based on electrophoretic and membrane potential measurements (37). This translates into a binding constant of $K_p = 1.6 \times 10^4 \text{ M}^{-1}$.

We also measured the molar reaction enthalpy of verapamil binding to POPC vesicles at pH 5.5. At this pH, verapamil is fully charged and no deprotonation takes place upon binding to the membrane. The binding enthalpy was found to be $\Delta H_D^0(\text{pH } 5.5) = -2.7 \text{ kcal/mol}$. On the other hand, the (extrapolated) binding enthalpy at pH 7.4 in the absence of a buffer dissociation reaction is $\Delta H_D(\text{pH } 7.4) = 1.5 \text{ kcal/mol}$ (see Fig. 9 for $\Delta H_{\text{Diss}} = 0$). The value $\Delta H_D(\text{pH } 7.4)$ is thus composed of the binding enthalpy of the fully charged drug, $\Delta H_D(\text{pH } 5.5)$, plus the dissociation enthalpy for 0.41 H^+ ,

$$\Delta H_D(\text{pH } 7.4) = \Delta H_D(\text{pH } 5.5) + 0.41 \Delta H_{\text{Diss}}^{\text{NH}}, \quad (14)$$

where $\Delta H_{\text{Diss}}^{\text{NH}}$ is the dissociation enthalpy of the verapamil amino group. The latter is then calculated as $\Delta H_{\text{Diss}}^{\text{NH}} = 10.2 \text{ kcal/mol}$. This result is consistent with data obtained for N-terminal amino group of peptides where the dissociation energy is $\sim 11 \pm 2 \text{ kcal/mol}$ (38).

Heat capacity change ΔC_p^0

We have measured the temperature-dependence of the verapamil-membrane partition equilibrium. For PC/PG (75:25 mol/mol) membranes in 50 mM HEPES at pH 7.4, ΔH_D^0 shows only a small temperature-dependence with a molar heat capacity of $\Delta C_p^0 = 14 \text{ cal/mol K}$. For pure PC SUVs in buffer (100 mM NaCl, 50 mM HEPES, pH 7.4), the heat capacity change is $\Delta C_p^0 = 12 \text{ cal/mol K}$.

Molecular cross-sectional area and air-water partition coefficient

Amphiphilic molecules such as verapamil, amlodipine, and nimodipine partition into the air-water and lipid-water interface such that the polar groups remain in either the aqueous phase ($\epsilon \approx 80$) or the polar headgroup region of the lipid membrane ($\epsilon \approx 30$). The hydrophobic group is then exposed to air (dielectric constant, $\epsilon \approx 1$) or inserts into the lipid core

region ($\epsilon \approx 2$). The approximate conformation of the three Ca^{2+} blockers, calculated by optimizing polar and nonpolar interactions, are shown in Fig. 1 (39). The cross-sectional areas of the three molecules, relevant for membrane insertion, were calculated as $A_D = 82 \text{ \AA}^2$ for verapamil, 66.2 \AA^2 for amlodipine, and 69.4 \AA^2 for nimodipine.

The surface activities of the three Ca^{2+} blockers were measured with the Wilhelmy plate method (data not shown) and were described by the Szyszkowski isotherm. The measured cross-sectional area of verapamil in aqueous solution is $A_D = 82 \pm 2 \text{ \AA}^2$ and in good agreement with the calculated value. The cross-sectional areas of amlodipine ($A_D = 122 \text{ \AA}^2$) and nimodipine ($A_D = 87 \text{ \AA}^2$) are, however, larger than the calculated data, which is caused by association effects at higher concentrations. For the following calculations, we use the calculated cross-sectional areas.

The air-water partition coefficients are $K_{A/W} = 1.7 \times 10^5 \text{ M}^{-1}$ for verapamil, $K_{A/W} = 1.9 \times 10^6 \text{ M}^{-1}$ for amlodipine, and $K_{A/W} = 7.1 \times 10^5 \text{ M}^{-1}$ for nimodipine. Insertion into the lipid bilayer expands the surface area and requires additional expansion work πA_D (40) where π is the monolayer-bilayer equivalence pressure (41). The lipid-water partition coefficient can then be calculated from the air-water partition coefficient as $K_{\text{lip}/W} = K_{A/W} \exp(-\pi A_D/kT)$ (26). For POPC LUVs (100 nm) and planar membranes with an equivalence pressure of $\pi \sim 30 \text{ mN/m}$, the lipid-water partition coefficient of charged verapamil is predicted to be $K_{\text{lip}/W} \approx 540 \text{ M}^{-1}$ in excellent agreement with the ITC measurements. For amlodipine $K_{\text{lip}/W} = 1.8 \times 10^4 \text{ M}^{-1}$, again in good agreement with previous ITC measurements ($K_p = 1.6 \times 10^4 \text{ M}^{-1}$ at pH 7.2, (11)). For nimodipine, the lipid water partition coefficient was calculated as $K_{\text{lip}/W} = 5.4 \times 10^3 \text{ M}^{-1}$. This value must be considered as a lower limit as nimodipine has a strong tendency to adsorb to the vessel walls. The data are summarized in Table 2.

P-glycoprotein transporter activity measurements with verapamil, amlodipine, and nimodipine

The P-glycoprotein transporter (Pgp) accepts its substrates from the cytosolic membrane leaflet. The Pgp transport efficiency is determined by 1), the lipid solubility of the substrate; and 2), the affinity of the substrate for the transporter in the lipid phase. The latter can be estimated on the basis of characteristic hydrogen-bonding patterns (6,7). Pgp shows basal activity in the absence of substrates. In the presence of substrates it follows a bell-shaped curve with an initial increase in activation (characterized by the concentration of half-maximum activation, K_1) followed by a decrease in activation at higher drug concentrations (characterized by the concentration of half-maximum inhibition, K_2). The model is detailed in references (6,15). Experimental results obtained with inside-out vesicles using a phosphate assay are shown in Fig. 10 for both verapamil and amlodipine. The quantitative analysis in terms of the model described by Litman

TABLE 2 Comparison of verapamil, amlodipine, and nimodipine; bilayer structure, binding thermodynamics, and P-glycoprotein activity

	Nimodipine	Amlodipine	Verapamil
Deuterium NMR			
Headgroup segments			
m_α (kHz/mol)	no effect*	-30.50*	-46.14
m_β (kHz/mol)	no effect*	15.25*	15.30
<i>cis</i> -double bond			
$m_{C-9'}$ (kHz/mol)			-11.50
$m_{C-10'}$ (kHz/mol)			-21.90
Surface activity measurements			
Cross-sectional area			
A_D (Å ²)	69.4	66.2	82
$K_{A/W}$ (M ⁻¹) [†]	$7.1 \times 10^{5\ddagger}$	1.9×10^6	1.7×10^5
$K_{lip/w}$ (M ⁻¹) at 30 mN/m	$5.4 \times 10^{3\ddagger}$	1.8×10^4	540
ITC measurements			
K_p (M ⁻¹) LUVS	nd	$7.6 \times 10^{3\S}$	470 [¶]
ΔG_{tw}^0 (kcal/mol)	-5.275	-5.484	-3.776
ΔH^0 (kcal/mol)	nd	-8.90 ^{\S}	-1.0 [¶]
Max. electric charge	0	1	1
pK	—	8.6	8.9
Pgp activity			
K_1 (M)	7.9×10^{-7}	1.1×10^{-7}	9.5×10^{-7}
ΔG_{tw}^0 (kcal/mol)	-8.624	-9.834	-8.511
K_2 (M)	—	3.9×10^{-5}	3.7×10^{-5}
V_1 (%)	2.06	2.13	2.6
Drug affinity in lipid bilayer			
ΔG_{li}^0 (kcal/mol)	-3.35	-4.350	-4.735
K_{li} (M ⁻¹)	234	1200	2240
No. of H-bond acceptors	4	4	5
ΔG_{li}^0 (J/mol)	-0.84	-1.088	-0.947

*Data taken from Bäuerle et al. (11).

[†]Data obtained with methanolic stock solutions (see Materials and Methods).

[‡]Lower limit due to adsorption to the Teflon trough.

^{\S}Multilamellar POPC liposomes, 0.1 M NaCl, 10 mM Tris, pH 7.25. Bäuerle et al. (11) gives $K_p = 1.55 \times 10^4$ M⁻¹ and $\Delta H^0 = -8.9$ kcal/mol at 23°C. Using van't Hoff's law and assuming a temperature-independent ΔH^0 , K_p was recalculated for 37°C.

[¶]100 nm POPC LUVs, 0.1 M NaCl, 50 mM HEPES, pH 7.4, 37°C.

et al. (15) yields the parameters K_1 , K_2 and also the corresponding reaction velocities V_1 and V_2 . The data are summarized in Table 2. As outlined previously, the parameters K_1 and K_2 can be interpreted as dissociation constants. Table 2 reveals that amlodipine has a higher affinity to Pgp than verapamil during the activation phase. Whereas the inhibition phase can be well measured for verapamil it cannot be measured to high concentrations for amlodipine and nimodipine due to drug association in solution. Partitioning into the lipid membrane requires the monomeric form of drugs and is not possible at concentrations which are higher than the critical micelles concentration.

Biophysical Journal 91(8) 2943–2955

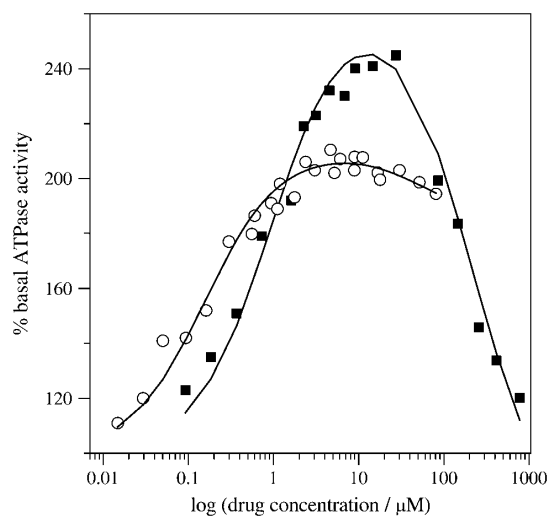


FIGURE 10 Pgp activation profiles obtained by a phosphate release assay with inside-out vesicles prepared from NIH-MDR-G185 cells. (■) Verapamil; (○) amlodipine.

DISCUSSION

Structural aspects of verapamil binding

Verapamil HCl is a calcium-ion influx inhibitor of wide clinical use. It is administered as a racemic mixture of R- and S-enantiomers. At low drug concentration and pH 7.4, a neutral (3%) and a charged species (97%) are in equilibrium in aqueous solution. The molecule exhibits amphiphilic properties and is well soluble in water, organic solvents, and lipid membranes. The pK_a-value of verapamil decreases distinctly with increasing temperature as the present ITC data show that the dissociation enthalpy is endothermic with $\Delta H_{Diss}^{NH} \sim 10$ kcal/mol.

Fig. 1 displays the conformations of verapamil, amlodipine, and nimodipine in the lipid membrane obtained by an energy minimization calculation (39). Verapamil adopts a folded conformation such that both aromatic ring systems can be inserted into the hydrophobic core of the membrane whereas the charged amino group remains at the lipid-water interface. Partitioning of verapamil into the lipid membrane modulates the lipid bilayer structure, as evidenced by deuterium NMR. The predominant effect in the hydrocarbon region is a disordering of the hydrocarbon chains and a weak complex formation of the *cis*-double bond with the aromatic rings of verapamil. Hydrocarbon chain disordering is a common phenomenon when proteins or other nonlipid components are inserted into the lipid bilayer (11,32). Particularly effective are detergent molecules (42,43), whereas cholesterol has the opposite effect; that is, the rodlike molecule induces a stiffening of the hydrocarbon chain (44–47). Membrane disordering has been implied in Pgp inactivation

but cannot play an important role for verapamil as this molecule is considered as the substrate per-excellence for specific drug-Pgp interactions. At the headgroup level, verapamil moves the ^+N end of the choline dipole toward the water phase. Verapamil is more efficient than amlodipine in turning the $^-P-N^+$ dipole since the change of the $\Delta\nu_Q(\alpha)$ quadrupole-splitting-per-mole-incorporated drug is $m_\alpha = -46.1$ kHz/mol for verapamil and only $m_\alpha = -30.5$ for amlodipine. Nimodipine as a noncharged molecule has no effect (11). The consequence of this change in dipole orientation is a change in the electric field across the bilayer membrane. The $^-P-N^+$ dipole has a large dipole moment of ~ 25 Debye (48). If the $^-P-N^+$ dipole is approximately parallel to the membrane surface, as in a pure POPC bilayer (49), the electric dipole field cannot penetrate deeply into the membrane. An orientation 20° away from the membrane surface can, however, creates a field of ~ 100 mV in the adjacent hydrophobic part of the membrane with its low dielectric constant of $\epsilon = 2$. Dipole fields are not efficiently screened by salt and are thus long-range. The electric effect of a single verapamil molecule will therefore extend over several layers of surrounding phospholipids. Electric fields of 100 mV across a distance of 2 nm thickness correspond to a field strength of 5×10^7 V/m and can induce conformational changes in proteins.

Thermodynamic binding parameters and Pgp activation

The extent of partitioning of verapamil into a lipid bilayer membrane is influenced by the electric charge of the membrane surface and the screening of Coulombic interactions through inert electrolytes. This is illustrated with the binding isotherms obtained for negatively charged (Fig. 7) and neutral (Fig. 8) membranes. In both cases, increasing NaCl concentrations decrease the amount of bound verapamil. Negatively charged POPC/POPG (75/25 mol/mol) membranes exhibit a surface potential of -40 mV in 150 mM NaCl, decreasing to -115 mV in 5 mM NaCl. The verapamil binding-affinity increases in parallel with the electrostatic attraction (Fig. 7). By using surface concentrations, $C_{D,M}$, instead of bulk concentrations, the variation of electrostatic attraction can be accounted for, leading to constant intrinsic binding constant. The solid lines in Fig. 7 were simulated with similar binding constants ($K_p = 410 \pm 30$ M $^{-1}$; see Table 1). The average electric charge of verapamil is $\langle z \rangle \sim 0.85$ – 0.99 .

A different situation is encountered for pure POPC bilayers. They are noncharged in the absence of verapamil and become positively charged upon drug binding. Under the present experimental conditions the surface potentials are small ($\psi \sim 5$ – 15 mV) and the binding constants determined with and without electrostatic correction differ by ~ 0 – 20% only. The insertion into the hydrophobic membrane entails a distinct pK_a -shift and the electric charge of verapamil in the membrane is only $\langle z \rangle \sim 0.5$. The binding constant of the charged species is $K_p \sim 400$ – 500 M $^{-1}$ for LUVs but $K_p \sim 900$ – 1200

for SUVs. Verapamil binding to phosphatidylcholine bilayers was determined previously by a centrifugation assay at 22°C (1). For multilamellar liposomes composed of egg lecithin (which typically contains 40% POPC), a verapamil partition coefficient of $P_{\text{Lipid}} \sim 267$ was determined (see also Fig. 4).

Verapamil binding to POPC LUVs can be compared to related data obtained for amlodipine and nimodipine leading to the following order of partition coefficients K_p , for POPC LUVs (at 37°C): verapamil 470 M $^{-1}$ < nimodipine $\sim 5.4 \times 10^3$ M $^{-1}$ < amlodipine 7.6×10^3 M $^{-1}$ (see Table 2).

Lipid solubility is a prerequisite for a drug to be recognized by Pgp, since the active center of this enzyme is located in the inner part of the lipid membrane. The Pgp activity can be measured with a phosphate release assay or, alternatively, a Cytosensor assay (6). Both assays refer to the overall process, that is, the binding of the drug from the aqueous phase to the active center of the transporter in the lipid phase. The corresponding free energy, ΔG_{tw}^0 , is given by $\Delta G_{\text{tw}}^0 = RT \ln(K_1)$, where K_1 has been defined above as the dissociation constant derived from the activation part of the bell-shaped curve given by Eq. 4. The value ΔG_{tw}^0 can be divided into two physically distinct processes, namely 1), the partitioning of the drug from water into the lipid membrane, ΔG_{lw}^0 , followed by 2), the binding of the drug to the transporter in the lipid matrix, ΔG_{tl}^0 (6):

$$\Delta G_{\text{tw}}^0 = \Delta G_{\text{lw}}^0 + \Delta G_{\text{tl}}^0. \quad (15)$$

ΔG_{lw}^0 is related to the lipid-water partition coefficient according to $\Delta G_{\text{lw}}^0 = -RT \ln K_p$. In this and previous studies we have measured K_p by ITC and by surface activity measurements. We thus know ΔG_{lw}^0 for all three drugs from physical-chemical experiments. On the other hand, Pgp activation has been measured in the present study for verapamil, amlodipine, and nimodipine with the phosphate release assay leading to the overall free energy ΔG_{tw}^0 (Table 2). Knowledge of ΔG_{lw}^0 and ΔG_{tw}^0 then allows the evaluation of ΔG_{tl}^0 , i.e., the affinity of the drug for the transporter in the lipid phase. The corresponding results for verapamil, amlodipine, and nimodipine are $\Delta G_{\text{tl}}^0 = -4.7$, -4.4 , and -3.4 kcal/mol, respectively.

ΔG_{tl}^0 can be further converted to lipid binding constants and it is thus possible, for the first time, to derive the binding constants of verapamil and amlodipine to Pgp in the lipid phase. The corresponding numbers are $K_{\text{tl}} = 2.24 \times 10^3$ for verapamil, 1.2×10^3 for amlodipine, and 230 for nimodipine.

We have previously proposed a model which explains the substrate versatility of Pgp on the basis of a modular binding concept, that is, Pgp recognizes well-defined hydrogen-bond acceptor groups (7). Not all hydrogen-bond acceptor groups form hydrogen bonds with same free energy. We distinguish among strong (oxygen atoms), intermediate (nitrogen and sulfur atoms, phenyl groups), and weak (fluorine atoms) hydrogen-bond acceptors, weighted with hydrogen-bond energy units of $EU_{\text{H}} = 1$, 0.5, and 0.25, respectively. This

model leads to $EU_H = 5$ for verapamil and $EU_H = 4$ for amlodipine and nimodipine, respectively. Based on the above free energy of binding in the lipid phase, ΔG_{H}^0 , the average bonding free energy per hydrogen bond is thus $\Delta G_{\text{H}}^0 = -0.95 \text{ kcal/mol} (-1.1 \text{ kcal/mol}, -0.85 \text{ kcal/mol})$ for verapamil (amlodipine, nimodipine). This is in good agreement with a larger set of 15 drug molecules where the free energy of binding from water to the transporter was derived from Cytosensor measurements monitoring the extracellular acidification rate (see (6), Table 1). The average free energy per hydrogen bond was found to be $\Delta G_{\text{H}}^0 \approx -0.79 \text{ kcal/mol}$.

Transport of calcium channel antagonists by Pgp

As Pgp accepts its substrates from the cytosolic leaflet, lipid solubility is an important prerequisite for a substrate to be recognized by Pgp. The second factor is the binding affinity of the drug to Pgp determined by the respective hydrogen-bonding patterns. The above analysis shows that verapamil exhibits the lowest lipid solubility but has the highest binding affinity to the transporter. If dissolved at equal concentrations in the lipid phase, verapamil is binding more efficiently than amlodipine or nimodipine. However, if dissolved at equal concentrations in the aqueous phase, amlodipine and nimodipine are more efficient in saturating Pgp because of their better lipid solubility. On the other hand, amlodipine and nimodipine diffuse more rapidly across the lipid membrane than verapamil due to the smaller cross-sectional area of the former two. Thus they can escape transport by Pgp more easily. Nimodipine, moreover, lacks the cationic charge and is thus not retained at the inner negatively charged membrane leaflet from which Pgp takes its substrates. Nimodipine can therefore be expected to cross the blood-brain barrier more easily. Indeed, in animal experiments, nimodipine had a strong effect on dilating the cerebral arteries, whereas the other two agonists act mainly on peripheral and cardiac vessels.

In conclusion, we have provided a complete binding analysis of verapamil and amlodipine to P-glycoprotein. We have dissected drug binding into a partitioning step into the lipid membrane, followed by the actual binding to the Pgp active site in the hydrophobic membrane. We could thus deduce the intrinsic binding constants of verapamil and amlodipine to Pgp in the lipid phase. All three drugs produce some disordering of the hydrocarbon chains. However, Pgp is not deactivated by membrane disordering as proposed previously.

G. Gerebtzoff was helpful in providing the computer figures and his scientific support is gratefully acknowledged.

This work was supported by the Swiss National Science Foundation grant No. 3100-107793.

REFERENCES

- Romsicki, Y., and F. J. Sharom. 1999. The membrane lipid environment modulates drug interactions with the P-glycoprotein multidrug transporter. *Biochemistry*. 38:6887–6896.
- Higgins, C. F., and M. M. Gottesman. 1992. Is the multidrug transporter a flippase? *Trends Biochem. Sci.* 17:18–21.
- Lu, P., R. Liu, and F. J. Sharom. 2001. Drug transport by reconstituted P-glycoprotein in proteoliposomes. Effect of substrates and modulators, and dependence on bilayer phase state. *Eur. J. Biochem.* 268:1687–1697.
- Omote, H., and M. K. Al-Shawi. 2006. Interaction of transported drugs with the lipid bilayer and P-glycoprotein through a solvation exchange mechanism. *Biophys. J.* 90:4046–4059.
- Seelig, A., and E. Gatlik-Landwojtowicz. 2005. Inhibitors of multidrug efflux transporters: their membrane and protein interactions. *Mini Rev. Med. Chem.* 5:135–151.
- Gatlik-Landwojtowicz, E., P. Aanismaa, and A. Seelig. 2006. Quantification and characterization of P-glycoprotein-substrate interactions. *Biochemistry*. 45:3020–3032.
- Seelig, A. 1998. A general pattern for substrate recognition by P-glycoprotein. *Eur. J. Biochem.* 251:252–261.
- Sauna, Z. E., M. B. Andrus, T. M. Turner, and S. V. Ambudkar. 2004. Biochemical basis of polyvalency as a strategy for enhancing the efficacy of P-glycoprotein (ABCB1) modulators: stipiamide homodimers separated with defined-length spacers reverse drug efflux with greater efficacy. *Biochemistry*. 43:2262–2271.
- Hasegawa, J., T. Fujita, Y. Hayashi, K. Iwamoto, and J. Watanabe. 1984. pKa determination of verapamil by liquid-liquid partition. *J. Pharm. Sci.* 73:442–445.
- Kass, R. S., J. P. Arena, and S. Chin. 1989. Cellular electrophysiology of amlodipine: probing the cardiac L-type calcium channel. *Am. J. Cardiol.* 64:351–411 (discussion 411–421).
- Bäuerle, H. D., and J. Seelig. 1991. Interaction of charged and uncharged calcium channel antagonists with phospholipid membranes. Binding equilibrium, binding enthalpy, and membrane location. *Biochemistry*. 30:7203–7211.
- Eytan, G. D., R. Regev, G. Oren, and Y. G. Assaraf. 1996. The role of passive transbilayer drug movement in multidrug resistance and its modulation. *J. Biol. Chem.* 271:12897–12902.
- Ferte, J. 2000. Analysis of the tangled relationships between P-glycoprotein-mediated multidrug resistance and the lipid phase of the cell membrane. *Eur. J. Biochem.* 267:277–294.
- Al-Shawi, M. K., M. K. Polar, H. Omote, and R. A. Figler. 2003. Transition state analysis of the coupling of drug transport to ATP hydrolysis by P-glycoprotein. *J. Biol. Chem.* 278:52629–52640.
- Litman, T., T. Zeuthen, T. Skovsgaard, and W. D. Stein. 1997. Structure-activity relationships of P-glycoprotein interacting drugs: kinetic characterization of their effects on ATPase activity. *Biochim. Biophys. Acta.* 1361:159–168.
- Landwojtowicz, E., P. Nervi, and A. Seelig. 2002. Real-time monitoring of P-glycoprotein activation in living cells. *Biochemistry*. 41:8050–8057.
- Gatlik-Landwojtowicz, E., P. Aanismaa, and A. Seelig. 2004. The rate of P-glycoprotein activation depends on the metabolic state of the cell. *Biochemistry*. 43:14840–14851.
- Ambudkar, S. V. 1998. Drug-stimulatable ATPase activity in crude membranes of human MDR1-transfected mammalian cells. *Methods Enzymol.* 292:504–514.
- Gally, H. U., W. Niederberger, and J. Seelig. 1975. Conformation and motion of the choline headgroup in bilayers of dipalmitoyl-3-sn-phosphatidylcholine. *Biochemistry*. 14:3647–3652.
- Seelig, J., and N. Waespe-Sarcevic. 1978. Molecular order in *cis* and *trans* unsaturated phospholipid bilayers. *Biochemistry*. 17:3310–3315.
- Macho, V., L. Brombacher, and H. W. Spiess. 2001. The NMR-WEPLAB: an internet approach to NMR lineshape analysis. *Appl. Magn. Reson.* 20:405–432.
- Aveyard, R., and D. A. Haydon. 1973. *Cambridge Chemistry Tests: An Introduction to the Principles of Surface Chemistry*. Cambridge University Press, New York.
- McLaughlin, S. 1977. Electrostatic potentials at membrane-solution interfaces. *Curr. Top. Membr. Transp.* 9:71–144.

24. Seelig, J., S. Nebel, P. Ganz, and C. Bruns. 1993. Electrostatic and nonpolar peptide-membrane interactions. Lipid binding and functional properties of somatostatin analogues of charge $z = +1$ to $z = +3$. *Biochemistry*. 32:9714–9721.
25. Goldberg, R. N., N. Kishore, and R. M. Lennen. 2002. Thermodynamic quantities for the ionization reactions of buffers. *J. Phys. Chem. Ref. Data*. 31:231–370.
26. Fischer, H., R. Gottschlich, and A. Seelig. 1998. Blood-brain barrier permeation: molecular parameters governing passive diffusion. *J. Membr. Biol.* 165:201–211.
27. Gerebtzoff, G., X. Li-Blatter, H. Fischer, A. Frentzel, and A. Seelig. 2004. Halogenation of drugs enhances membrane binding and permeation. *ChemBioChem*. 5:676–684.
28. Seelig, J. 1978. ³¹P nuclear magnetic resonance and the headgroup structure of phospholipids in membranes. *Biochim. Biophys. Acta*. 515:105–140.
29. Seelig, J., P. M. Macdonald, and P. G. Scherer. 1987. Phospholipid headgroups as sensors of electric charge in membranes. *Biochemistry*. 26:7535–7541.
30. Seelig, A., and J. Seelig. 2002. Membrane structure. In *Encyclopedia of Physical Science and Technology*, 3rd Ed. Academic Press, New York.
31. Seelig, J., L. Tamm, L. Hymel, and S. Fleischer. 1981. Deuterium and phosphorus nuclear magnetic resonance and fluorescence depolarization studies of functional reconstituted sarcoplasmic reticulum membrane vesicles. *Biochemistry*. 20:3922–3932.
32. Tamm, L. K., and J. Seelig. 1983. Lipid solvation of cytochrome c oxidase. Deuterium, nitrogen-14, and phosphorus-31 nuclear magnetic resonance studies on the phosphocholine headgroup and on *cis*-unsaturated fatty acyl chains. *Biochemistry*. 22:1474–1483.
33. Bienvenue, A., M. Bloom, J. H. Davis, and P. F. Devaux. 1982. Evidence for protein-associated lipids from deuterium nuclear magnetic resonance studies of rhodopsin-dimyristoylphosphatidylcholine recombinants. *J. Biol. Chem.* 257:3032–3038.
34. Fogel, M., and R. L. Biltonen. 1975. The pH dependence of the thermodynamics of the interaction of 3'-cytidine monophosphate with ribonuclease A. *Biochemistry*. 14:2610–2615.
35. Biltonen, R. L., and N. Langerman. 1979. Microcalorimetry for biological chemistry: experimental design, data analysis, and interpretation. *Methods Enzymol.* 61:287–318.
36. Morin, P. E., and E. Freire. 1991. Direct calorimetric analysis of the enzymatic activity of yeast cytochrome c oxidase. *Biochemistry*. 30:8494–8500.
37. Pohl, E. E., A. V. Krylov, M. Block, and P. Pohl. 1998. Changes of the membrane potential profile induced by verapamil and propranolol. *Biochim. Biophys. Acta*. 1373:170–178.
38. Martin, B. R. 1964. *Introduction to Biophysical Chemistry*. McGraw-Hill, New York.
39. Gerebtzoff, G., and A. Seelig. 2006. In-silico prediction of blood-brain barrier permeation using the calculated molecular cross-sectional area as main parameter. *J. Chem. Inf. Model*. In press.
40. Boguslavsky, V., M. Rebecchi, A. J. Morris, D. Y. Jhon, S. G. Rhee, and S. McLaughlin. 1994. Effect of monolayer surface pressure on the activities of phosphoinositide-specific phospholipase C- β 1, $-\gamma$ 1, and $-\delta$ 1. *Biochemistry*. 33:3032–3037.
41. Seelig, A. 1987. Local anesthetics and pressure: a comparison of dibucaine binding to lipid monolayers and bilayers. *Biochim. Biophys. Acta*. 899:196–204.
42. Heerklotz, H., T. Wieprecht, and J. Seelig. 2004. Membrane perturbation by the lipopeptide surfactin and detergents as studied by deuterium NMR. *J. Phys. Chem. B*. 108:4909–4915.
43. Wenk, M. R., and J. Seelig. 1997. Interaction of octyl- β -thioglucopyranoside with lipid membranes. *Biophys. J.* 73:2565–2574.
44. Blume, A., and R. G. Griffin. 1982. Carbon-13 and deuterium nuclear magnetic resonance study of the interaction of cholesterol with phosphatidylethanolamine. *Biochemistry*. 21:6230–6242.
45. Gally, H. U., A. Seelig, and J. Seelig. 1976. Cholesterol-induced rod-like motion of fatty acyl chains in lipid bilayers a deuterium magnetic resonance study. *Hoppe Seylers Z. Physiol. Chem.* 357:1447–1450.
46. Haberkorn, R. A., R. G. Griffin, M. D. Meadows, and E. Oldfield. 1977. Deuterium nuclear magnetic resonance investigation of the dipalmitoyl lecithin-cholesterol-water system. *J. Am. Chem. Soc.* 99:7353–7355.
47. Oldfield, E., M. Meadows, D. Rice, and R. Jacobs. 1978. Spectroscopic studies of specifically deuterium labeled membrane systems. Nuclear magnetic resonance investigation of the effects of cholesterol in model systems. *Biochemistry*. 17:2727–2740.
48. Shepherd, J. C., and G. Buldt. 1978. Zwitterionic dipoles as a dielectric probe for investigating headgroup mobility in phospholipid membranes. *Biochim. Biophys. Acta*. 514:83–94.
49. Buldt, G., H. U. Gally, A. Seelig, J. Seelig, and G. Zaccai. 1978. Neutron diffraction studies on selectively deuterated phospholipid bilayers. *Nature*. 271:182–184.

3.3 – Appendix

Gouy-Chapman binding model

Binding isotherms of charged drugs or peptides to lipid membranes are obtained by standard isothermal titration calorimetry protocols (see previous paper). Such a binding isotherm (see figure 7 in the article) describes the binding ratio, X_b , as function of the free drug concentration in bulk, $C_{D,free}$ according to

$$X_b = f(C_{D,free}) \quad (A1)$$

where X_b is defined as the ratio of bound drug or peptide, $n_{D, bound}$, to the fraction of lipids, accessible for binding, $\gamma \cdot n_L$. Whereas such a binding isotherm is directly obtained from the experimental ITC data, a specific binding model has to be applied to evaluate the binding parameters. The term "drug" will be used in the following representative for the ligand. Differences in the binding theory between drugs and peptides are quoted in the text.

The binding model applied to the experimental data assumes that membrane binding of charged drugs will be described as surface partition equilibrium^{1,2}

$$X_b = \frac{n_{D,bound}}{\gamma \cdot n_L} = K \cdot C_{D,M} \quad (A2)$$

where K is the equilibrium constant and $C_{D,M}$ the concentration of the drug immediately above the membrane surface. The fraction of lipid accessible for binding depends on the ligand. For charged drugs, that have only access to the outer leaflet of the lipid bilayer, γ is about 0.6 in small unilamellar vesicles, whereas for drugs that can cross the bilayer both leaflets of the membrane have to be accounted for, and therefore γ is 1. Note, that (A2)

uses the surface concentration of the drug, $C_{D,M}$, whereas a partition equilibrium is commonly defined via the bulk concentration such as in A1. Here, the surface concentration is connected to the bulk concentration, $C_{D,eq}$, and the surface potential ψ_0 , via a Boltzmann distribution

$$C_{D,M} = C_{D,eq} \exp\left(-\frac{z_D e_0 \psi_0}{kT}\right) \quad (\text{A3})$$

where z_D is the signed valency of the ligand, e_0 the elementary charge, T the temperature and k the Boltzmann constant. The corresponding surface potential can be determined by solving the Gouy-Chapman equation^{3,4} (for review see^{5,6})

$$\sigma^2 = 2000 \varepsilon_0 \varepsilon_r RT \sum_i c_i \left\{ \exp\left(-\frac{z_i \psi_0 F}{RT}\right) - 1 \right\} \quad (\text{A4})$$

where σ is the two-dimensional density of charge on the surface, ε_0 is the permittivity of the free space, ε_r the dielectric constant of the solution, R the universal gas constant, F the Faraday constant, c_i the concentration of the i^{th} electrolyte in the bulk aqueous phase and z_i is the signed valency of the i^{th} species. The summation in A4 is done over all ions in solution. Since, the charge density and the effective charge of the ligand are not known *ab initio* for the calculation of the membrane potential, a second independent model must be applied to find a self-consistent solution. The derivation of the surface charge density model for a lipid bilayer is given under (A8) to (A17). At his point by definition, the surface charge density can be written as

$$\sigma = \left(\frac{e_0}{A_L}\right) \frac{-z_L X_L^{+/-} (1 - X_{lon}) + z_D X_b}{1 + \left(\frac{A_D}{A_L}\right) X_b} \quad (\text{A5})$$

where A_L is the surface area of lipid ($A_L = 68 \text{ \AA}^2$ for POPC and POPG^{7, 8}), A_D is the surface area requirement of the inserting component, z_L the effective charge of the ligand, and $X_L^{+/-}$ the mol fraction of charged lipid in the membrane. The ligand's surface area, A_D , is not known for most drugs and peptides but can be estimated². Accordingly, A_D is in the range between 50 to 150 \AA^2 for most drugs and peptides, and therefore the contribution from the corrected term of peptide insertion, $(A_D / A_L)X_b$, is small compared to unity. The approximation of A_D is thus not critical and the correction term can be even neglected for substances that only adsorb to the membrane surface. The reduction of the surface charge density due to counterion binding is accounted for by X_{Ion} , which denotes the mole fraction of charged lipids associated with Na^+ or Cl^- . X_{Ion} is calculated by assuming a Langmuir adsorption isotherm for the monovalent ions to the membrane surface

$$X_{Ion} = \frac{K_{Ion} \cdot C_{Ion,M}}{1 + K_{Ion} \cdot C_{Ion,M}} \quad (\text{A6})$$

Here, K_{Ion} is the binding constant for monovalent ions. For sodium ion binding to POPG, the K_{Ion} is 0.6 M^{-1} ^{9, 10} and the binding constant of chloride ions to DOTAP is set equal to K_{Na^+} . Finally, $C_{Ion,M}$ is the concentration of the ion in close proximity to the membrane surface and is connected to the bulk equilibrium concentration, $C_{Ion,eq}$ via a Boltzmann distribution

$$C_{Ion,M} = C_{Ion,eq} \exp\left(-\frac{F\psi_0}{RT}\right) \quad (\text{A7})$$

This binding model can now be linked to the experimental isothermal titration calorimetry data. Unfortunately, two parameters are unknown, the effective charge of the drug and the surface potential. The equation (A3) to (A7) can be solved for each experimentally

obtained pair of X_b and $C_{D,free}$, when a z_D value is given. This procedure has to be repeated for a range of z_D values, in search of the drug binding constant and valency of the drug that corresponds to the best fit to the experimental data according to equation (A1).

Model for the derivation of the surface charge density in lipid bilayers

The surface charge density, σ , at a lipid surface is defined as

$$\sigma = \frac{Q}{A_T} \quad (\text{A8})$$

where Q is the electric charge of the lipid surface and A_T is the surface area of the lipid bilayer. The surface area of the lipid bilayer is given by the moles of the lipid molecules within the lipid bilayer and their surface area, A_L ,

$$A_T = A_L (n_{L^0} + n_{L^{+/-}}^{free} + n_{L^{+/-}}^{bound}) \quad (\text{A9})$$

Furthermore equation (A9) distinguishes between the moles of uncharged lipids, n_{L^0} , charged lipids free of counter ions, $n_{L^{+/-}}^{free}$, and charged lipids bound to counter ions, $n_{L^{+/-}}^{bound}$.

The electric charge of the surface can be expressed by

$$Q = e_0 (-z_L \cdot n_{L^{+/-}}^{free}) \quad (\text{A10})$$

where z_L is the signed valency of the charged lipid and ϵ_0 is the permittivity of the free space. Substitution of (A10) and (A9) into (A8) leads to

$$\sigma = \frac{e_0}{A_L} \left(\frac{-z_L \cdot n_{L^{+/-}}^{free}}{n_{L^0} + n_{L^{+/-}}^{free} + n_{L^{+/-}}^{bound}} \right) \quad (\text{A11})$$

The molar amount of free charged lipids can be written due to mass conservation

$$n_{L^{+/-}}^{free} = n_{L^{+/-}}^{total} - n_{L^{+/-}}^{bound} = n_{L^{+/-}}^{total} - X_{Ion} \cdot n_{L^{+/-}}^{total} = n_{L^{+/-}}^{total} (1 - X_{Ion}) \quad (\text{A12})$$

where $n_{L^{+/-}}^{total}$ is the total amount of charged lipids. $n_{L^{+/-}}^{bound}$ can be deviated from $n_{L^{+/-}}^{total}$ by knowing the mol fraction of charged lipids associated with counterions, X_{Ion} . X_{Ion} is described by (A6) and (A7). Substitution of (A12) into (A10) leads than to

$$\sigma = \frac{e_0}{A_L} \left(\frac{-z_L \cdot n_{L^{+/-}}^{total} (1 - X_{Ion})}{n_{L^0} + n_{L^{+/-}}^{free} + n_{L^{+/-}}^{bound}} \right) \quad (A13)$$

Equation (A14) can be simplified to

$$\sigma = \frac{e_0}{A_L} \left(-z_L \cdot X_L^{+/-} (1 - X_{Ion}) \right) \quad (A14)$$

where $X_L^{+/-}$ denotes for the mol fraction of charged lipids. To this point, the surface charge density of the lipid bilayer was derived in dependence of the molar fraction of charged lipids by taking only the effect of counterions at the membrane surface into consideration. However, upon binding of charged drugs to the membrane the surface charge density is altered. Therefore, incorporation of drugs into the lipid bilayer changes the surface area of the lipid bilayer according to

$$A_T = A_L (n_{L^0} + n_{L^{+/-}}^{free} + n_{L^{+/-}}^{bound}) + n_{Pep} \cdot A_{Pep}. \quad (A15)$$

The electric surface charge also changes upon incorporation and/or adsorption of drugs according to

$$Q = e_0 (z_L \cdot n_{L^{+/-}}^{free} + z_D n_D) \quad (A16)$$

Following the derivation from (A11) to (A14) with the additional terms of peptide or drug binding we find in analogy to A14

$$\sigma = \left(\frac{e_0}{A_L} \right) \frac{-z_L X_L^{+/-} (1 - X_{Ion}) + z_D X_b}{1 + \left(\frac{A_D}{A_L} \right) X_b} \quad (A17)$$

References

1. Beschiaschvili, G. & Seelig, J. Melittin binding to mixed phosphatidylglycerol/phosphatidylcholine membranes. *Biochemistry* 29, 52-8 (1990).
2. Seelig, J., Nebel, S., Ganz, P. & Bruns, C. Electrostatic and nonpolar peptide-membrane interactions. Lipid binding and functional properties of somatostatin analogues of charge $z = +1$ to $z = +3$. *Biochemistry* 32, 9714-21 (1993).
3. Gouy, G. *Journal of Physics*, 457 (1910).
4. Chapman, D. L. *Phil Mag* 6, 475 (1913).
5. McLaughlin, S. Electrostatic potentials at membrane-solution interfaces. *Curr Top Membr Transp* 9, 71-144 (1977).
6. Aveyard, R. & Hydon, D. A. *An introduction to principles of surface chemistry* (Cambridge University Press, London, 1973).
7. Altenbach, C. & Seelig, J. Ca^{2+} binding to phosphatidylcholine bilayers as studied by deuterium magnetic resonance. Evidence for the formation of a Ca^{2+} complex with two phospholipid molecules. *Biochemistry* 23, 3913-20 (1984).
8. Evans, R. W., Williams, M. A. & Tinoco, J. Surface areas of 1-palmitoyl phosphatidylcholines and their interactions with cholesterol. *Biochem J* 245, 455-62 (1987).
9. Eisenberg, M., Gresalfi, T., Riccio, T. & McLaughlin, S. Adsorption of monovalent cations to bilayer membranes containing negative phospholipids. *Biochemistry* 18, 5213-23 (1979).
10. Macdonald, P. M. & Seelig, J. Calcium binding to mixed cardiolipin-phosphatidylcholine bilayers as studied by deuterium nuclear magnetic resonance. *Biochemistry* 26, 6292-8 (1987).

4. Thermodynamics of the Coil \rightleftharpoons β -Sheet Transition in a Membrane Environment

Matthias Meier and Joachim Seelig

Department of Biophysical Chemistry, Biozentrum, University of Basel,
Klingelbergstrasse 50/70, CH-4056 Basel, Switzerland
Tel: +41-61-267 2190, Fax: +41-61-267 2189, e-mail: joachim.seelig@unibas.ch

4.1 – Summary: Thermodynamics of the Coil \rightleftharpoons β -Sheet Transition in a Membrane Environment

As discussed in the introduction, there are good reasons to believe that peptide adsorption to lipid membranes is the starting point of a various human diseases, e.g. the Alzheimer's disease. In the case of amyloid peptides adsorption or binding is generally accompanied by a structural transition from the native to an aggregating state rich in β -sheet structure. Hydrogen bonds within β -sheets can be formed intra- and intermolecular, while formation of the latter can also be regarded as an aggregation process. To investigate the membrane-induced random coil \rightleftharpoons β -sheet transition a model system was developed utilizing of a designed peptide, namely (KIGAKI)₃ (see Chapter 1.6). Briefly, upon binding to anionic lipid membranes the (KIGAKI)₃ peptide forms a highly amphipathic β -sheet, whereas in aqueous solution it adopts a random coil conformation.

Within the studies the (KIGAKI)₃ sequence was systematically modified to vary the extent of the β -sheet formation on the membrane surface. To achieve this we have taken advantage of synthetic analogs of the KIGAKI repeat in which two adjacent amino acids were replaced by their D-enantiomers. For a set of (KIGAKI)₃ peptides in which D-enantiomers of Ala-Lys were introduced we found that the membrane inducible extent of the β -sheet formation is dependent on the number and position of the double D amino acid substitution. In conclusion, substitution of double D amino acids results in a local disturbance of the β -sheet structure. Aggregation size was investigated with deuterium magnetic resonance using (KIGAKI)₃ peptides in which a single Ala residue carried a deuterated methyl group (-CD₃). The NMR analysis revealed that the (KIGAKI)₃ peptide without double D amino acids substitution forms a rigid extended β -sheet, whereas a KIGAKI peptide, in which several D-enantiomers were introduced, freely diffuses at the lipid membrane surface. Additionally, the extent of β -sheet formation on the surface of negatively charged vesicles could be monitored and quantified with circular dichroism (CD) spectroscopy. For example the (KIGAKI)₃ peptide without D-amino acids forms β -sheets of 13.4 residues on average, whereas the stereo-analog (KIGakI)₃ (small letters denote for D amino acids) formed a β -sheet of 3.4 residues.

The thermodynamic parameters of the overall peptide binding process to anionic lipid vesicles, which combines the folding and intrinsic binding process, were determined for all peptides with high-sensitivity isothermal titration calorimetry (ITC). By correlating the overall thermodynamic parameters of the binding process with the structural change of β -sheet formation (gained from CD spectroscopy), it was possible to separate the intrinsic peptide binding to the lipid membrane from the process of β -sheet formation. The results showed that the β -sheet folding reaction in the case of the (KIGAKI)₃ peptide is driven by enthalpy ($\Delta H_{\beta} = -0.2$ kcal/mol per residue) and disfavored by entropy ($T\Delta S_{\beta} = -0.08$ kcal/mol per residue), where the free energy of β -sheet folding reaction is -0.15 kcal/mol per residue. These are the first thermodynamic β -sheet folding and concomitant peptide aggregation parameters in a membrane environment.

4.2 – Published Article

doi:10.1016/j.jmb.2007.02.082

J. Mol. Biol. (2007) xx, xxx–xxx

JMBAvailable online at www.sciencedirect.com

ScienceDirect


Thermodynamics of the Coil \rightleftharpoons β -Sheet Transition in a Membrane Environment

Matthias Meier and Joachim Seelig*

Department of Biophysical
Chemistry, Biozentrum
University of Basel
Klingelbergstrasse 50/70
CH-4056 Basel, Switzerland

Biologically important peptides such as the Alzheimer peptide A β (1–40) display a reversible random coil \rightleftharpoons β -structure transition at anionic membrane surfaces. In contrast to the well-studied random coil \rightleftharpoons α -helix transition of amphipathic peptides, there is a dearth on information on the thermodynamic and kinetic parameters of the random coil \rightleftharpoons β -structure transition. Here, we present a new method to quantitatively analyze the thermodynamic parameters of the membrane-induced β -structure formation. We have used the model peptide (KIGAKI) $_3$ and eight analogues in which two adjacent amino acids were substituted by their D-enantiomers. The positions of the d,d pairs were shifted systematically along the three identical segments of the peptide chain. The β -structure content of the peptides was measured in solution and when bound to anionic lipid membranes with circular dichroism spectroscopy. The thermodynamic binding parameters were determined with isothermal titration calorimetry and the binding isotherms were analysed by combining a surface partition equilibrium with the Gouy–Chapman theory. The thermodynamic parameters were found to be linearly correlated with the extent of β -structure formation. β -Structure formation at the membrane surface is characterized by an enthalpy change of $\Delta H_{\beta} = -0.23$ kcal/mol per residue, an entropy change of $\Delta S_{\beta} = -0.24$ cal/mol K residue and a free energy change of $\Delta G_{\beta} = -0.15$ kcal/mol residue. An increase in temperature induces an unfolding of β -structure. The residual free energy of membrane-induced β -structure formation is close to that of membrane-induced α -helix formation.

© 2007 Elsevier Ltd. All rights reserved.

Keywords: random coil- β -sheet transition; peptide-membrane interaction; peptide-aggregation; (KIGAKI) $_3$ peptide

*Corresponding author

Introduction

The thermodynamics and kinetics of the coil \rightleftharpoons helix transition of peptides and proteins have been studied intensively for several decades. In contrast, little is known about the thermodynamic and kinetic factors that influence the stability of β -sheet folds.¹ β -Sheets form a significant proportion of protein

structure and are found to be associated with protein misfolding; in particular, in the formation of amyloid fibrils and other non-native protein aggregates that have been implicated in a variety of human diseases. The origin of the stability of β -sheets in proteins has been attributed to conformational preferences of residues in the strands,^{2–4} to the hydrophobic effect,⁵ inter-strand hydrogen bonds,^{6,7} and solvent properties.⁸

A closer insight into the thermodynamics of β -sheet formation might be obtained from small model peptides forming β -sheets and β -hairpins; that is, two-stranded antiparallel β -sheet structures, rather than from whole proteins. Homooligopeptides such as poly-lysine, poly-tyrosine, and polycysteine,^{9–11} have been the first model peptides for β -sheet formation and aggregation. Examples of naturally occurring β -sheets were derived, for example, from protein G and ubiquitin.^{12,13} More recently designed peptides like the Gellman peptides¹⁴

Abbreviations used: ITC, isothermal titration calorimetry; SUV, small unilamellar vesicles; POPC, 1-palmitoyl-2-oleoyl-*sn*-glycero-3-phosphocholine; POPE, 1-palmitoyl-2-oleoyl-*sn*-glycero-3-phosphoethanolamine; POPG, 1-palmitoyl-2-oleoyl-*sn*-glycero-3-phosphoglycerol; mPEG 2000 PE, 1,2-dioleoyl-*sn*-glycero-3-phosphoethanolamine-*N*[(methoxy)(polyethylene glycol)-2000].

E-mail address of the corresponding author:
joachim.seelig@unibas.ch

and the WW domain¹⁵ have contributed to the thermodynamic understanding of β -sheet stability.

The free energy of β -sheet formation varies in the range of $-1.6 \text{ kcal/mol} \leq \Delta G_{\beta} \leq 1.2 \text{ kcal/mol}$ per residue depending on the model system under investigation.^{4,16–18} Both enthalpy-driven and entropy-driven β -sheet stabilization is documented in the literature.^{9,19–21} The thermodynamic analysis is hampered by the relatively low tendency of model peptides to form β -sheets in aqueous solution, as intramolecular hydrogen bond formation is in competition with binding to water molecules.

Even less is known about β -sheet formation in a membrane environment. Experimental studies on the energetics of peptide folding in a lipid membrane are still limited to a few examples. The best investigated systems for the coil \rightleftharpoons α -helix equilibrium are amphipathic peptides such as melittin, magainin, or signal peptides that form α -helices at the lipid–water interface.^{22–27} The membrane-induced β -sheet formation, on the other hand, has been investigated with the model peptide AcWL₅,^{28–30} with the Alzheimer peptides β AP(25–35) and β AP(1–40),^{31–33} and with a designed 18 residue peptide, (KIGAKI)₃-NH₂.³⁴ The latter has no amphipathic character as an α -helix but can form a highly amphipathic β -sheet when bound to lipid membranes.

In the present study we have systematically modified the (KIGAKI)₃ sequence to vary the extent of β -sheet formation on the membrane surface. In analogy to previous work on linear amphipathic peptides³⁵ and Alzheimer β AP(1–40) peptides,³⁶ we have taken advantage of synthetic analogues of the KIGAKI repeat in which two adjacent amino acids were replaced by their D-enantiomers. Substitution of double D amino acids results in a local dis-

turbance of β -sheet structure without modifying other characteristics such as hydrophobicity and side-chain functionality.³⁷ Figure 1 shows the envisaged perturbation of the β -structure if an L-Ala-L-Lys pair in a β -sheet is replaced by its D,D-enantiomers. A Lys side-chain that is above or below the β -sheet in the L-enantiomer is rotated into the plane of the β -sheet causing a steric repulsion between neighbouring strands. We have synthesized eight different (KIGAKI)₃ peptides in which D-enantiomers of Ala-Lys were introduced in each of the three repeats, either as a single substitution in one repeat or as multiple substitutions in two or three repeats (D-enantiomers are denoted with lower case letters ak). The extent of β -sheet formation on the surface of negatively charged vesicles was monitored and quantified with circular dichroism (CD) spectroscopy. Aggregate size was investigated with deuterium magnetic resonance (²H-NMR) using a (KIGAKI)₃ peptide in which a single alanine carried a deuterated methyl group (²H₃). The thermodynamic parameters of the binding process were determined with high-sensitivity isothermal titration calorimetry (ITC). By correlating the thermodynamic parameters with the percentage of β -sheet formation, it was possible to separate binding to the lipid membrane from β -sheet formation.

Results

The peptide–membrane binding equilibrium measured with isothermal titration calorimetry

Table 1 shows the set of synthesized peptides with their corresponding short-hand notation. For accurate

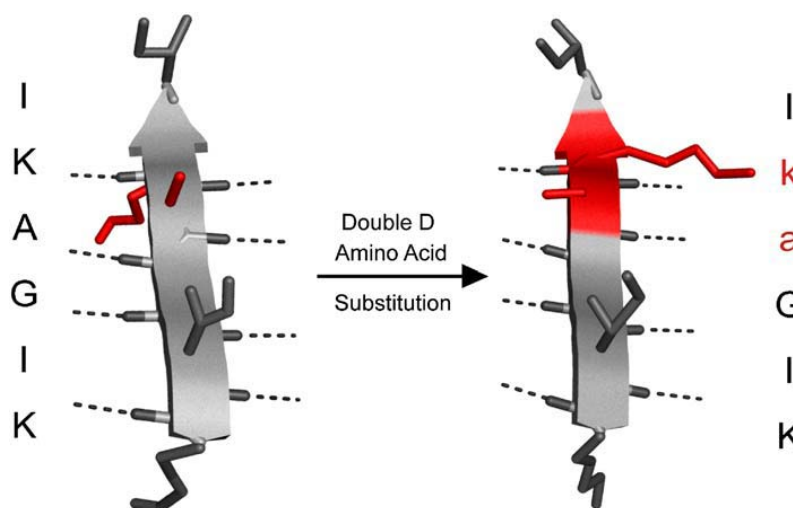


Figure 1. β -Sheet conformation of one KIGAKI unit with and without double D amino acid substitution. The broad arrow indicates the direction of the peptide backbone involved in β -sheet building. The L-Lys and L-Ala side-chains are above the β -sheet. Changing the stereochemistry at the C ^{α} atom to D-Lys and D-Ala rotates the side-chain of the Lys from an orientation perpendicular to the plane of the backbone-backbone hydrogen bonds into a parallel alignment. Lys was chosen for D-substitution as its side-chain is particularly large.

Table 1. Amino acid sequences of the synthesized peptides

Peptide	Abbreviation used in the text
KWGAKI- KIGAKI- KIGAKI-NH ₂	1 ^a
KWGakI- KIGAKI- KIGAKI-NH ₂	2
KWGAKI- KIGakI- KIGAKI-NH ₂	3
KWGAKI- KIGAKI- KIGakI-NH ₂	4
KWGakI- KIGakI- KIGAKI-NH ₂	5
KWGAKI- KIGakI- KIGakI-NH ₂	6
KWGakI- KIGAKI- KIGakI-NH ₂	7
KWGakI- KIGakI- KIGakI-NH ₂	8
KWGakI- KIGakI- KIGakI-NH ₂	9

Amino acids with small letters denote a D stereochemistry at the C^α atom. Underscored Ala residues are deuterium-labelled at the C^β methyl group and are in the L configuration. All peptides are amidated at the C terminus.

^a Peptide 1 was synthesized with and without a deuterium label.

determination of the peptide concentration, Ile2 was replaced by Trp and peptide concentrations were calculated using the Trp molar extinction coefficient (5500 M⁻¹ cm⁻¹). The C-terminal carboxyl groups of all peptides were amidated.

In the following, the term binding is used in a general sense to describe the adsorption of the cationic peptide from bulk solution to the anionic membrane surface. Binding isotherms were determined by injecting lipid vesicles into a peptide solution.³⁸ A typical example is shown in Figure 2. The calorimeter cell contained a 25 μM solution of peptide 8, and 10 μl aliquots of a 12 mM 1-palmitoyl-2-oleoyl-*sn*-glycero-3-phosphoethanolamine (POPE)/1-palmitoyl-2-oleoyl-*sn*-glycero-3-phosphoglycerol (POPG)/1,2-dioleoyl-*sn*-glycero-3-phosphoethanolamine-N [methoxy(polyethylene glycol)-2000 (mPEG 2000 PE) (70:25:5 mol%) SUV suspension were injected (measuring temperature 25 °C). The Figure demonstrates that the heat of reaction, h_i , is endothermic and thus unfavourable for binding (Figure 2(a)). h_i decreases with increasing injections as less and less peptide is available for binding. Control experiments of 10 μl injections of lipid suspension into pure buffer revealed a constant heat of dilution of -1.8 μcal, which was subtracted from the actual measurement. The heat of reaction approaches zero after ~20 injections, indicating that essentially all peptide is bound to the lipid vesicles. The molar binding enthalpy, ΔH^0 , can then be calculated according to:

$$\Delta H^0 = \sum_{i=1}^n h_i/n^0 \quad (1)$$

where n^0 is the total molar amount of peptide in the calorimeter cell and is the cumulative heat of reaction (Figure 2(b)). The measured binding enthalpies for all eight peptides are summarized in Table 2. They vary between 6.5 kcal/mol and 8.7 kcal/mol, depending on the position and extent of the d,d substitution of the peptide. ΔH^0 is a consequence of peptide binding and of β -sheet formation. The variation in ΔH^0 can be correlated with the extent of β -structure formation (see below).

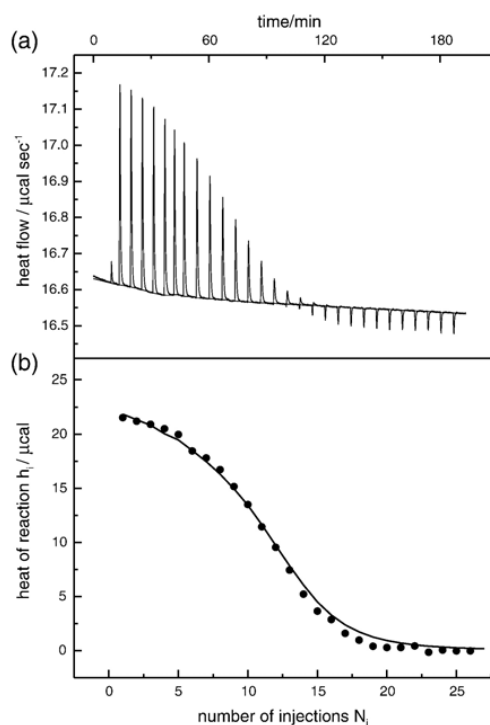


Figure 2. Titration calorimetry of a (KIGakI)₃ (peptide 8) solution (18.8 μM) with small unilamellar vesicles (POPE/POPG/mPEG 2000 POPE (70:25:5 mol%)) with a total lipid concentration of C_L⁰ = 12 mM. (a) Each peak corresponds to the injection of 10 μl of lipid suspension into the reaction cell (V = 1.4053 ml) containing the peptide solution. The reference cell contained 25 mM Tris-HCl (pH 7.4), 50 mM NaCl, T = 25 °C. (b) Heat of reaction h_i as a function of the injection number N_i . The continuous line was calculated by combining a surface partition equilibrium with electrostatic attraction ($\Delta H^0 = 9.0$ kcal/mol, $K_0 = 40$ M⁻¹, $z_p = 4.9$). Binding was assumed to occur only outside the vesicle (60% of total lipid).

Binding can be observed only for membranes that are negatively charged. If the anionic POPG in our vesicles is replaced by an equal amount of zwitterionic 1-palmitoyl-2-oleoyl-*sn*-glycero-3-phosphocholine

Table 2. Thermodynamic parameters for the binding of peptides 1–8 to small unilamellar vesicles composed of POPG/POPE/POPE-PEG 2000 (25:70:5 mol%) at 25 °C

Peptide	ΔH^0 (kcal/mol)	K_0 (M ⁻¹)	z_p	ΔG^0 (kcal/mol)	$T\Delta S^0$ (kcal/mol)
1	6.3±0.3	890±150	4.0	-6.38	12.7
2	7.2±0.3	420±140	4.2	-5.93	13.1
3	8.3±0.25	230±100	4.5	-5.58	13.8
4	7.1±0.3	400±120	4.1	-5.91	13.0
5	8.4±0.3	80±5	4.6	-4.95	13.3
6	8.6±0.15	85±10	4.9	-5.0	13.6
7	7.9±0.1	200±10	4.7	-5.50	13.4
8	8.8±0.4	50±20	4.9	-4.72	13.6

Measurements were performed in triplicate or duplicate.

(POPC), no heat of reaction can be measured in an ITC experiment.

The binding isotherm can be derived from the lipid-into-peptide titration,^{24,38} and is shown in Figure 3 for the ITC data of the previous Figure. The binding isotherm, $X_b = f(c_f)$, describes the amount of bound peptide per lipid, X_b , a function of the equilibrium concentration of free peptide c_f . X_b is defined as $X_b = n_{p,\text{bound}}/n_L^0$ where n_L^0 is the molar amount of lipid available for binding. In the present case, the charged peptides cannot penetrate the lipid membrane and only the outer membrane leaflet (60% of the total lipid) is available for peptide binding. $n_{p,\text{bound}}$ is the molar amount of lipid-bound peptide.

In the case of i injections, X_b can be determined from the measured heats of reaction as follows. $n_{p,\text{bound}}^{(i)}$ is given by

$$n_{p,\text{bound}}^{(i)} = \sum_{k=1}^i h_k / (\Delta H^0 V_{\text{cell}} c_p^0) \quad (2)$$

$n_L^{(i)}$ is calculated from the concentration of lipid in the injection syringe and the number of injections i . Knowledge of the amount of bound peptide allows calculation of the concentration of peptide free in solution from mass conservation. The binding isotherm can thus be determined in a model-independent fashion. Small dilution effects due to the increase in reaction volume must be taken into account.

The further analysis of the binding isotherm requires models for the binding mechanism. One possibility would be a complex formation such that the peptide interacts with a defined number of lipids. Such a model is unlikely, however, since no change in the orientation or motion of the phospholipid head-

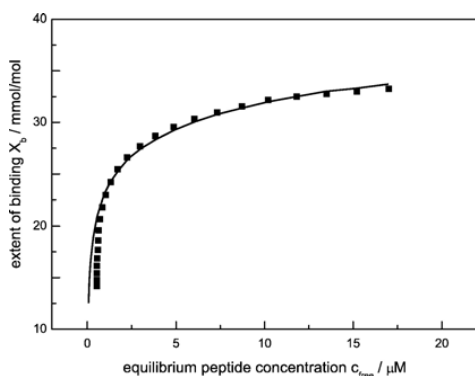


Figure 3. Binding isotherm of (KIGAKI)₃ (peptide 8) for small unilamellar vesicles ($d \sim 30$ nm) as derived from titration calorimetry. The degree of binding X_b (i.e. mmol peptide bound per mol lipid) is plotted against c_{free} , the equilibrium concentration of peptide in bulk solution. The experimental points are derived from the ITC data shown in Figure 2 without assuming a specific binding model. In contrast, the continuous line is the theoretical binding isotherm calculated by combining the Gouy–Chapman theory with a surface partition equilibrium with a partition constant $K_0 = 40 \text{ M}^{-1}$ and an electric charge $z = 4.9$.

groups is observed by ³¹P-NMR (see below). The model employed in the following is a surface partition model in which the peptide adsorption is related to the concentration of peptide c_M found immediately above the plane of binding:^{24,39}

$$X_b = K_0 c_M \quad (3)$$

The model is based on the observation that the negatively charged membrane surface will attract cationic species in its vicinity. The concentration of peptide will thus increase from its equilibrium value, c_f , far away from the membrane surface to the much higher value c_M in the lipid–water interface, an equilibrium governed by the Boltzmann relation:

$$c_M = c_f e^{-z_p F_0 \psi / RT} \quad (4)$$

z_p is the effective peptide charge (usually smaller than the nominal charge), ψ is the membrane surface potential, F_0 is the Faraday constant, and RT is the thermal energy. Using the Gouy–Chapman theory,^{40,41} it is possible to calculate the surface potential ψ and the surface concentration c_M for each datum point of the ITC curve (and the binding isotherm) leading to the surface partition constant K_0 . A detailed description of this binding model as applied to the binding of an α -helix-forming amphipathic peptide has been given.^{24,38,39} As an additional feature of this model, the well-known binding of sodium ions to phosphatidylglycerol was taken into account with a Langmuir adsorption isotherm and a Na^+ binding constant of 0.6 M^{-1} . Tris–HCl buffer was counted as a 1–1 salt. The continuous line in Figure 3 is the theoretical fit to the experimental data. The effective peptide charge is $z_p = 4.2$ and the surface potential varies between $\psi = -45$ mV in the absence of peptide to $\psi = -9$ mV at the highest X_b value. The binding constant according to equation (2) is $K_0 = 300 \text{ M}^{-1}$. An excellent agreement between the model and the experimental data is obtained for all peptides. The corresponding binding constants K_0 are listed in Table 2.

The free energy of binding, ΔG^0 , follows from:

$$\Delta G^0 = -RT \ln 55.5 K_0 \quad (5)$$

where the factor 55.5 is the molar concentration of water. It corrects for the fact that the concentration of free peptide in the aqueous phase is given in mol/l and not as mole fraction, whereas the concentration of the bound peptide is given as mole fraction. ΔG^0 corresponds to the transfer of peptide from the lipid–water interface (peptide concentration c_M) into the lipid bilayer surface. The reaction entropy can then be calculated from $\Delta G^0 = \Delta H^0 - T \Delta S^0$. The thermodynamic parameters for all eight peptides are given in Table 2.

Peptide secondary structure determination of (KIGAKI)₃ peptides in aqueous solution

The thermodynamic results can be correlated with the changes in peptide conformation. For this

purpose, CD spectra of all (KIGAKI)₃ analogues were measured in buffer and in the presence of lipid vesicles (POPE/POPG/mPEG 2000 PE; 45:50:5 mol %). Figure 4(a) shows the CD spectra of the eight peptides measured in buffer. The analysis of the CD spectrum of peptide 1, which has only L-amino acids, yields 23% β -sheet and 77% random coil conformation, but no contribution from α -helix or β -turn. Peptides 2–4 have one d,d substitution, peptides 5–7 have two d,d substitutions and peptide 8 has three such substitutions. Peptides with the same number of d,d pairs have rather similar CD spectra in buffer. However, the substitution with D-amino acids reduces the spectral intensity distinctly. Peptides 2–4 have a single d,d pair (11% of total amino acids). An almost perfect simulation of the CD spectra in buffer is achieved if the CD spectrum of peptide 1 is superimposed with its mirror image at a ratio of 89:11. The shape of the resulting CD spectrum is identical with that of peptide 1 but its ellipticity is reduced to 78% (89%–11%). (A detailed justification of this approach is given in the Material and Method section.) The same model may be applied to peptides 5–7 with two d,d pairs (22% of all amino acids) and predicts a reduced ellipticity of 56% (78%–22%) compared to

peptide 1. Indeed, the shape of all three CD spectra is still very similar to that of the all-L amino acid peptide 1. For peptide 7, the reduction is 56%, in agreement with the theory; for peptides 5 and 6, the reduction is larger, with 36% and 40% of the peptide 1 ellipticity, respectively. This can be explained by a small increase in β -structure (see Material and Method section). Peptide 8 has three d,d substitutions (33% D-amino acids). Its CD spectrum has reduced intensity, since L and D-amino acids almost compensate each other but its shape also differs from the random coil spectrum of peptide 1 as the result of an increased β -content.

The spectral shape and the molar ellipticity of all peptides are independent of the concentration of peptide in the range 25 μ M to 1 mM. The solutions remain optically clear, arguing against the formation of large peptide aggregates. Using the method described in the Material and Method section, we have analysed the CD spectra of all eight peptides in terms of their random coil and β -structure content. The results are summarized in Table 3.

Structure of (KIGAKI)₃ peptides interacting with lipid membranes

Addition of POPE/POPG/mPEG 2000 PE vesicles (45:50:5 mol%) to (KIGAKI)₃ solutions induces a distinct conformational change for peptide 1 (as first reported using POPG vesicles³⁴), and for the d,d substituted peptides 2–8. The corresponding spectra are displayed in Figures 4(b) and 5. Figure 4(b) compares the CD spectra of peptides 1–8 recorded at a lipid-to-protein molar ratio of \sim 20 to ensure complete peptide binding. Peptide 1, composed of L-amino acids only, has the CD spectrum with the largest ellipticity and corresponds to an almost perfect β -sheet spectrum (Table 3). The CD spectra of peptides 2 and 4 have shapes similar to that of peptide 1 but the ellipticity is reduced to 80% and 65%, respectively. For peptide 2, this is consistent with a prediction of 78% if the spectrum of lipid-bound, all-L peptide 1 (89%) is superimposed with its all-D mirror image (11%). The remaining peptides have smaller β -contents. The spectra were analysed as described in Material and Method section, and the structural elements are quantified in Table 3.

It is obvious from the above that the extent of β -structure formation is dependent on the number and position of double D amino acid substitution in the peptide sequence. The largest effect is observed when the d,d pair is placed in the middle of the KIGAKI sequence. Table 3 displays the percentage change of β -structure, $\Delta\beta$, and the number of amino acids, $\Delta\beta_{aa}$, involved in this change.

The lipid-induced random coil to β -structure transition is a two-state equilibrium, as illustrated for peptide 1 in Figure 5, which displays the variation of the CD spectra of 50 μ M peptide 1 upon addition of anionic phospholipid SUVs composed of POPE/POPG/mPEG 2000 PE (45:50:5 mol%) added in small portions of a 25 mM SUV stock solution. The random coil spectrum is gradually replaced by a

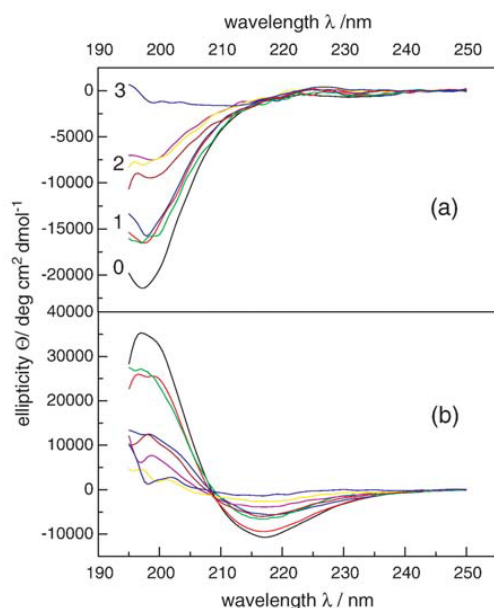


Figure 4. (a) CD spectra of peptides 1–8 in aqueous solution. The spectra were recorded at a peptide concentration of 50 μ M in 5 mM cacodylate buffer (pH 7.4). The numerals indicate the number of d,d substitutions. Peptides with the same number of d,d pairs have similar CD spectra. (b) CD spectra of peptides 1–8 recorded in excess of POPE/POPG/mPEG-2000-POPE (70:25:5 mol%) SUVs (lipid to peptide mol ratio of 15). The peptide concentration was 50 μ M in 5 mM cacodylate buffer (pH 7.4). The largest intensity is observed for peptide 1 with no d,d substitution. The smallest intensity is recorded for peptide 8 with three d,d pairs.

Table 3. CD spectral analysis of peptides 1–8 in buffer and when bound to lipid vesicles

Peptide	Peptide in buffer		Peptide with excess lipid		Change in	
	Random coil (%)	β -Structure (%)	Random coil (%)	β -Structure (%)	$\Delta\beta$ -Structure (%)	$\Delta\beta$ -Structure ^a (residues)
1	77	23	2	98	75	13.5
2	77	23	17	83	60	10.8
3	75	25	28	72	47	8.5
4	77	23	8	92	69	12.4
5	67	33	31	69	36	6.5
6	68	32	43	57	25	4.5
7	73	28	18	82	54	9.7
8	55	46	36	64	19	3.4

The percentages of random coil and β -structure are listed for peptide in buffer and bound to lipid.

^a The column lists the number of amino acid residues (aa) that change from random coil to β -structure ($\Delta\beta(\text{aa}) = 18\Delta\beta(\%) / 100$).

spectrum characteristic of β -structure. The transition shows an isosbestic point at 210 nm, indicating that only two types of structures are involved, one predominantly random coil, the other almost 100% β -sheet.

Mobility of KIGAKI peptides on the membrane surface: NMR measurements

We wished to determine whether β -structure formation is an intra- or intermolecular process. We labelled two peptides with deuterated alanine ($\text{C}^2\text{H}_3\text{-Ala}$) and measured the deuterium NMR spectra of the pure peptide in the solid state and when bound to the liquid-like lipid membrane.

Figure 6(a) and (c) show the ^2H -NMR spectra of the Ala- d_3 label attached to peptide 1 (all-L amino acids) and peptide 9 (two d,d pairs) in lyophilized powder. The characteristic parameter of a deuterium spectrum is the quadrupole splitting, $\Delta\nu_Q$, which is defined as the separation of the two most intense peaks. The quadrupole splitting of the methyl group deuterons provides a direct measure of the order parameter ($S_{\text{c-c}} = 0.5 \langle 3 \cos^2 \Theta - 1 \rangle$) of the methyl rotor axis. The quadrupole splitting of the alanine deuterons of peptides 1 and 9 are 39.5 kHz

and 39 kHz, respectively, at 298 K. The rigid limit of the quadrupole splitting of methyl group deuterons in Ala- d_3 is about 126 kHz. Rapid ($\sim 10^9 \text{ s}^{-1}$) rotation around the methyl $\text{C}^\alpha\text{-C}^\beta$ bond axis reduces the static quadrupole splitting of 126 kHz by a factor of 1/3 to ~ 42 kHz. Thus, the observed quadrupole splitting of about 39 kHz for the lyophilized peptide powder is close to this limit. For rigid molecules undergoing only rapid axial symmetric reorientation about a single axis, the quadrupole splitting is independent of the temperature, which was found for both peptides in the powder state in the temperature range between 248 K and 298 K.

Next, ^2H -NMR spectra were recorded for peptides 1 and 9 in the presence of multilamellar lipid bilayer dispersions composed of POPC/POPG (3:1 mol%) at a lipid-to-peptide ratio of 40 (Figure 6(b) and (d)). Obviously, the deuterium spectra differ distinctly. Deuterons attached to peptide 1 have a motionally averaged quadrupole splitting of 38.2 kHz, a value close to that of the lipid-free solid powder (Figure 6(b)). The only motion is the rotation around the $\text{C}^\alpha\text{-C}^\beta$ threefold symmetry axis. Peptide 1 thus exhibits a rigid structure when bound to negatively charged liposomes. This result can be explained by the formation of extended intermolecular β -sheet aggregates of peptide 1 at the membrane surface. In contrast, the deuterons attached to peptide 9 produce an isotropic deuterium signal (single sharp line) when lipid-bound, suggesting a high level of mobility (Figure 6(d)). The rotational motion of peptide 9 at the membrane surface is fast on the time-scale of the deuterium NMR experiment ($> 10^5 \text{ s}^{-1}$), which leads to the isotropic averaging of the quadrupole splitting. The D amino acids in peptide 9 prevent the formation of an extended intermolecular β -sheet at the negatively charged membrane surface, and peptide 9 appears to be bound as a monomer. The membrane spectra of peptide 9 show a temperature-dependent quadrupole splitting. At 248 K, a quadrupole splitting of 38 kHz is observed, and the molecular motion is completely frozen in. Only the rotation of the methyl group is observed at this temperature.

The bilayer structure of the multilamellar vesicles remains unchanged upon addition of peptides 1 and 9, as evidenced by the ^{31}P phosphorus NMR spectra, shown in Figure 6(e). The ^{31}P phosphorus NMR

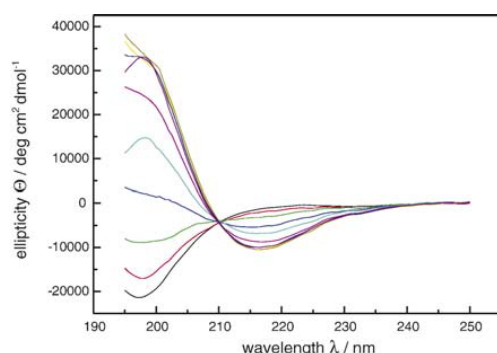


Figure 5. Random coil-to- β -sheet transition of peptide 1 (50 μM) upon titration with POPE/POPG/mPEG 2000 POPE (70:25:5 mol%) SUVs (5 mM cacodylate buffer, pH 7.4). CD spectra were recorded at lipid/peptide ratios of 0, 1, 2, 4, 8, 12, 15, and 20, respectively, reading from bottom to top at 198 nm. The structural transition comes to completion at a lipid to peptide mol ratio of 15.

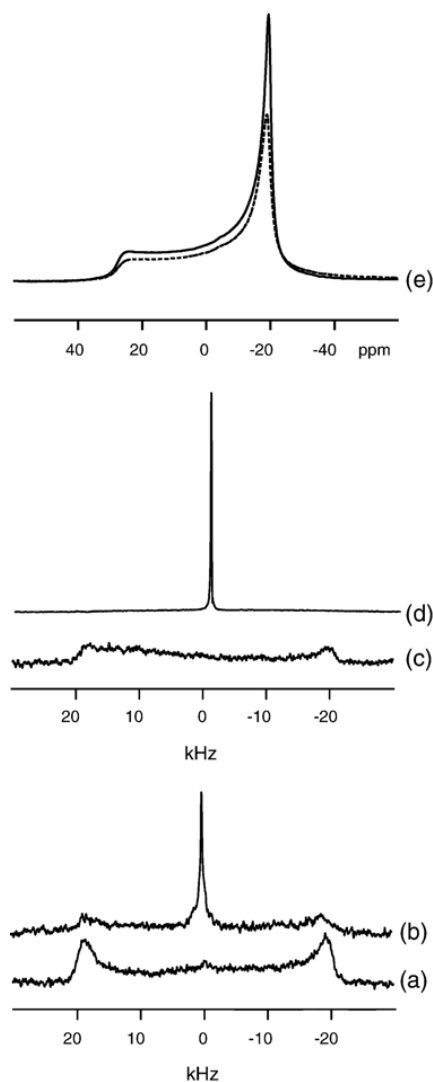


Figure 6. (a) and (c) Deuterium NMR powder spectra of ~ 3 mg of freeze-dried peptide 1 and peptide 9, respectively. Both peptides are labelled with Ala- d_3 at position 9. Peptide 1 consists of L-amino acids only; in peptide 9 the L-amino acid residues at position 4, 5, 10, 15, and 16 are substituted by their D-enantiomers. (b) and (d) Deuterium NMR spectra of peptides 1 and 9 bound to POPC/POPG (3:1 mol%) liposomes, at a lipid to peptide mol ratio of 50. (e) ^{31}P NMR spectra of the POPC/POPG bilayer without peptide (continuous line) and in the presence of peptide 1 (broken line). The ^{31}P phosphorus spectrum was recorded with the same sample of peptide 1 used to obtain the deuterium NMR spectrum in (b).

spectra of the POPC/POPG bilayer with and without peptides are very similar and exhibit the typical signature of the bilayer phase. The chemical shielding anisotropy is $\Delta\sigma = -49.2$ ppm and remains constant at a lipid-to-peptide mol ratio above 40.

From the shape of the ^{31}P phosphorus NMR spectra, it can be concluded that the long-range structure of the bilayer remains unaltered. At higher peptide contents (i.e. lower lipid-to-peptide mol ratios) the (KIGAGI) $_3$ peptide will perturb the bilayer structure. An isotropic component was observed, contributing 30%–70% to the total spectra intensity when the lipid to protein mol ratio was reduced to 25 or 12.5.⁴²

This was further supported by deuterium NMR experiments with and without peptide 8 (three d,d substitutions) using deuterated POPC membranes (spectra not shown). In these experiments, it was the lipid membrane that was deuterated. To be more specific, POPC was deuterated selectively at the β -position of the choline moiety ($-\text{NC}^2\text{H}_2\text{CH}_2\text{OP}-$) and mixed with non-deuterated POPG (3:1 mol%).⁴³ The quadrupole splitting was $\Delta\nu_Q = 5.9$ kHz in the absence of peptide 8 and did not change up to the highest peptide/lipid mol ratio measured (50). The only noticeable effect was a broadening of the line shape. This is in distinct contrast to observations made with, for example, amphiphilic peptides such as melittin or magainin, where the binding to the lipid membrane induces a large change in the quadrupole splitting of the headgroup as the headgroup moves more into the aqueous phase.^{44–46} The present results exclude a conformational change or a spatial reorientation of the $^-\text{P}-\text{N}^+$ dipole.

Peptide β -structure formation and correlation with thermodynamic parameters

The binding of peptides 1–8 to lipid membranes entails two different processes: (i) the association with the membrane surface; and (ii) the conformational change of the peptide. As all peptides adopt virtually identical structures in solution ($\sim 70\%$ random coil, $\sim 30\%$ β -sheet) we assume rather similar association energies. The differences in the experimentally measured thermodynamic parameters are then caused by the change in secondary structure following binding to the membrane surface. Table 3 shows the increase in β -structure upon lipid binding for peptide 1 to peptide 8, both in percentage of β -structure and with the number of amino acid residues involved.

A correlation between the thermodynamic parameters ΔH^0 , ΔG^0 , and ΔS^0 of the peptide binding reaction and the change in β -structure can now be established, and is displayed in Figure 7, which reveals a linear dependence of the thermodynamic binding parameters on the change in β -structure and regression analysis yields the following expressions:

$$\Delta H^0 = -0.23\Delta n_\beta + 9.8(\text{kcal/mol}) \quad R = 0.90 \quad (6)$$

$$\Delta G^0 = -0.15\Delta n_\beta - 4.2(\text{kcal/mol}) \quad R = 0.93 \quad (7)$$

$$\Delta S^0 = -0.24\Delta n_\beta + 46.5(\text{kcal/mol}) \quad R = 0.82 \quad (8)$$

where Δn_β denotes the number of random coil segments that change to β -structure. The contribu-

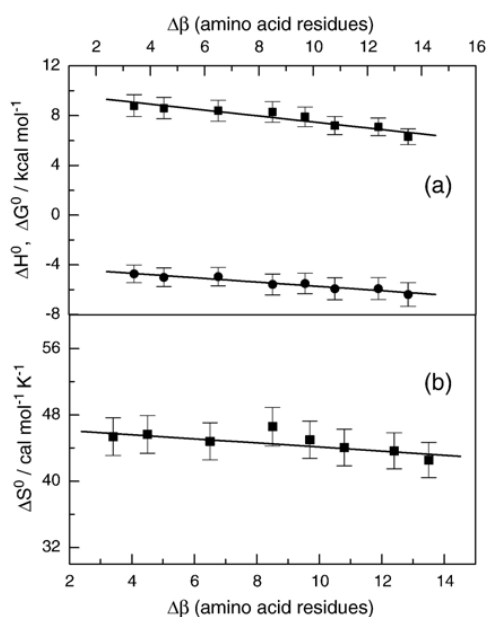


Figure 7. Variation of the thermodynamic parameters of peptide-lipid interaction with the extent of β -sheet formation of peptides 1–8. (a) Enthalpy ΔH^0 (■) and free energy ΔG^0 (●). (b) Entropy ΔS^0 . All data were recorded at 25 °C.

tion of β -structure formation to the binding process is thus given by the slopes of the regression lines:

$$\begin{aligned}\Delta H_{\beta} &= -0.23 \text{ kcal/mol per residue} \\ \Delta G_{\beta} &= -0.15 \text{ kcal/mol per residue} \\ \Delta S_{\beta} &= -0.24 \text{ cal/mol K per residue}\end{aligned}$$

From the intercepts with the ordinate, the thermodynamic binding parameters of a hypothetical (KIGAKI) $_3$ peptide with no conformational change can be estimated as:

$$\begin{aligned}\Delta H^0 &= 9.8 \text{ kcal/mol,} \\ \Delta G^0 &= -4.2 \text{ kcal/mol} \\ \Delta S^0 &= 46.5 \text{ cal/mol K}\end{aligned}$$

We have also measured the temperature dependence of ΔH^0 for the (KIGAKI) $_3$ peptide as $\Delta C_p^0 \approx -100$ cal/mol K.

Discussion

Structural aspects of membrane-peptide interactions

We have used the (KIGAKI) $_3$ peptide and its d,d analogues to obtain information on the thermodynamics of the random coil \rightleftharpoons β -structure transition at the membrane surface. Formation of β -structure

requires either a folding of the peptide chain onto itself or a lateral association of two or more peptides. Thermodynamics allows no distinction between these two processes. On the basis of the deuterium NMR spectra of deuterated (KIGAKI) $_3$ peptides, both possibilities appear to be realized in the present set of peptides. When bound to the membrane the all-L peptide 1 molecule exhibits a deuterium NMR spectrum characteristic of a solid powder, suggesting extensive lateral aggregation. On the other hand, peptide 9 with two d,d pairs gives rise to a sharp deuterium NMR resonance when bound to the lipid membrane. This result argues against the formation of solid-like aggregates. Small aggregates with internal mobility, however, cannot be excluded.

The deuterium and phosphorus NMR measurements provide no evidence that the (KIGAKI) $_3$ peptide changes the bilayer structure, or the conformation and orientation of the P-N^+ choline dipoles. The chemical shift anisotropy of the phosphate segment and the deuterium quadrupole splitting of the choline β -segment (POCH $_2$ CD $_2$ N) remain unchanged up to a lipid to peptide mol ratio of 40.

The quadrupole splitting of the β -segment in mixed POPC/POPG bilayers (3:1) is $\Delta\nu(\beta) = 3.6$ kHz. This is smaller than that observed in the absence of POPG, which is $\nu_Q \sim 5.9$ kHz and can be explained by the influence of the negative POPG charge on the P-N^+ dipole.⁴⁷ As only a single quadrupole splitting is observed, this requires a homogeneous distribution of anionic POPG molecules in the electrically neutral POPC matrix.

The quadrupole splitting in the presence of (KIGAKI) $_3$ peptide is almost identical with that in the absence of peptide with $\Delta\nu(\beta) = 3.3$ kHz. Again, a single quadrupole splitting is observed. This is possible only if the P-N^+ dipoles sense a similar surface charge as before. The POPG molecules hence remain distributed randomly in the lipid bilayer. A phase separation of the anionic lipids induced by the binding of cationic peptides can be excluded.

Thermodynamics of β -sheet formation

The peptides employed have the same sequence with respect to side-chain functionality and, in turn, similar intrinsic hydrophobicities. In water, they adopt a conformation that is mainly random coil, with about 30% β -structure. The percentage of β -structure is independent of the concentration of peptide up to 1 mM, arguing against an aggregation of the peptides in buffer solution. Binding of peptides 1–8 to negatively charged membranes increases the fraction of β -conformation and induces the formation of aggregates at the membrane surface.

The binding process is an endothermic reaction and makes an energetically unfavourable contribution to the binding process. This is in distinct contrast to the membrane binding of helix-forming peptides such as magainin^{23,24,34,48} and the mitochondrial signal sequence RDH,²⁵ which exhibit exothermic reactions of considerable magnitude. Binding of melittin and melittin analogues (E. Gonçalves and

J.S., unpublished results) to lipid bilayers entails reaction enthalpies between +4 kcal/mol and -4 kcal/mol, depending on temperature.³⁰

The free energy of binding, however, is negative for β -structure as well as for α -helix formation, and contains two contributions: (i) the electrostatic attraction to the membrane surface; and (ii) the binding step proper driven by hydrophobic and hydrogen bonding interactions and aggregation. As the membrane is negatively charged, the concentration of the cationic peptide is larger at the membrane surface (c_M) than in bulk solution (c_f) and the electrostatic contribution to the free energy, ΔG_{el} , is given by:

$$\Delta G_{el} = -RT \ln(c_M/c_f) \quad (9)$$

The hydrophobic/hydrogen bonding part of the free energy is more important in the present context, as it includes the energy change of the conformational transition from random coil to β -sheet. It is given by:

$$\Delta G^0 = -RT \ln 55.5 K_0 \quad (10)$$

where the factor 55.5 corrects for the cratic contribution. K_0 can be determined from the ITC binding isotherms, using the Gouy-Chapman theory to eliminate electrostatic effects.^{24,39} K_0 is independent of salt concentration, peptide concentration, and membrane surface charge, provided the structure of the membrane remains unchanged.

Table 2 summarizes the binding constants K_0 , the effective charge z_p , and the free energy ΔG^0 , calculated from K_0 . The charge z_p was determined to yield an optimum fit to the individual ITC curves and varies between 4.0 and 4.9. However, it is equally possible to analyse all ITC curves with a common average electric charge of $z_p=4.5$ for all eight peptides. The numerical results are not essentially different from those presented in Table 2. The binding constants shown in Table 2 fall in the range of 50–890 M^{-1} and are thus relatively weak. The change in free energy, ΔG^0 , is of the order of -4.7 to -6.4 kcal/mol.

The electrostatic energy must be added to the chemical adsorption process. ΔG_{el} varies continuously during an ITC titration requiring a point-by-point correction of the ITC curve. The surface potential of a POPC/POPG (3:1 mol%) membrane in 50 mM NaCl plus 25 mM Tris and in the absence of peptide is $\psi_0=-45$ mV. If the peptide concentration is 10 μM in bulk solution, the surface concentration is $c_M \sim 68 \mu M$ for peptide 1. The corresponding electrostatic energy thus amounts to $\Delta G_{el}=-1.16$ kcal/mol. At the same time, the surface potential is reduced to $\psi_0=-13$ mV due to neutralization of the membrane charge by peptide adsorption. For less concentrated peptide solutions, the electric energy, ΔG_{el} , is higher.

Membrane-induced β -structure versus α -helix formation

We may now compare the β -structure formation of (KIGAKI)₃ with the corresponding membrane-

induced α -helix formation of magainin and related amphipathic peptides.²³ From the slope of the ΔG^0 line in Figure 7, we deduce that the incremental change in the free energy for β -structure formation of (KIGAKI)₃ is $\Delta G_{\beta}=-0.15$ kcal/mol per amino acid residue. Almost the same value, $\Delta G_{helix}=-0.14$ kcal/mol per residue, has been reported for the helix formation of magainin 2 amide on the membrane surface.²³ The numerical agreement is probably accidental, as other amphipathic peptides such as the mitochondrial signal peptide RDH and melittin display ΔG_{helix} values in the range of -0.2 to -0.4 kcal/mol per residue.^{22,25} Nevertheless, the comparison illustrates two different aspects. First, induction of β -structure and helix formation appear to involve very similar free energies. This is not surprising, as both processes entail the formation of H bonds, be it intra- or intermolecular. Secondly, though energetically favourable, the change in free energy, ΔG_{β} , from random coil to β -structure is small and can be reversed easily. On the other hand, if a longer stretch of peptide is involved and the segmental contributions accumulate cooperatively, the interaction with the membrane can produce a more stable conformational change.

A similar comparison can be made for the reaction enthalpy ΔH^0 . From the slope of the ΔH^0 line in Figure 7 one finds $\Delta H_{\beta}=-0.23$ kcal/mol per residue, which is smaller by a factor of 3 than $\Delta H_{helix}=-0.78$ kcal/mol per residue for magainin 2 amide. As an immediate consequence, it follows that both secondary structures are destabilized at higher temperatures but that this effect is less pronounced for the β -sheet conformation than for the α -helix.

An even larger difference is found for the segmental entropy which is $\Delta S_{helix} \approx -1.9$ cal/mol K per residue for α -helix formation but only $\Delta S_{\beta}=-0.25$ cal/mol K for β -sheet structure. It can be speculated that α -helix formation imposes more drastic steric constraints on distances and bond angles than a loosely packed β -sheet.

The intercepts of the straight lines in Figure 7 provide the binding thermodynamics of a hypothetical (KIGAGKI)₃ peptide that binds to the membrane surface without a conformational change. As the binding enthalpy is endothermic, with $\Delta H_0=9.8$ kcal/mol, the driving force for the association with the membrane is the entropic contribution with $\Delta S_0=47$ cal/mol K. This result is quite different from data reported for a (hypothetical) random coil magainin 2 amide, where the enthalpy is favourable with $\Delta H_0=-4.7$ kcal/mol and is counteracted by a negative entropy term. The thermodynamic difference between the two types of peptides probably arises from the fact that (KIGAKI)₃ aggregates at the membrane surface, while magainin 2 amide binds as a monomer. Lateral association itself will reduce the entropy due to motional restrictions. The large positive entropy term must then arise from the release of hydration water.

Membrane-induced β -sheet formation has been investigated with a hydrophobic hexapeptide acetyl-Trp-Leu₅.²⁹ The mechanism of β -sheet formation is,

however, different from that observed for the charged (KIGAKI)₃ peptide. As AcWL₅ is hydrophobic, it partitions as a monomer from the aqueous phase into the hydrophobic part of the bilayer, where it assembles cooperatively into β -sheet aggregates containing 10–20 monomers. At about 60 °C the aggregates undergo a relatively sharp and reversible unfolding to random coil monomers. Using equilibrium dialysis and spectroscopic methods, β -sheet formation could be analyzed quantitatively and described by a cooperative model. The free energy change per residue was calculated for two different membranes to be in the range of –0.46 kcal/mol to –0.61 kcal/mol per residue.²⁹ These values are larger than those observed here for the (KIGAKI)₃ peptides. However, AcWL₅ penetrates deeply into the membrane, while (KIGAKI)₃ remains adsorbed in the lipid–water interface.

Using ITC and differential scanning calorimetry, the partitioning of AcWL₅ monomers into the lipid membrane as well as the thermal unfolding of the β -sheet aggregates in the membrane were investigated.³⁰ Membrane partitioning is associated with an enthalpy close to zero, while the enthalpy of unfolding is estimated as 1.3 kcal/mol per residue. The corresponding process of peptide folding thus has $\Delta H_{\beta} = -1.3$ kcal/mol and is again distinctly larger than the value of –0.23 kcal/mol observed for the (KIGAKI)₃ peptide. The differences demonstrate the influence of the solvent on the physical parameters of the random coil \rightleftharpoons β -structure transition.

A related example without the involvement of a lipid membrane is the β -hairpin formation of the G-peptide, a short linear peptide consisting of only 16 amino acid residues. It folds into a β -hairpin structure in water and the unfolding process was investigated with NMR and differential scanning calorimetry.⁴⁹ A heat of unfolding of $\Delta H = 12.2$ kcal/mol was derived from the differential scanning calorimetry experiments. If all amino acids are involved in β -hairpin formation, this leads to $\Delta H_{\beta} = -0.76$ kcal/mol per residue for the folding process. The above examples demonstrate that a large variability exists for the enthalpy of β -sheet formation. This is in contrast to α -helix formation, which is always associated with $\Delta H_{\text{helix}} \sim -0.7$ to –1.1 kcal/mol.

The (KIGAKI)₃ model peptide was developed primarily as a new antimicrobial peptide.³⁴ However, the formation of β -structure when bound to membranes makes it a model compound for other amyloid-forming peptides such as the Alzheimer peptides. The Alzheimer peptide A β (1–40) undergoes a two-state random coil \rightleftharpoons β -structure transition when titrated with anionic lipid vesicles.^{31–33} Like (KIGAKI)₃ the A β (1–40) molecule does not penetrate into the lipid membrane, at least when added from the aqueous phase. ITC experiments at ambient temperature reveal an exothermic binding reaction. However, the quantitative analysis of this process is difficult because: (i) A β (1–40) aggregates in solution even without lipid; and (ii) because the random coil \rightleftharpoons β -structure transition in the mem-

brane is followed by a β -structure \rightleftharpoons α -helix transition at high lipid-to-protein ratios. Knowledge of the thermodynamics of the (KIGAKI)₃ reaction is helpful in unravelling the more complex A β membrane interaction.

A number of conclusions can be drawn from the present studies that may be of interest in other areas. First, the enthalpy for β -structure formation, ΔH_{β} , shows a greater variability than that of α -helix formation. The influence of the environment (membrane surface, membrane interior, or aqueous solution) appears to have an important role. Secondly, comparing ΔS_{β} of (KIGAKI)₃ and ΔS_{helix} of magainin 2 amide, the reduction in entropy is much less for β -structure formation. Finally, the method of multiple d,d substitutions appears to be a general approach to study the conformational and thermodynamic properties of other amyloid-forming peptides. A corresponding study on Alzheimer peptide A β (1–40) is in progress.

Material and Methods

1-Palmitoyl-2-oleoyl-*sn*-glycero-3-phosphocholine (POPC), 1-palmitoyl-2-oleoyl-*sn*-glycero-3-phosphoethanolamine (POPE), 1-palmitoyl-2-oleoyl-*sn*-glycero-3-phosphoglycerol (POPG), and 1,2-dioleoyl-*sn*-glycero-3-phosphoethanolamine-*N*[methoxy(polyethylene glycol)-2000] (mPEG 2000 PE) were purchased from Avanti Polar Lipids (Alabaster, AL). All other chemicals were purchased from commercial sources at the highest purity available.

All peptides were synthesized using Fmoc (*N*-(9-fluorenyl)methoxycarbonyl) chemistry on an Applied Biosystems model 433A peptide synthesizer. The crude peptides were purified by reverse phase HPLC. Purity was assessed by HPLC and mass spectrometry. The concentration of peptide in all experiments was determined by measuring the absorbance at 280 nm ($\epsilon = 5500 \text{ M}^{-1} \text{ cm}^{-1}$) as the N-terminal repeat contained Trp2 instead of Ile2.

Preparation of lipid vesicles

Small unilamellar vesicles (SUVs) of ~30 nm diameter were prepared as follows. Defined amounts of lipid were dissolved in chloroform and were dried first with a stream of N₂ and then over night *in vacuo*. For ternary lipid mixtures, the second and third lipid in chloroform were added to the dried film and the mixed solution was treated as before. Subsequently, buffer solution was added to the lipid film and the mixture was vortex mixed extensively. Next, the lipid dispersion was sonicated with a G112SP1 Special Ultrasonic Cleaner (Laboratory Supplies CO., Inc.) until an opalescent solution was obtained.

For CD spectroscopy and ITC, we used SUVs with 5 mol % mPEG 2000 PE. Incorporation of mPEG 2000 PE into SUVs was crucial, because binding of the polycationic (KIGAKI)₃ peptide to negatively charged lipids leads to charge neutralization with concomitant formation of large aggregates. Aggregation produces a noisy ITC baseline and causes extensive light-scattering in CD spectroscopy. The inclusion of grafted hydrophilic polymers, such as PEG chains, into phospholipid vesicles prevented vesicle aggregation without influencing peptide–lipid binding. The vesicle composition was POPE/POPG/mPEG 2000

PE at molar ratios 70:25:5 for ITC and 45:50:5 for CD spectroscopy. mPEG 2000 PE is negatively charged as the amino group is no longer protonated.

NMR measurements

All NMR experiments were performed on a Bruker Avance 400 MHz spectrometer. Deuterium NMR spectra (^2H -NMR) were recorded at 64 MHz with the quadrupole echo technique with full-phase cycling. ^{31}P -NMR spectra were recorded at 161 MHz using a Hahn echo sequence with broadband proton decoupling (WALTZ-16). The chemical shielding anisotropy, $\Delta\sigma$, was measured as full width at 10% maximum intensity.

Peptides observed by deuterium NMR were labelled with Ala- d_3 ($\text{HC}_\alpha\text{-C}_\beta^2\text{H}_3$) at amino acid position 9. About 3 mg of the lyophilized peptides was used for the ^2H -NMR powder spectra. To obtain ^2H -NMR spectra of peptides bound to non-oriented multilamellar vesicles, a defined amount of lipid was transferred into an NMR sample tube (typically 50 mg of lipid), and buffer solution was added to achieve a predefined water/lipid ratio of 2:1 (v/w). For all NMR samples, we used a POPC/POPG molar ratio of 75:25 and 25 mM Tris-HCl (pH 7.4), 50 mM NaCl as buffer. In order to achieve a homogenous suspension, the sample was vortex mixed extensively at room temperature, followed by several freeze-thaw cycles and further vortex mixing. The lyophilized peptide was added in 0.2 mg steps in small volumes of buffer. After peptide addition, the sample was again vortex mixed extensively between at least five freeze-thaw cycles. The procedure was repeated until the final lipid/peptide ratio was achieved.

Isothermal titration calorimetry (ITC)

ITC was performed on a VP ITC instrument (Microcal, Northampton, MA). Unless noted otherwise, all measurements were made at 25 °C in 25 mM Tris-HCl (pH 7.4), 50 mM NaCl. Buffer solutions were freshly prepared. The sample cell contained the peptide solution at a concentration of, typically, 25 μM . Lipid vesicles were suspended in the same buffer as the peptide (~12–15 mM lipid) and 10 μl was injected into the peptide solution every 5 min *via* a 300 μl syringe. As a control, lipid vesicles were injected into pure buffer containing no peptide.

Circular dichroism spectroscopy (CD)

CD measurements were performed on a Jasco J-720 spectropolarimeter. Spectra were recorded from 250 nm to 197 nm at room temperature, with resolution of 0.5 nm, a response time of 2 s, a bandwidth of 1 nm, a scan speed of 20 nm/min and six accumulations. CD samples were prepared by adjusting the peptide concentration to 50 μM in 2.5 mM cacodylate buffer at pH 7.4, and by subsequently adding aliquots of POPE/POPG/mPEG 2000 PE (45/50/5) SUVs suspended in the same buffer, to the peptide solution. A blank of pure buffer solution was subtracted from all samples.

Evaluation of CD spectra of peptides containing D-amino acids

Figure 5 shows the titration of peptide 1 with anionic lipid vesicles. An isosbestic point is observed at 209 nm,

providing evidence for a two-state equilibrium. The analysis yields the following composition of ellipticity:

$$\epsilon_{\text{buffer}}^{\text{pep-1}} = 0.77\epsilon_{\text{rc}} + 0.23\epsilon_{\beta} \equiv C_{\text{buffer}} \quad \text{lipid/peptide} = 0 \quad (11)$$

$$\epsilon_{\text{buffer}}^{\text{pep-1}} = 0.22\epsilon_{\text{rc}} + 0.98\epsilon_{\beta} \equiv C_{\text{buffer}} \quad \text{lipid/peptide} = 10 \quad (12)$$

where $\epsilon_{\text{rc}}(\epsilon_{\beta})$ is the ellipticity of the pure random coil (β -sheet) spectrum at a given wavelength. Peptide 1 in buffer has a spectrum that is 77% random coil and 23% β -structure.

All intermediate spectra can be simulated by a superposition of these two spectra. The observed conformation C_i can be described as:

$$C_i = f_{i,\text{buffer}}C_{\text{buffer}} + f_{i,\text{lipid}}C_{\text{lipid}} = f_{i,\text{buffer}}C_{\text{buffer}} + (1 - f_{i,\text{buffer}})C_{\text{lipid}}$$

$$C_i = f_{i,\text{buffer}}(C_{\text{buffer}} - C_{\text{lipid}}) + C_{\text{buffer}} \quad (13)$$

Here, f_{buffer} is the fraction of the initial spectrum at lipid/peptide=0 and $f_{\text{lipid}}=1-f_{\text{buffer}}$ is the spectral contribution of the peptide bound to lipid (lipid/peptide=10).

By combining equations (11)–(13) it is possible to evaluate the random coil and β -content of all intermediate spectra shown in Figure 5.

Figure 8(a) displays the CD spectra of peptide 2 in buffer and in excess lipids. The continuous lines represent the corresponding spectra of peptide 1 but at a reduced ellipticity of 78% and an almost perfect agreement is obtained.

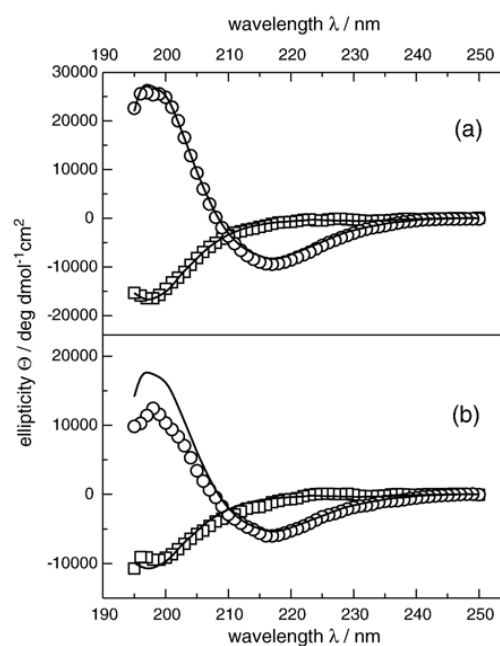


Figure 8. Comparison of experimental and calculated CD spectra of peptides containing D-amino acids. (a) Peptide 2 with one d,d pair: (□) peptide in buffer solution; (○) peptide bound to lipid. The continuous lines are the corresponding spectra of the all-L peptide 1 but with a reduced intensity of 78% (theory 78%). (b) Peptide 7 with two d,d pairs: (□) peptide in buffer solution; (○) peptide with excess lipid. The continuous lines correspond to the spectra of peptide 1 with 56% intensity (theory 56%).

A quantitative explanation of this result can be given as follows. If peptide 1 is synthesized from all-D amino acids, the corresponding CD spectra without and with lipid would be mirror images of those shown in Figure 5 (mirrored at the x -axis), that is:

$$\varepsilon_D(\lambda) = -\varepsilon_L(\lambda)$$

Considering the peptide in buffer, the conformation is essentially unstructured (random coil). The observed ellipticity can be predicted as:

$$\begin{aligned} \varepsilon_{\text{obs}} &= X_D \varepsilon_D(\lambda) + X_L \varepsilon_L(\lambda) \\ &= (1 - X_L)(-\varepsilon_L(\lambda)) + X_L \varepsilon_L(\lambda) \\ &= -2X_L \varepsilon_L + \varepsilon_L = \varepsilon_L(2X_L - 1) \end{aligned} \quad (14)$$

X_D and X_L are the mole fractions of the D and L-amino acids. Peptide 2 with a total length of 18 residues contains two D-amino acids (11%) and this simple model predicts $\varepsilon_{\text{obs}} = 0.78 \varepsilon_L$, in agreement with the experiment. For an essentially random coil conformation, this result can perhaps be anticipated, as each amino acid contributes its CD increment (L or D) to the non-structured peptide. However, it is surprising that the same model leads to the correct prediction of peptide 2 bound to the lipid membrane. This means that the D-amino acids in the β -conformation of peptide 2 make the same contribution to the spectrum as if they were incorporated into an all-D peptide 1 molecule.

A further reduction of intensity occurs if two d,d pairs (peptides 5–7) or three d,d pairs (peptide 8) are incorporated. Equation (14) then predicts only 56% and 33% intensity compared to peptide 1. For the peptide spectra in buffer, this prediction is only approximately fulfilled (Figure 4(a)). The deviations of the experimental results from the theoretical spectra are significant, however, and cannot be ignored. They must be traced back to changes in the conformation. An optimal fit is obtained by first reducing the intensity of the basic spectra of peptide 1 (Figure 1) according to the D-amino acid fraction and, secondly, by mixing the reduced basic spectra. Figure 8(b) shows the optimal fit for peptide 7 with and without lipid. The continuous lines correspond to 50% intensity (theoretical value 56%) of the CD spectra of the all-L peptide 1. It is possible to calculate the random coil and β -structure content for all spectra by this method. The results are summarized in Table 3 and discussed above.

Acknowledgements

This work was supported by the Swiss National Science Foundation grant no. 3100–107793.

References

- Kuznetsov, S. V., Hilario, J., Keiderling, T. A. & Ansari, A. (2003). Spectroscopic studies of structural changes in two beta-sheet-forming peptides show an ensemble of structures that unfold noncooperatively. *Biochemistry*, **42**, 4321–4332.
- Kim, C. A. & Berg, J. M. (1993). Thermodynamic beta-sheet propensities measured using a zinc-finger host peptide. *Nature*, **362**, 267–270.
- Ramirez-Alvarado, M., Blanco, F. J. & Serrano, L. (1996). De novo design and structural analysis of a model beta-hairpin peptide system. *Nature Struct. Biol.* **3**, 604–612.
- Smith, C. K., Withka, J. M. & Regan, L. (1994). A thermodynamic scale for the beta-sheet forming tendencies of the amino acids. *Biochemistry*, **33**, 5510–5517.
- Maynard, A. J., Sharman, G. J. & Searle, M. S. (1998). Origin of β -hairpin stability in solution: Structural and thermodynamic analysis of the folding of model peptide supports hydrophobic stabilization in water. *J. Am. Chem. Soc.* **120**, 1996–2007.
- Constantine, K. L., Mueller, L., Andersen, N., Tong, H., Wandler, C. F., Friedrichs, M. S. & Brucoleri, R. E. (1995). Structural and dynamic properties of a β -hairpin-forming linear peptide. 1. Modeling using ensemble-averaged constraints. *J. Am. Chem. Soc.* **117**, 10841–10854.
- Hutchinson, E. G., Sessions, R. B., Thornton, J. M. & Woolfson, D. N. (1998). Determinants of strand register in antiparallel beta-sheets of proteins. *Protein Sci.* **7**, 2287–2300.
- Searle, M. S., Zerella, R., Williams, D. H. & Packman, L. C. (1996). Native-like beta-hairpin structure in an isolated fragment from ferredoxin: NMR and CD studies of solvent effects on the N-terminal 20 residues. *Protein Eng.* **9**, 559–565.
- Pederson, D., Gabriel, D. & Hermans, J., Jr (1971). Potentiometric titration of poly-L-lysine: the coil-to-beta transition. *Biopolymers*, **10**, 2133–2145.
- Auer, H. E. & McKnight, R. P. (1978). Two classes of beta-pleated-sheet conformation in poly(L-tyrosine): a model for tertiary structure in native proteins. *Biochemistry*, **17**, 2798–2805.
- Nakaishi, A., Maeda, H., Tomiyama, T., Ikeda, S., Kobayashi, Y. & Kyogoku, Y. (1988). Chain-length dependence of solubility of monodisperse polypeptides in aqueous-solutions and the stability of the β -structure. *J. Phys. Chem.* **92**, 6161–6166.
- Blanco, F. J., Rivas, G. & Serrano, L. (1994). A short linear peptide that folds into a native stable beta-hairpin in aqueous solution. *Nature Struct. Biol.* **1**, 584–590.
- Searle, M. S., Williams, D. H. & Packman, L. C. (1995). A short linear peptide derived from the N-terminal sequence of ubiquitin folds into a water-stable non-native beta-hairpin. *Nature Struct. Biol.* **2**, 999–1006.
- Gellman, S. H. (1998). Minimal model systems for beta sheet secondary structure in proteins. *Curr. Opin. Chem. Biol.* **2**, 717–725.
- Chen, H. I., Einbond, A., Kwak, S. J., Linn, H., Koepf, E., Peterson, S. *et al.* (1997). Characterization of the WW domain of human yes-associated protein and its polyproline-containing ligands. *J. Biol. Chem.* **272**, 17070–17077.
- Wang, M., Wales, T. E. & Fitzgerald, M. C. (2006). Conserved thermodynamic contributions of backbone hydrogen bonds in a protein fold. *Proc. Natl Acad. Sci. USA*, **103**, 2600–2604.
- Munoz, V., Ghirlando, R., Blanco, F. J., Jas, G. S., Hofrichter, J. & Eaton, W. A. (2006). Folding and aggregation kinetics of a beta-hairpin. *Biochemistry*, **45**, 7023–7035.
- Deechongkit, S., Nguyen, H., Powers, E. T., Dawson, P. E., Gruebele, M. & Kelly, J. W. (2004). Context-dependent contributions of backbone hydrogen bonding to beta-sheet folding energetics. *Nature*, **430**, 101–105.
- Ciani, B., Jourdan, M. & Searle, M. S. (2003). Stabilization of beta-hairpin peptides by salt bridges: role of preorganization in the energetic contribution of weak interactions. *J. Am. Chem. Soc.* **125**, 9038–9047.

20. Streicher, W. W. & Makhatadze, G. I. (2006). Calorimetric evidence for a two-state unfolding of the beta-hairpin peptide trpzip4. *J. Am. Chem. Soc.* **128**, 30–31.
21. Munoz, V., Thompson, P. A., Hofrichter, J. & Eaton, W. A. (1997). Folding dynamics and mechanism of beta-hairpin formation. *Nature*, **390**, 196–199.
22. Ladokhin, A. S. & White, S. H. (1999). Folding of amphipathic alpha-helices on membranes: energetics of helix formation by melittin. *J. Mol. Biol.* **285**, 1363–1369.
23. Wieprecht, T., Apostolov, O., Beyermann, M. & Seelig, J. (1999). Thermodynamics of the alpha-helix-coil transition of amphipathic peptides in a membrane environment: implications for the peptide-membrane binding equilibrium. *J. Mol. Biol.* **294**, 785–794.
24. Wenk, M. R. & Seelig, J. (1998). Magainin 2 amide interaction with lipid membranes: calorimetric detection of peptide binding and pore formation. *Biochemistry*, **37**, 3909–3916.
25. Wieprecht, T., Apostolov, O., Beyermann, M. & Seelig, J. (2000). Interaction of a mitochondrial presequence with lipid membranes: role of helix formation for membrane binding and perturbation. *Biochemistry*, **39**, 15297–15305.
26. Wieprecht, T., Beyermann, M. & Seelig, J. (2002). Thermodynamics of the coil-alpha-helix transition of amphipathic peptides in a membrane environment: the role of vesicle curvature. *Biophys. Chem.* **96**, 191–201.
27. Li, Y., Han, X. & Tamm, L. K. (2003). Thermodynamics of fusion peptide-membrane interactions. *Biochemistry*, **42**, 7245–7251.
28. Bishop, C. M., Walkenhorst, W. F. & Wimley, W. C. (2001). Folding of beta-sheets in membranes: specificity and promiscuity in peptide model systems. *J. Mol. Biol.* **309**, 975–988.
29. Wimley, W. C., Hristova, K., Ladokhin, A. S., Silvestro, L., Axelsen, P. H. & White, S. H. (1998). Folding of beta-sheet membrane proteins: a hydrophobic hexapeptide model. *J. Mol. Biol.* **277**, 1091–1110.
30. Wimley, W. C. & White, S. H. (2004). Reversible unfolding of beta-sheets in membranes: a calorimetric study. *J. Mol. Biol.* **342**, 703–711.
31. Terzi, E., Holzemann, G. & Seelig, J. (1994). Alzheimer beta-amyloid peptide 25–35: electrostatic interactions with phospholipid membranes. *Biochemistry*, **33**, 7434–7441.
32. Terzi, E., Holzemann, G. & Seelig, J. (1995). Self-association of beta-amyloid peptide (1–40) in solution and binding to lipid membranes. *J. Mol. Biol.* **252**, 633–642.
33. Terzi, E., Hölzemann, G. & Seelig, J. (1997). Interaction of Alzheimer beta-amyloid peptide(1–40) with lipid membranes. *Biochemistry*, **36**, 14845–14852.
34. Blazyk, J., Wiegand, R., Klein, J., Hammer, J., Epanand, R. M., Epanand, R. F. *et al.* (2001). A novel linear amphipathic beta-sheet cationic antimicrobial peptide with enhanced selectivity for bacterial lipids. *J. Biol. Chem.* **276**, 27899–27906.
35. Wieprecht, T., Dathe, M., Schumann, M., Krause, E., Beyermann, M. & Bienert, M. (1996). Conformational and functional study of magainin 2 in model membrane environments using the new approach of systematic double-D-amino acid replacement. *Biochemistry*, **35**, 10844–10853.
36. Janek, K., Rothmund, S., Gast, K., Beyermann, M., Zipper, J., Fabian, H. *et al.* (2001). Study of the conformational transition of A beta(1–42) using D-amino acid replacement analogues. *Biochemistry*, **40**, 5457–5463.
37. Rothmund, S., Beyermann, M., Krause, E., Krause, G., Bienert, M., Hodges, R. S. *et al.* (1995). Structure effects of double D-amino acid replacements: a nuclear magnetic resonance and circular dichroism study using amphipathic model helices. *Biochemistry*, **34**, 12954–12962.
38. Seelig, J. (1997). Titration calorimetry of lipid-peptide interactions. *Biochim. Biophys. Acta*, **1331**, 103–116.
39. Seelig, J., Nebel, S., Ganz, P. & Bruns, C. (1993). Electrostatic and nonpolar peptide-membrane interactions. Lipid binding and functional properties of somatostatin analogues of charge $z = +1$ to $z = +3$. *Biochemistry*, **32**, 9714–9721.
40. Aveyard, R. & Haydon, D. A. (1973). *An Introduction to the Principles of Surface Chemistry*. Cambridge University Press, London.
41. McLaughlin, S. (1977). Electrostatic potentials at membrane-solution interfaces. *Curr. Top. Membr. Transport*, **71**–144.
42. Lu, J. X., Damodaran, K., Blazyk, J. & Lorigan, G. A. (2005). Solid-state nuclear magnetic resonance relaxation studies of the interaction mechanism of antimicrobial peptides with phospholipid bilayer membranes. *Biochemistry*, **44**, 10208–10217.
43. Gally, H. U., Niederberger, W. & Seelig, J. (1975). Conformation and motion of the choline head group in bilayers of dipalmitoyl-3-sn-phosphatidylcholine. *Biochemistry*, **14**, 3647–3652.
44. Seelig, J., Macdonald, P. M. & Scherer, P. G. (1987). Phospholipid head groups as sensors of electric charge in membranes. *Biochemistry*, **26**, 7535–7541.
45. Kuchinka, E. & Seelig, J. (1989). Interaction of melittin with phosphatidylcholine membranes. Binding isotherm and lipid head-group conformation. *Biochemistry*, **28**, 4216–4221.
46. Matsuzaki, K. & Seelig, J. (1995). NMR study on interactions of an antibiotic peptide, magainin-2, with lipid bilayers. In *Peptide Chemistry 1994* (Ohno, N., ed.), pp. 129–132, Protein Research Foundation, Osaka.
47. Scherer, P. G. & Seelig, J. (1987). Structure and dynamics of the phosphatidylcholine and the phosphatidylethanolamine head group in L-M fibroblasts as studied by deuterium nuclear magnetic resonance. *EMBO J.* **6**, 2915–2922.
48. Wieprecht, T., Beyermann, M. & Seelig, J. (1999). Binding of antibacterial magainin peptides to electrically neutral membranes: thermodynamics and structure. *Biochemistry*, **38**, 10377–10387.
49. Honda, S., Kobayashi, N. & Munekata, E. (2000). Thermodynamics of a beta-hairpin structure: evidence for cooperative formation of folding nucleus. *J. Mol. Biol.* **295**, 269–278.

Edited by J. E. Ladbury

(Received 29 November 2006; received in revised form 21 February 2007; accepted 22 February 2007)

5. Length dependence of the Coil \rightleftharpoons β -sheet Transition in a membrane environment

M. Meier and J. Seelig

Department of Biophysical Chemistry, Biozentrum, University of Basel,

Klingelbergstrasse 50/70, CH-4056 Basel, Switzerland

Tel: +41-61-267 2190, Fax: +41-61-267 2189, e-mail: joachim.seelig@unibas.ch

5.1 – Summary: Length dependence of the Coil \rightleftharpoons β -Sheet Transition in a Membrane Environment

In the previous chapter we determined the thermodynamic parameters for the β -sheet folding reaction of the (KIGAKI)₃ peptide in a membrane environment. In the following we investigate the difference between the β -sheet folding reaction in a native and aggregated protein.

To this purpose we increase the length of the β -sheet forming (KIGAKI)₃ peptide by one and two KIGAKI repeats or we shorten it to a total length of 12, 10, 8, or 7 amino acids residues. The thermodynamic overall binding parameters, which combines the folding and binding process, were determined by ITC for all peptides. Structural changes upon binding to lipid vesicles were monitored by CD spectroscopy. For peptides with one KIGAKI repeat longer and shorter than (KIGAKI)₃ we applied the double D amino acid substitution strategy to divide the overall binding reaction contributions from β -sheet folding and the binding process proper. A length-dependence of the β -sheet folding and binding reaction can be deduced from the thermodynamic parameters measured for (KIGAKI)₂, (KIGAKI)₃, and (KIGAKI)₄. Upon extending the length of the β -sheet the thermodynamic driving forces changed dramatically. For β -sheets shorter than 10 residues the folding reaction is driven by entropy, whereas for longer β -sheets the folding reaction is driven by enthalpy. Considering that β -strands in proteins are statistically 2 to 6 residues in length and current models of β -sheet in protein aggregates, i.e. amyloid fibrils, predict a length of at least 10 residues, our results may explain a fundamental thermodynamic difference in the folding reaction of the two β -sheet folds. We further demonstrate that the stability of the β -sheet folds increases only slightly upon lengthening the β -sheet and that cooperativity effects are rather small compared to the random coil to α -helices transition. The present findings provide evidence that small changes of pH or temperature can have a profound effect on the β -sheet aggregation reaction.

In addition to the length-dependence of the β -sheet folding reaction we also studied the binding of the polycationic peptides to anionic membrane surfaces. Binding of the peptides is mainly driven by electrostatic interactions, although hydrophobic and dehydration effects also play a role. Finally, we show thermodynamic parameters derived

for the three peptides discussed above to shorter or longer chain length explains the experimental data observed for KIGAKI peptides with chain length of 8, 10 and 30 residues.

5.2 – Manuscript: Length dependence of the Coil \rightleftharpoons β -Sheet Transition in a Membrane Environment

Introduction

β -sheet folds in proteins are typically 2 to 6 residues in length, with few longer than 12 residues^{1, 2}. In comparison to α -helices which on the average have 7-20 residues^{3, 4}, β -sheet structures tend to be distinctively shorter. Interestingly, current models of β -sheets in non-native protein structures, i.e. amyloid fibrils, are about 10 residues in length⁵⁻⁷. Length stabilization is well known for the α -helix^{8, 9}, but is still controversial for the β -sheet structure. Isolated helices become more stable as the length of the α -helix increases. However, a more complex situation is encountered in the case of β -sheets since two orthogonal dimensions must be considered for β -sheet stabilization¹⁰, namely along and perpendicular to the strands. A closer insight into stabilization forces of β -sheets is obtained from small model peptides forming β -hairpins, that is a two-stranded antiparallel β -sheet, ^{7, 10}. In such model peptides the length dependence of the β -sheet stability has been examined in both dimensions. Extension of the β -sheet structure perpendicular to the strand has been shown to gradually stabilize the β -sheet ¹¹⁻¹³, whereas a discontinuous effect was found upon strand lengthening along the peptide axis. It has been suggested that β -sheet stability may not increase beyond seven to nine residues¹⁴.

The thermodynamic analysis of β -sheet formation in aqueous solution is hampered by the low solubility of the specific peptides in water. Chain extension usually reduces the solubility even further. Both β -sheet formation and peptide solubility are, however, increased in hydrophobic environments such as organic solvents and lipid membranes¹⁵.

Few experimental studies on the stabilization of a β -sheet fold in a membrane environment are available to date. We have recently determined the thermodynamic parameters of the membrane-induced random coil \rightleftharpoons β -sheet folding reaction of the (KIGAKI)₃ peptide using isothermal titration calorimetry (ITC)¹⁶. ITC data were obtained for the binding of the (KIGAKI)₃ peptide to anionic lipid vesicles. The thermodynamic data are the result of two processes, namely the transfer of the peptide from the aqueous phase to the lipid surface, $\Delta G_{\text{Binding}}$, and the conformational change of the peptide from a random coil conformation to a β -sheet structure, $\Delta G_{\text{Folding}}$. The contribution of the folding reaction to the overall process was determined with analogs of the KIGAKI repeat, in which two adjacent amino acids were replaced by their D-enantiomers. Substitution of L amino acids by their D enantiomers led to a local disturbance of the β -sheet structure^{17, 18}, the extent of which was dependent on the number and position of the D amino acid substitutions. The extent of β -sheet formation on the surface of negatively charged membranes was measured with circular dichroism (CD) spectroscopy. By correlating the thermodynamic parameters with the percentage of β -sheet formation of peptides with and without D-amino acids it was possible to separate the binding thermodynamics from the process of β -sheet formation.

In the present study we were interested in the influence of the peptide chain length on the thermodynamic parameters of β -sheet formation. To this purpose we increased the length

of the (KIGAKI)₃ peptide by one and two KIGAKI repeats or shortened the peptide to 12, 10, 8, or 7 amino acid residues. The thermodynamic binding parameters and structural changes of all peptides were determined with ITC and circular dichroism spectroscopy, respectively. By comparing the different peptides distinct differences were observed between short ($n \leq 12$) and long peptides ($12 < n \leq 30$).

Materials and Methods

1-Palmitoyl-2-oleoyl-*sn*-glycero-3-phosphoethanolamine (POPE), 1-palmitoyl-2-oleoyl-*sn*-glycero-3-phosphoglycerol (POPG), and 1,2-dioleoyl-*sn*-glycero-3-phosphoethanolamine-N-[methoxy (polyethylene glycol)-2000] (mPEG 2000 POPE) were purchased from Avanti Polar Lipids (Alabaster, AL). All other chemicals were purchased at highest purity from various sources.

All peptides were synthesized using the Fmoc (N-(9-fluorenyl)methoxycarbonyl) chemistry on an Applied Biosystems model 433A peptide synthesizer. The crude peptides were purified by reverse phase high performance liquid chromatography (HPLC). Purity was proven by HPLC and mass spectrometry. Peptide concentration in all experiments was determined by absorbance at 280 nm using an extinction coefficient of $\epsilon = 5500 \text{ M}^{-1} \text{ cm}^{-1}$ for Trp.

Preparation of Lipid Vesicles

Small unilamellar vesicles (SUV) of ~30 nm diameter were prepared as follows. Defined amounts of lipid were dissolved in chloroform and were dried first with a stream of N₂ and then over night under high vacuum. The second and third lipid for the ternary lipid

mixtures was added to the dried film in chloroform solution and treated as before. Subsequently, buffer solution was added to the lipid film and the mixture was vortexed extensively. The lipid dispersion was sonicated with a G112SP1 Special Ultrasonic Cleaner (Laboratory Supplies CO., Inc.) until a clear solution was obtained. To prevent vesicle aggregation all small unilamellar vesicles (SUVs) contained 5 mol% of 1,2-dioleoyl-*sn*-glycero-3-phosphoethanolamine-N-[methoxy (polyethylene glycol)-2000] (mPEG 2000 POPE).

Circular Dichroism Spectroscopy

Circular dichroism (CD) measurements were performed with a Jasco J-720 spectropolarimeter. Spectra were recorded at room temperature from 250 to 198 nm, with resolution of 0.5 nm, response time of 2 s, bandwidth of 1 nm, scan speed of 20 nm/min and 6 accumulations. CD samples were prepared by adjusting the peptide concentration to 50 μ M or 75 μ M in 2.5 mM cacodylate buffer at pH 7.4. Aliquots of a 25 mM 45/50/5 POPE/POPG/mPEG 2000 POPE SUV dispersion in the same buffer were added to the peptide solution. A blank of pure buffer solution was subtracted from all samples.

Isothermal Titration Calorimetry

Isothermal titration calorimetry (ITC) was performed with a VP ITC instrument (Microcal, Northampton, MA). All measurements were made at 25 °C in buffer (25 mM Tris/HCl, 50 mM NaCl, pH 7.4). Buffer solutions were freshly prepared. The sample cell contained the peptide solution at a concentration of 25-50 μ M. Lipid vesicles were prepared in the same buffer (lipid concentration varied from 5 to 25 mM) and injected into the peptide solution

in 10 μL aliquots. As a control, lipid vesicles were injected into pure buffer containing no peptide.

Results

The peptide-membrane binding equilibrium of the KIGAKI repeats measured with isothermal titration calorimetry

Table 1 shows the set of synthesized peptides with their corresponding short-hand notation. For accurate determination of the peptide concentration, Ile-2 was replaced by Trp, and peptide concentrations were calculated using the Trp molar extinction coefficients ($5500 \text{ M}^{-1} \text{ cm}^{-1}$). The C-terminal carboxyl groups of all peptides were amidated.

Table 1

In the following the term “binding” is used in a general sense to describe the adsorption of the cationic peptide from the bulk solution to the anionic membrane surface. Binding of the KIGAKI peptides with length of 7 to 30 residues to negatively charged lipid vesicles was studied by ITC. Following the standard protocol for lipid-into-peptide titration¹⁹ a diluted peptide solution was filled into the calorimeter cell and 10 μL aliquots of a lipid suspension were injected at constant time intervals. Figure 1A shows a representative calorimetric trace obtained at 25 °C by titration of 50 μM pep-8 with 25 mM SUVs composed of POPE/POPG/mPEG 2000 POPE (70:25:5 molar ratio).

Figure 1

Each lipid injection causes an endothermic reaction as illustrated by the calorimetric trace. The size of the titration peak becomes smaller with increasing number of injections as less peptide is available for binding. After about 20 injections all peptide is bound and further lipid injections entail no additional heat of reaction (except of dilution effects). The molar binding enthalpy, ΔH^0 , can then be calculated according to

$$\Delta H^0 = \sum_{i=1}^n h_i / n_{\text{pep}}^0 \quad (1)$$

where n_{pep}^0 is the total molar amount of peptide in the calorimeter cell and $\sum_{i=1}^n h_i$ is the cumulative heat of reaction. The measured binding enthalpies for all peptides except for pep-7 are summarized in table 2. For pep-7 we observed only small heat peaks upon titration with anionic lipid vesicles.

Table 2

The ITC data can be translated into binding isotherms as described elsewhere²⁰. Figure 1 B shows the binding isotherm corresponding to the ITC measurement of figure 1A. The binding isotherm, $X_b = f(c_f)$, describes the extent of binding, X_b , as a function of the equilibrium concentration of the free peptide c_f . X_b is defined as $X_b^{(i)} = n_{\text{pep, bound}}^{(i)} / n_L^{(i)}$, where $n_{\text{pep, bound}}^{(i)}$ is the molar amount of bound peptide after i injections, and $n_L^{(i)}$ is the molar amount of injected lipid available for binding. $n_L^{(i)}$ is known from the lipid

concentration in the injection syringe and the number of injections i . In the present case the charged peptides are not able to translocate across the membrane and only the outer membrane leaflet of the SUVs (60% of the total lipid) is available for peptide binding. $n_{\text{pep, bound}}^{(i)}$ can be calculated from the experimental heats of reaction, h_i , according to

$$n_{\text{p, bound}}^{(i)} = \sum_{k=1}^i h_k / (\Delta H^0 V_{\text{Cell}} c_{0,\text{pep}}) \quad (2)$$

$c_{0,\text{pep}}$ is the total peptide concentration in the calorimeter cell. Knowledge of the amount of bound peptide allows the calculation of the peptide concentration free in solution from mass conservation. The binding isotherm can thus be determined in a model-independent fashion.

The further analysis of the binding isotherm is based on a *surface partitioning model*, in which the peptide adsorption is related to the peptide concentration c_M found immediately above the plane of binding^{18, 21}

$$X_b = K_0 c_M \quad (3)$$

The model is based on the observation that the negatively charged membrane surface will attract cationic species in its vicinity. The peptide concentration will thus increase from its equilibrium value, c_f , far away from the membrane surface to the much higher value c_M in the lipid water interface. The electrostatic equilibrium governed by the Boltzmann relation

$$c_M = c_f \exp(-z_{\text{pep}} F_0 \psi / RT) \quad (4)$$

z_{pep} is the effective peptide charge (usually smaller than the nominal charge), ψ is the membrane surface charge potential, F_0 is the Faraday constant, and RT the thermal energy. Using the Gouy-Chapman theory it is possible to calculate the surface potential ψ and the

surface concentration c_M for each data point of the ITC curve and for the binding isotherm leading to a surface partition constant K_0 ^{22,23}. A detailed description of this binding model has been given elsewhere²⁰. As an additional feature the binding of Na^+ ions to phosphatidylglycerol was taken into account with a Langmuir adsorption isotherm and a Na^+ binding constant of 0.6 M^{-1} ²⁴. Tris/HCl buffer was counted as a 1-1 salt. The continuous line in figure 1B is the best theoretical fit to the experimental data. The effective peptide charge is $z_{\text{pep}} = 3.1\text{-}3.3$ and the surface potential varies between $\psi = -45$ mV at low X_b to $\psi = -17$ mV at the highest X_b value. The binding constant according to eq. (4) is $K_0 = 170 \text{ M}^{-1}$. An excellent agreement between the model and the experimental data is obtained for all peptides. The corresponding binding constants K_0 are listed in table 2. The free energy of binding, ΔG^0 , follows from

$$\Delta G^0 = -RT \ln(55.5 K_0) \quad (5)$$

where the factor 55.5 is the molar concentration of water and corrects for the cratic contribution. The binding entropy can then be calculated from $\Delta G^0 = \Delta H^0 - T \Delta S^0$.

Circular dichroism spectroscopy of KIGAKI peptides with and without lipid

The CD spectra of KIGAKI peptides of chain length $n = 8$ to 30 in buffer are displayed in figure 2A. All spectra are characteristic of a predominantly random coil conformation.

Figure 2

The ellipticity decreases with decreasing peptide length. The spectra can be simulated with conventional CD simulation programs and the random coil content is in the range of 71 to 85%. The detailed analysis is given in table 3.

Upon addition of anionic lipid vesicles the cationic peptides bind to the membrane surface and undergo a conformational change to a β -structured conformation. Figure 2B displays the

Table 3

corresponding CD spectra recorded in excess of anionic lipid vesicles. The β -sheet content increases from 38% for $n=8$ to 90-100% for $n=18, 24$ and 30 . The detailed analysis is again listed in table 3. We have also synthesized peptides with a chain length of 6 and 7 residues. They bind only weakly and the changes in the CD spectra are small.

The last two columns in table 3 quantitate the observed spectral change in terms of the fraction of β -structure, Δf_{β} , and the total number of amino acids, $\Delta\beta(\text{aa})$ involved in the random coil-to- β -structure transition. $\Delta\beta(\text{aa})$ is obtained by multiplying Δf_{β} with the peptide chain length n_{total} . A plot of $\Delta\beta(\text{aa})$ vs the total peptide length n_{total} is shown in figure 3 and

Figure 3

yields a straight line with

$$\Delta\beta(\text{aa}) = 1.13n_{\text{total}} - 7.86 \quad (6)$$

The figure predicts that for peptides with a chain length $n_{\text{total}} \leq 7$ no conformational change should be observed. This agrees with the experimental finding by ITC and CD that neither a heat signal nor a change in the CD signal can be observed if peptides with $n_{\text{total}} = 6$ are titrated with anionic lipid vesicles. The binding of short peptides appears to be too weak to be measured.

As the KIGAKI peptides in solution have up to 20% β -content it is physically more meaningful to plot the number of new β -segments, $\Delta\beta(\text{aa})$, on the membrane vs. the number of random coil segments of the same peptide in solution, n_{rc} (plot not shown). Again a straight line is obtained with

$$\Delta\beta(\text{aa}) = 1.23 n_{\text{rc}} - 4.96 \quad (7)$$

The latter equation allows the following conclusion. Once a threshold of about 5 random coil segments is passed, each increase in the chain length by 1 rc-element will produce 1.23 β -segments upon binding to the lipid surface. This yields a first approximation of the free energy for the membrane induced random coil \rightleftharpoons β -structure transition of $\Delta G_{\beta} = -RT \ln 1.23 = -0.12$ kcal/mol. In a previous study using D,D substitution of pep-18 ΔG_{β} was found to be -0.15 kcal/mol.

Thermodynamics of β -structure formation

The thermodynamic parameters measured in the ITC experiment are composed of the binding process and the conformational change induced by the interaction with the lipid matrix. Figure 3 shows a *linear* correlation between the total chain length, n , and the

number of amino acid residues, $\Delta\beta(\text{aa})$, changing from random coil to β -structure. A plot of the thermodynamic parameters ΔH^0 , ΔG^0 , and $T\Delta S^0$ against the chain length n or the increase in β -structure, $\Delta\beta(\text{aa})$, will lead to qualitatively similar diagrams. Figure 4 displays the variation of the thermodynamic parameters as a function of the peptide chain length.

Figure 4

Two regions can be discerned. For small n ($8 \leq n \leq 12$; $1.5 \leq \Delta\beta(\text{aa}) \leq 6$) the thermodynamic parameters show a linear *increase*, whereas for large n ($18 \leq n \leq 30$; $13 \leq \Delta\beta(\text{aa}) \leq 25$) the thermodynamic parameters *decrease*. In particular figure 4 reveals that for stretches of amino acids longer than $n = 12$ the formation of β -structure is an exothermic process. A temperature-increase will decrease the β -content of long aggregates. For shorter chains ($n = 8-12$) ΔH^0 is endothermic and the β -structure will be stabilized upon increasing the temperature.

However, it has to be taken into account that the peptide binding process to the membrane (without conformational change) varies with the peptide chain length. To exclude a strong contribution of the binding process to the β -sheet folding and to quantify the β -sheet folding reaction, we deduce the thermodynamic parameters of the β -sheet folding process by keeping the chain length constant but replacing pairs of L-amino acids by their D-enantiomers.

β -structure formation of KIGAKI peptides with 12 and 24 residues containing D-amino acids

It can be assumed that the basic binding properties of the all-L peptide and its D,D analogs are identical and that the differences in the thermodynamic parameters can be ascribed to different extents of β -sheet formation. The systematic D,D substitutions at different chain positions have been successfully employed to quantitatively describe the membrane-induced α -helix formation of the antibacterial peptide magainin ²⁵ and the β -structure formation of pep-18 ¹⁶. In the present study we have extended this method to a longer (KIGAKI)₄ peptide (pep-24) with 2 or 3 D,D pairs and a shorter (KIGAKI)₂ peptide (pep-12) with 1 or 2 D,D pairs.

Figure 5 summarizes the CD spectra of the three pep-24 analogs in buffer (fig 5A) and in the

Figure 5

presence of excess lipid (fig. 5B). The figure demonstrates a distinct change from a random coil spectrum in buffer to a β -structured CD spectrum upon addition of lipids. The figure also reveals that the ellipticity is reduced as D-amino acids are incorporated into the sequence. An isosbestic point is observed at about $\lambda = 210$ nm suggesting a 2-state equilibrium. The evaluation of the CD spectra with D-amino acids has been described previously ¹⁶. In short, we start from the pep-24 or the pep-12 spectrum without D-amino acids, which can be analyzed by the conventional CD simulation programs. The results are given in table 3. Next, we reduce the ellipticities according to the fraction of D-amino

acids in the analog. If the fraction of D-amino acids in the sequence is X_D , the ellipticities of the all-L peptide in buffer and with lipid is multiplied by $(1 - 2X_D)$. In a third step we generate linear combinations of the buffer and lipid spectra with reduced ellipticities to reproduce the experimental spectra. The results of this conformational analysis are also listed in table 3.

The structural changes can then be correlated with the changes in ΔH^0 , $T\Delta S^0$, and ΔG^0 as shown for pep-24, pep-12, and pep-18 in figure 6. The slopes of the linear regression lines yield the parameters of β -sheet folding per amino acid residue, whereas the intersections with the y-axis yields the binding parameters for a hypothetical peptide which binds without folding. The results are summarized in table 4. It is obvious that the regression analysis yields for all thermodynamic parameters a linear decrease of the binding enthalpy for pep-24, and pep-18 with increasing β -structure.

Figure 6

A different behavior is observed for pep-12. The plot of ΔH^0 , $T\Delta S^0$, and ΔG^0 vs. $\Delta\beta(\text{aa})$ is only approximately linear with a *positive* slope. This result is consistent with the biphasic behaviour described above in figure 4, which shows a positive slope for short chains and a negative slope for long chains.

In the following figure 7 we use $\Delta\beta(\text{aa})$ as the physically more relevant parameter to quantify length dependence of the β -sheet folding process per residue. Therefore the

thermodynamic parameters of the β -sheet folding process of pep-12, pep-18, and pep-24, obtained from the DD amino acid substitution study, are correlated with $\Delta\beta(\text{aa})$.

Figure 7

All thermodynamic parameters correlate linearly with a correlation coefficient higher than 0.9. The change for the residual thermodynamics of β -sheet formation with the β -sheet length for the KIGAKI peptides are described by

$$\Delta\Delta H_{\text{folding}} = -0.04 \cdot n_{\beta} + 0.31 \quad (8)$$

$$-T\Delta\Delta S_{\text{folding}} = 0.03 \cdot n_{\beta} - 0.36 \quad (9)$$

$$\Delta\Delta G_{\text{folding}} = -0.02 \cdot n_{\beta} + 0.19 \quad (10)$$

where n_{β} is the length of the β -sheet. Regression functions of the intrinsic binding reaction are given in the legend of table 4.

Specific heat capacities

Electrostatic as well as hydrophobic interactions contribute to membrane binding and peptide aggregation. In particular, the large entropic contribution to the binding reactions suggests a prominent contribution of the hydrophobic effect to the binding reaction. The hallmark of the hydrophobic effect is a large change in the specific heat capacity, which is associated with the adsorption or release of water from the hydrophobic surface. The last column in table 2 shows measured heat capacities for selected peptides. The heat

capacities are large (-150 to -400 cal mol⁻¹ K⁻¹) and negative confirming the role of the hydrophobic effect in the binding process.

Discussion

We have studied the influence of the peptide chain length on the β -sheet \rightleftharpoons random coil transition in a membrane environment using a set of peptides with the KIGAKI repeat. The chain length varied from 7 to 30 residues. As deduced from the CD spectra all peptides are predominantly random coil in water but adopt β -sheet structures of different extent when bound to an anionic membrane surface.

The overall binding process of the KIGAKI peptides to the membrane can be dissected into two steps. The first is an electrostatic attraction of the cationic peptides to the negatively charged membrane surface which leads to a higher peptide concentration near the membrane surface, c_M , than the bulk concentration, c_{eq} . This peptide concentration was calculated with the Gouy-Chapman theory. The ensuing binding equilibrium between peptide in the water-lipid interface and peptide bound to the membrane surface is governed by the interfacial concentration c_M and follows a simple partition law (eq. 4). The bound peptide remains localized at the membrane surface as deduced from solid state NMR¹⁶, and peptide partitioning into the hydrophobic core of the membrane can be excluded. The membrane binding step is coupled to a transition from a random coil to a β -sheet structure. The β -sheet folding reaction entails additional enthalpic and entropic contributions, which are the theme of the present study.

For three peptides with chain lengths of 24, 18 and 12 amino acids, we have synthesized stereo-analogs with double D amino acid substitution at different positions. The

replacement of L-amino acids by their D-enantiomers leads to a local disruption of hydrogen bonds and produces an enhanced flexibility in the regions around the D-amino acids^{17,18}. On the other hand, other peptide properties such as the hydrophobicity and side chain functionality are maintained. We have recently shown that the overall binding enthalpy (as determined from ITC), the free energy (as determined from the analysis of the binding isotherm), and the entropy of pep-18 and its stereo-analogs varied linearly with the extent of β -sheet formation at the membrane surface¹⁶. In the present work, a linear correlation is also found for the KIKAGI derivatives pep-24 and pep-12 and their corresponding stereo-analogs. At the same time, our data demonstrate that the intrinsic thermodynamic parameters for β -sheet formation are not constant but depend on the total chain length of the peptides investigated (see table 4).

Which are the thermodynamic driving forces for the β -sheet formation, and is β -sheet folding a cooperative process? These topics have been partially addressed in the literature, but the results are controversial^{12,26}. Stabilization energies of β -sheets appear to depend on the particular model protein or peptide investigated, but it is generally believed that hydrophobic interactions are the dominant driving force for the β -sheet folding reaction in *aqueous* solution^{27,28}. In particular, interactions between non-polar side chains on adjacent strands were shown to stabilize β -sheet structure²⁹⁻³¹. However, in a *membrane environment* or in the interior of globular proteins, polar interactions, in particular hydrogen bonds, are expected to drive β -sheet formation^{32,33}.

Inspection of table 2 reveals endothermic reaction enthalpies for all peptides investigated. For the binding to the lipid membrane the enthalpic contribution to the free energy is therefore unfavorable and binding is exclusively driven by entropy. The measured ΔH^0

values vary considerably between the different peptides ($\delta\Delta H^0 \sim 9$ kcal/mol between largest and smallest value). However, an entropy-enthalpy compensation mechanism smoothes out the enthalpy variations and leads to rather constant free energies ($\delta\Delta G^0 = 2.5$ kcal/mol). The peptides pep-24-1 D,D and pep-24-2 D,D have the most unfavorable ΔH^0 parameters but, at the same time, possess the largest $T\Delta S^0$ values. The D-amino acids make these peptides more flexible than their parent compounds explaining the large positive entropy and this flexibility is retained upon binding to the lipid membrane.

Although the detailed structure of the β -sheet aggregates is not known, previous NMR results obtained with pep-18 suggest some general features. ^2H -NMR studies on pep-18 have shown that β -sheet formation leads to large, immobile peptide aggregates at the membrane surface. In the present study, the percentage change of residues transferred from random coil to β -sheet increases with the peptide chain length and is only 17% for pep-8 but 85% for pep-30. It can thus be expected that longer peptides form larger aggregates than shorter peptides.

Table 2 provides no immediate insight into the thermodynamics of β -structure formation as the experimental data are the sum of the consecutive binding steps. The characteristics of β -structure growth can, however, be extracted by comparing peptides of identical chain length and different extents of D,D substitution. This comparison is based on the assumption that the initial attachment of the peptides to the membrane surface has identical thermodynamic characteristics for all members of a given set. The experimentally observed differences between the individual peptides are then ascribed exclusively to the conformational change from random coil to β -structure.

As mentioned above, enthalpy-entropy compensation leads to only small changes in the free energy. Figure 4 shows a small increase in ΔG^0 for short peptides ($n \leq 12$) and a decrease in ΔG^0 for long peptides. Considering the pure folding thermodynamics, free of the peptide membrane binding contributions, the incremental change $\Delta\Delta G_{\text{Folding}}$ decreases linearly by -0.02 kcal/mol per residue. As a general conclusion it follows from these studies that the random coil \rightleftharpoons β -structure transition makes a small negative contribution to the free energy and favours the binding to the membrane for long peptides ($n > 12$).

The analogous analysis can also be performed for enthalpic changes. Figure 4 shows that the variation of ΔH^0 with β -structure formation is negative, whereas for long peptides and positive. The folding enthalpy H_{Folding} varies from 0.13 kcal/mol per residue for shorter peptides ($n \leq 12$) to -0.4 kcal/mol per residue for longer peptides ($n > 12$). The incremental change $\Delta\Delta H_{\text{Folding}}$ is -0.04 kcal/mol per residue. Other factors unchanged, an increase in temperature will reduce the β -structure content for long peptides but increase it for short peptides.

It is obvious from the above that the random coil conformation and the β -structure have almost equal probabilities in a membrane environment with a small bias of $\Delta G_{\text{Folding}} = 0.08$ to -0.2 kcal/mol per residue towards the β -structure. For long peptides the free energies accumulate and a 10 amino acid stretch is 5-10 times more likely to adopt the β -conformation than random coil.

The random coil \rightleftharpoons β -structure transition is, however, not the driving force for membrane binding as such. The dominant factor here are (i) the Coulombic attraction between the anionic membrane lipids and the cationic peptides and (ii) hydrophobic interactions with the membrane and between the peptides. Each KIGAKI repeat carries two positive

changes and the Coulombic interaction is established by the observation that no peptide binding occurs if the membrane is composed of electrically neutral phospholipids only.

At high peptide concentrations saturation of the membrane surface is reached at about 5-10 peptides per 100 lipids (depending on the chain length) for a membrane containing 25% anionic phosphatidylglycerol. Each KIGAKI repeat carries 2 positive charges, but not all charges are sensed at the membrane surface. The effective peptide charge as deduced from the ITC experiments is $z_p \sim 3-4$, on the average, but may reach $z_p \sim 6.5$ (cf. table 2). At saturation, the membrane charge is then almost neutralized by the polycation. Expressed in terms of amino acid residues, a saturation level of $X_b = 70$ mmol/mol for pep-24 corresponds to an amino acid residue-to-phospholipid ratio of 1.7. As the area of a lipid headgroup is $\sim 60 \text{ \AA}^2$ and thus larger than the projected area of most amino acids, even at the saturation limit enough space is available that the KIGAGI peptides can be stretched out flat on the membrane surface. On the other hand, the adsorbed peptides must be packed rather tightly allowing sufficient hydrophobic interactions between neighboring molecules. Hydrophobic interactions are suggested by large negative heat capacities of the binding reaction (cf. table 2) and are consistent with the large positive binding entropies, $T\Delta S^0$. Both effects can be traced back to the release of hydration water as the hydrophobic peptidic side chains come into close contact.

Concluding remarks

We have modified the original (KIGAKI)₃ peptide by lengthening or shortening the peptide chain and have investigated the membrane-binding characteristics of the new analogs. A minimum chain length of $n = 7$ amino acids is required to observe binding and

detect conformational changes with CD spectroscopy. For a chain length of $8 \leq n \leq 30$ the thermodynamic parameters can be derived with ITC measurements. Membrane-binding requires an anionic surface and all bound peptides show an increased β -structure content compared to their conformation in solution. The β -content of the bound peptides $\Delta\beta(\text{aa})$, i.e. the number of amino acids changed from random coil to β -structure, is linearly dependent on the chain length. A more detailed analysis reveals actually two different thermodynamics for short and long peptides. For short peptides $n \leq 12$, β -structure formation has a positive free energy of $\Delta G_{\text{Folding}} = 0.08 \text{ kcal mol}^{-1}$ per residue and counteracts binding. For long chains with $n \leq 18$ $\Delta G_{\text{Folding}} = -0.15 \text{ kcal mol}^{-1}$ per residue is slightly favorable for membrane binding. These conclusions are supported by studies with peptides with D,D substitutions. The peptide binding to the membrane is an endothermic reaction and is hence driven exclusively by entropy. The large positive entropies and the large negative heat capacities suggest a prominent role of hydrophobic interactions in binding and peptide aggregation. As initially mentioned, β -sheets in biological proteins are generally shorter than 10 residues². In conclusion, this process is predominantly driven by the hydrophobic interaction, i.e. by the hydrophobic effect. On the other hand, it is thought that peptides in amyloid fibrils generally form β -sheet than about 10 residues³⁴. Interestingly, at a β -sheet length of 10 residues the thermodynamic driving forces of the β -sheet folding processes changed. These results suggest for the first time fundamental differences in the folding thermodynamics of native and aggregated protein structures. Further the small stabilization effects of the β -sheet structure serves as an explanation why only small changes of environmental parameters like pH or temperature can have a profound effect on aggregation reactions, for example in amyloid fibril formation.

References

1. Kabsch, W. & Sander, C. Dictionary of protein secondary structure: pattern recognition of hydrogen-bonded and geometrical features. *Biopolymers* 22, 2577-637 (1983).
2. Penel, S., Morrison, R. G., Dobson, P. D., Mortishire-Smith, R. J. & Doig, A. J. Length preferences and periodicity in beta-strands. Antiparallel edge beta-sheets are more likely to finish in non-hydrogen bonded rings. *Protein Eng* 16, 957-61 (2003).
3. Barlow, D. J. & Thornton, J. M. Helix geometry in proteins. *J Mol Biol* 201, 601-19 (1988).
4. Kumar, S. & Bansal, M. Geometrical and sequence characteristics of alpha-helices in globular proteins. *Biophys J* 75, 1935-44 (1998).
5. Jaroniec, C. P. et al. High-resolution molecular structure of a peptide in an amyloid fibril determined by magic angle spinning NMR spectroscopy. *Proc Natl Acad Sci U S A* 101, 711-6 (2004).
6. Petkova, A. T. et al. A structural model for Alzheimer's beta -amyloid fibrils based on experimental constraints from solid state NMR. *Proc Natl Acad Sci U S A* 99, 16742-7 (2002).
7. Chan, J. C., Oyler, N. A., Yau, W. M. & Tycko, R. Parallel beta-sheets and polar zippers in amyloid fibrils formed by residues 10-39 of the yeast prion protein Ure2p. *Biochemistry* 44, 10669-80 (2005).
8. Zimm, B. H., Doty, P. & Iso, K. Determination of the parameters for helix formation in poly-gamma-benzyl-L-glutamate. *Proc Natl Acad Sci U S A* 45, 1601-7 (1959).
9. Scholtz, J. M., Qian, H., York, E. J., Stewart, J. M. & Baldwin, R. L. Parameters of helix-coil transition theory for alanine-based peptides of varying chain lengths in water. *Biopolymers* 31, 1463-70 (1991).
10. Gellman, S. H. Minimal model systems for beta sheet secondary structure in proteins. *Curr Opin Chem Biol* 2, 717-25 (1998).
11. Syud, F. A. et al. Influence of strand number on antiparallel beta-sheet stability in designed three- and four-stranded beta-sheets. *J Mol Biol* 326, 553-68 (2003).
12. Sharman, G. J. & Searle, M. S. Cooperative Interaction between the Three Strands of a Designed Antiparallel Beta-Sheet. *J. Am. Chem. Soc.* 120, 5291-5300 (1998).
13. Searle, M. S., Williams, D. H. & Packman, L. C. A short linear peptide derived from the N-terminal sequence of ubiquitin folds into a water-stable non-native beta-hairpin. *Nat Struct Biol* 2, 999-1006 (1995).
14. Stanger, H. E. et al. Length-dependent stability and strand length limits in antiparallel beta -sheet secondary structure. *Proc Natl Acad Sci U S A* 98, 12015-20 (2001).
15. Sharman, G. J. et al. Prion protein fragments spanning helix 1 and both strands of beta sheet (residues 125-170) show evidence for predominantly helical propensity by CD and NMR. *Fold Des* 3, 313-20 (1998).
16. Meier, M. & Seelig, J. Thermodynamics of the Coil to Beta-Sheet Transition in a Membrane Environment. *J Mol Biol* (in press) (2007).
17. Rothmund, S. et al. Structure effects of double D-amino acid replacements: a nuclear magnetic resonance and circular dichroism study using amphipathic model helices. *Biochemistry* 34, 12954-62 (1995).

18. Wieprecht, T. et al. Conformational and functional study of magainin 2 in model membrane environments using the new approach of systematic double-D-amino acid replacement. *Biochemistry* 35, 10844-53 (1996).
19. Seelig, J. Titration calorimetry of lipid-peptide interactions. *Biochim Biophys Acta* 1331, 103-16 (1997).
20. Seelig, J., Nebel, S., Ganz, P. & Bruns, C. Electrostatic and nonpolar peptide-membrane interactions. Lipid binding and functional properties of somatostatin analogues of charge $z = +1$ to $z = +3$. *Biochemistry* 32, 9714-21 (1993).
21. Wenk, M. R. & Seelig, J. Interaction of octyl-beta-thioglucopyranoside with lipid membranes. *Biophys J* 73, 2565-74 (1997).
22. McLaughlin, S. Electrostatic potentials at membrane-solution interfaces. *Current Topics in Membrane Transport*, 71-144 (1977).
23. Aveyard, R. & Haydon, D. A. *Cambridge Chemistry Tests: An Introduction to the Principles of Surface Chemistry* (1973).
24. Eisenberg, M., Gresalfi, T., Riccio, T. & McLaughlin, S. Adsorption of monovalent cations to bilayer membranes containing negative phospholipids. *Biochemistry* 18, 5213-23. (1979).
25. Wieprecht, T., Apostolov, O., Beyermann, M. & Seelig, J. Thermodynamics of the alpha-helix-coil transition of amphipathic peptides in a membrane environment: implications for the peptide-membrane binding equilibrium. *J Mol Biol* 294, 785-94 (1999).
26. de Alba, E., Jimenez, M. A. & Rico, M. Turn Residue Sequence Determines Beta-Hairpin Conformation in Designed Peptides. *J. Am. Chem. Soc.* 119, 175-183 (1997).
27. Chou, K. C., Nemethy, G. & Scheraga, H. A. Role of interchain interactions in the stabilization of the right-handed twist of beta-sheets. *J Mol Biol* 168, 389-407 (1983).
28. Smith, C. K., Withka, J. M. & Regan, L. A thermodynamic scale for the beta-sheet forming tendencies of the amino acids. *Biochemistry* 33, 5510-7 (1994).
29. Espinosa, J. F., Munoz, V. & Gellman, S. H. Interplay between hydrophobic cluster and loop propensity in beta-hairpin formation. *J Mol Biol* 306, 397-402 (2001).
30. Ramirez-Alvarado, M., Blanco, F. J. & Serrano, L. Elongation of the BH8 beta-hairpin peptide: Electrostatic interactions in beta-hairpin formation and stability. *Protein Sci* 10, 1381-92 (2001).
31. Russell, S. J., Blandl, T., Skelton, N. J. & Cochran, A. G. Stability of cyclic beta-hairpins: asymmetric contributions from side chains of a hydrogen-bonded cross-strand residue pair. *J Am Chem Soc* 125, 388-95 (2003).
32. Wimley, W. C. & White, S. H. Experimentally determined hydrophobicity scale for proteins at membrane interfaces. *Nat Struct Biol* 3, 842-8 (1996).
33. Roseman, M. A. Hydrophobicity of the peptide C=O...H-N hydrogen-bonded group. *J Mol Biol* 201, 621-3 (1988).
34. Tycko, R. Molecular structure of amyloid fibrils: insights from solid-state NMR. *Q Rev Biophys* 39, 1-55 (2006).
35. Meier, M. & Seelig, J. Thermodynamics of the Coil to Beta-Sheet Transition in a Membrane Environment. in prep. (2006).

Tables

Table 1. Amino acid sequences of the synthesized peptides	
Short-Hand notation used in the text	Peptide Sequence
pep-7	KWGAKI-K-NH ₂
pep-8	KWGAKI-KI-NH ₂
pep-10	KWGAKI-KIGA-NH ₂
pep-12	KWGAKI-KIGAKI-NH ₂
pep-18*	KWGAKI-(KIGAKI) ₂ -NH ₂
pep-24	KWGAKI-(KIGAKI) ₃ -NH ₂
pep-30	KWGAKI-(KIGAKI) ₄ -NH ₂
pep-12-1DD	KWG <u>ak</u> I-KIGAKI-NH ₂
pep-12-2DD	KWG <u>ak</u> I-KIG <u>ak</u> I-NH ₂
pep-24-2DD	KWGAKI-KIG <u>ak</u> I-KIG <u>ak</u> I-KIGAKI-NH ₂
pep-24-3DD	KWGAKI-KIG <u>ak</u> I-KIG <u>ak</u> I-KIG <u>ak</u> I-NH ₂

The underlined small letters in the peptide sequences denote for D amino acids. The first number of the short hand notation represents the peptide length, the second the number of double D amino acid substitutions.

*Data of the length series of 18 residues were taken from reference³⁵

Table 2. Thermodynamic binding parameters of the KIGAKI peptides to POPE/POPG/mPEG 2000 PE (70:25:5) SUVs at 25 °C

Peptide	K_0 ^{a)} (M^{-1})	ΔH^0 ^{b)} (kcal/mol)	$T\Delta S^0$ ^{c)} (kcal/mol)	ΔG^0 ^{d)} (kcal/mol)	z_{eff}	ΔC_p cal/molK
pep-7	No ITC data at 25 °C					
pep-8	170 ± 40	1.3 ± 0.1	6.7	-5.4 ± 0.12	3.2	
pep-10	80 ± 20	2.7 ± 0.1	7.6	-5.0 ± 0.1	3.2	
pep-12	55 ± 10	3.6 ± 0.3	8.3	-4.7 ± 0.1	3.7	-157
pep-18*	890 ± 150	6.3 ± 0.3	12.7	-6.4 ± 0.1	3.4	-84
pep-24	1200 ± 200	6.4 ± 0.3	12.6	-6.6 ± 0.1	3.7	-192
pep-30	2000 ± 400	5.2 ± 0.3	12.1	-6.85 ± 0.1	3.5	
pep-12-1DD	100 ± 20	3.35 ± 0.1	8.4	-5.1 ± 0.1	2.7	-141
pep-12-2DD	85 ± 10	3.0 ± 0.1	8.0	-5.0 ± 0.1	4.1	-134
pep-24-2DD	160 ± 30	9.8 ± 0.5	15.2	-5.4 ± 0.1	5.8	-325
pep-24-3DD	30 ± 40	10.7 ± 0.5	16.2	-4.35 ± 0.1	6.5	-411

a) Gained from the theoretical calculation using a model, which combines a surface partition equilibrium with the Gouy Chapman theory.

b) The enthalpy of the peptide binding reaction was determined directly from the ITC experiment see text.

c) The entropy of the peptide binding reaction was calculated according to $\Delta G^0 = \Delta H^0 - T\Delta S^0$

d) The free energy of the peptide binding reaction was calculated according to $\Delta G^0 = -RT \ln(K_0 * 55.5)$ using the given binding constant.

*Data taken from reference³⁵

Table 3. Results of the CD spectra simulation of the KIGAKI peptides with and without double D-amino acid substitution in aqueous solution and presence of excess lipid.

Peptide	CD spectra in aqueous solution				CD spectra with excess lipids			Change of β -structure	
	f_{rc}	$f_{\beta}^{\text{a)}}$	f_{α}	f_{rc}	f_{β}	f_{α}	Δ (β -structure)	$\Delta\beta(\text{aa})$	
Pep-8	0.71	0.29	0	0.54	0.46	0	0.17	1.4	
Pep-10	0.70	0.30	0	0.44	0.56	0	0.22	2.2	
Pep-12	0.76	0.24	0.01	0.18	0.82	0	0.56	6.7	
Pep-18 ^{b)}	0.77	0.19	0.04	0.02	0.98	0	0.75	13.5	
Pep-24	0.81	0.16	0.03	0	0.995	0.005	0.835	20.0	
Pep-30	0.85	0.2	0.12	0	0.95	0.05	0.85	25.5	
% D-amino acids									
Pep-12-1DD	0.63	0.30	0.07	0.32	0.47	0.20	0.31	3.7	
Pep-12-2DD	0.58	0.42	0	0.18	0.82	0	0.392	2.2	
Pep-24-2DD	0.74	0.23	0.03	0.25	0.74	0.01	0.51	12.2	
Pep-24-3DD	0.73	0.24	0.03	0.49	0.49	0.02	0.38	9.0	

^{a)} f_{β} is the sum of β -sheet and β -turn

^{b)} Data taken from reference¹⁶.

Table 4. Thermodynamic parameters of the binding reaction to negatively charged lipid vesicles and the accompanied β -sheet folding reaction for the KIGAKI peptides with 12, 18, and 24 amino acid residues.

Peptide	Intrinsic peptide binding				β -sheet Folding			
	Peptide length	$\Delta H_{\text{binding}}$ (kcal/mol)	$-T\Delta S_{\text{binding}}$ (kcal/mol)	$\Delta G_{\text{binding}}$ (Kcal/mol)	Length of the β -sheet	$\Delta H_{\text{folding}}$ (kcal/mol)	$-T\Delta S_{\text{folding}}$ (kcal/mol)	$\Delta G_{\text{folding}}$ (cal/mol)
pep-12	12	2.79	-7.59	-5.31	6.7	0.13	-0.12	0.08
pep-18*	18	9.79	-13.99	-4.18	13.5	-0.23	0.08	-0.15
pep-24	24	14.45	-19.11	-2.77	20	-0.40	0.33	-0.2

Correlation of the intrinsic thermodynamic binding parameters with the peptide length leads to the following linear regression functions: $\Delta H_{\text{binding}} = 0.97 \cdot n_p - 8.48$, $-T\Delta S_{\text{binding}} = 0.96 \cdot n_p - 3.77$, $\Delta \Delta G_{\text{binding}} = 0.12 \cdot n_p - 6.37$, where n_p is the peptide length.

Linear regression functions for the β -sheet folding parameters are given in the text.

*Data of the length series of 18 residues were taken from reference¹⁶.

Figure Captions

Figure 1. (A) Calorimetric trace obtained at 25 °C by titration of 25 mM POPE/POPG/mPEG 2000 POPE (70/25/5 mol/mol/mol) SUVs into a 50 μ M pep-8 solution. Buffer conditions: 25 mM Tris, pH 7.4 and 50 mM NaCl. The injection volume of the lipid vesicles was 10 μ L, injections occurred at 5 min intervals. (B) Corresponding binding isotherm of pep-8 derived from the ITC experiment shown in 1A. The extent of bound peptide per lipid (lipid of outer vesicle layer) is plotted vs. the equilibrium concentration of peptide in solution. The solid line is the theoretical binding isotherm derived by combining the Gouy Chapman theory with a surface partition equilibrium.

Figure 2. Circular dichroism spectra of KIGAKI peptides with different chain lengths recorded in (A) aqueous solution and (B) excess of POPE/POPG/mPEG 2000 POPE (45/50/5) SUVs (L/P = 15). The CD spectra correspond to a chain length of $n = 30, 24, 18, 12, 8,$ and $10,$ respectively, reading from the bottom to the top at 198 nm in (A) or 217 nm in (B). The spectra were recorded at peptide concentrations of 50-75 μ M in 5 mM cacodylate buffer (pH 7.4).

Figure 3. Membrane-induced β -structure. Binding of KIGAKI peptides to anionic lipid vesicles leads to an increase in β -structure. The increase in β -structure, $\Delta\beta(\text{aa})$, is given as the number of amino acid residues which change from random coil to β -structure. $\Delta\beta(\text{aa})$ is plotted as a function of the total peptide chain length. A minimum chain length of $n = 7$ is required to observe a conformational change.

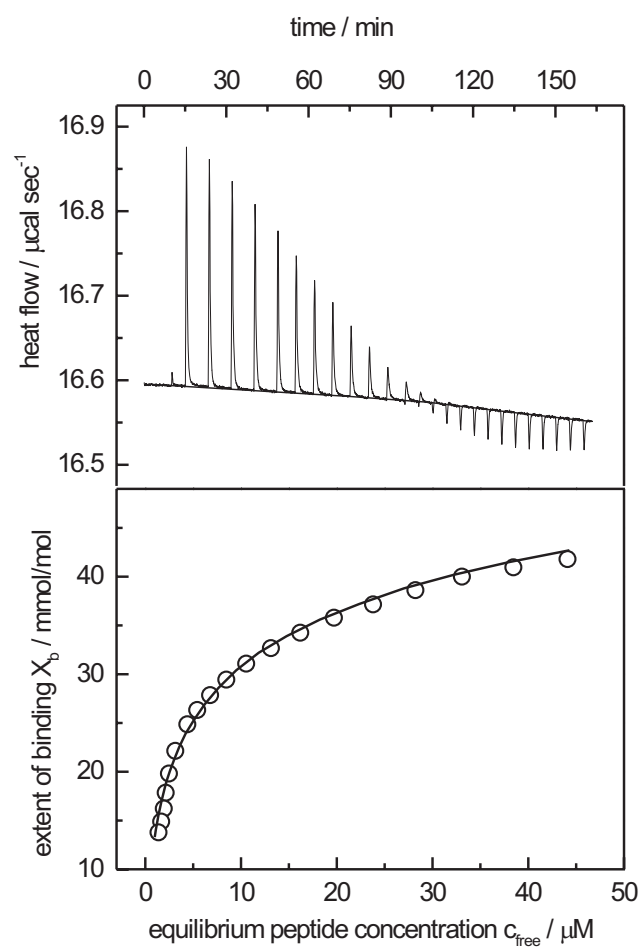
Figure 4. Thermodynamic parameters for the binding of KIGAKI peptides to anionic membranes. The membrane composition and the experimental conditions are the same as in figure 1. The reaction enthalpy ΔH^0 (●), the reaction free energy ΔG^0 (■) and the entropy term $T\Delta S^0$ (▲) are plotted as a function of peptide chain length. The dotted line differentiates between the two thermodynamic regions of short and long peptides.

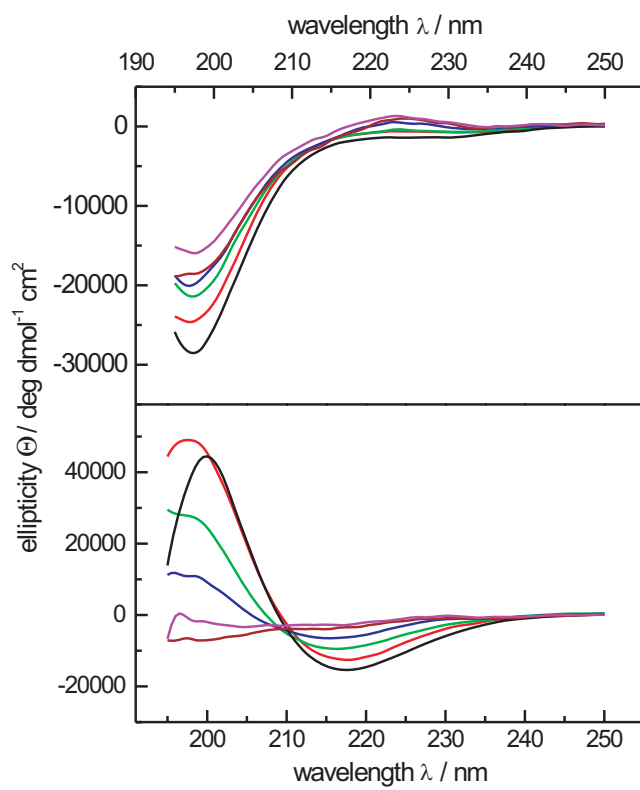
Figure 5. Circular dichroism spectra of pep-24 and two D,D analogs in buffer (A) and in the presence of excess lipid (B).

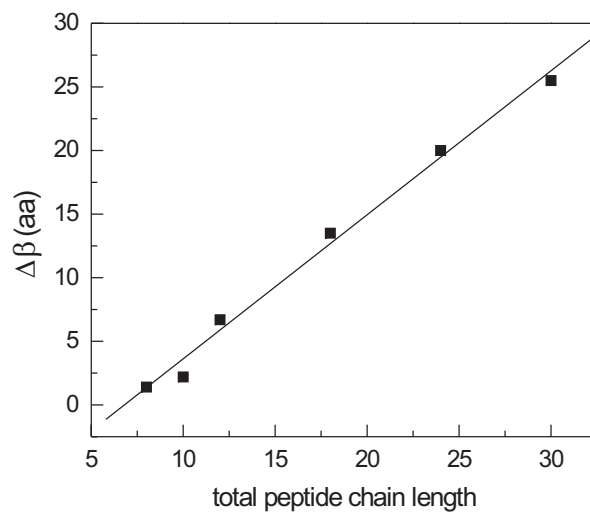
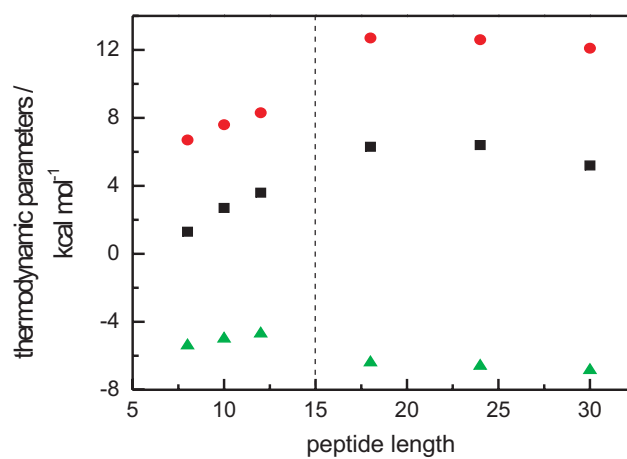
Spectra from top to bottom at 198 nm in (A) and at 210 nm in (B): pep-24, pep-24-1DD, pep-24-2DD. The lipid vesicles (SUVs 30 nm) were composed of POPE/POPG/mPEG-2000 POPE in a molar ratio of 45:50:5. The lipid-to-peptide ratio was ~ 15 . Spectra were recorded at peptide concentrations of 50-75 μM in 5 mM cacodylate buffer (pH 7.4).

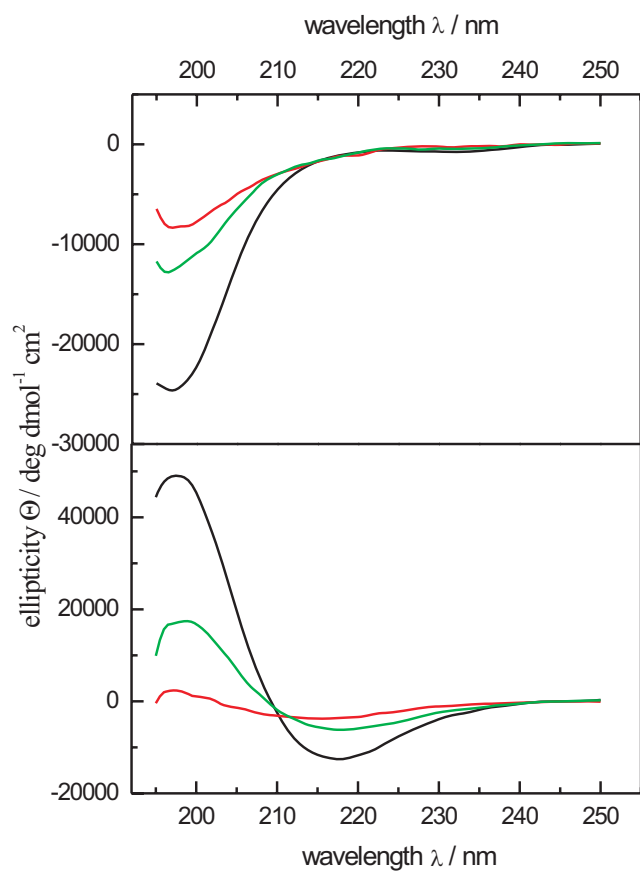
Figure 6. The membrane binding enthalpy ΔH^0 , free energy ΔG^0 , and entropy $T\Delta S^0$ of pep-24 (\blacktriangle), pep-18 (\blacksquare), pep-12 (\bullet) and their stereo analogs. The structural change from random coil to β -structure is largest for pep-24 and decreases with increasing D-substitution. The figure shows the variation of all thermodynamic parameters with increasing conformational change. $\Delta\beta(\text{amino acids})$ denotes the number of amino acid residues changing from random coil to β -structure.

Figure 7. The correlation of the structural changes $\Delta\beta(\text{aa})$ of pep-12, pep-18, and pep-24 with the thermodynamic folding parameters $\Delta H_{\text{Folding}}$ (\square), $-T\Delta S_{\text{Folding}}$ (\circ), and $\Delta G_{\text{Folding}}$ (\blacktriangle) shows a entropy-enthalpy compensation point at a β -sheet length of about 10 residues. Slopes of the linear regression lines are given in the text.

**Figure 1**

**Figure 2**

**Figure 3****Figure 4.**

**Figure 5**

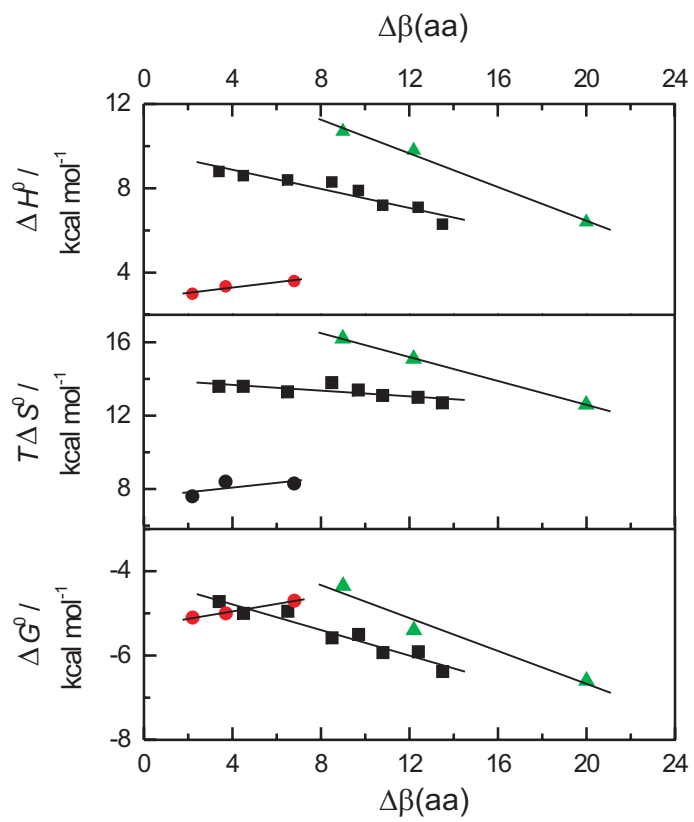
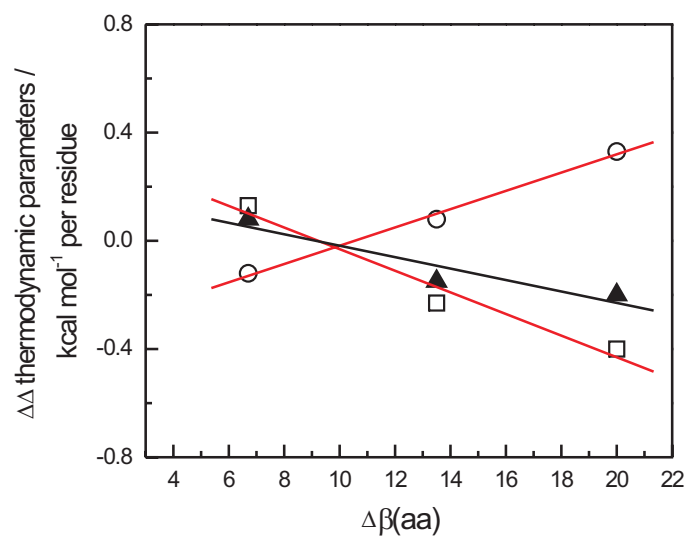


Figure 6

**Figure 7**

6. Structure analysis of encapsulated Peptide- Aggregates in reverse micelles

M. Meier and J. Seelig

Department of Biophysical Chemistry, Biozentrum, University of Basel,

Klingelbergstrasse 50/70, CH-4056 Basel, Switzerland

Tel: +41-61-267 2190, Fax: +41-61-267 2189, e-mail: joachim.seelig@unibas.ch

6.1 – Summary: Structure analysis of encapsulated Peptide-Aggregates in reverse micelles

Solid-state NMR spectroscopy is the method of choice to obtain structural insights of peptides forming an extended β -sheet at the membrane surface. However, high-resolution structures and relative orientation of the peptides to the membrane surface are inaccessible with all known NMR techniques so far. A new approach to obtain structural information about β -sheet aggregated peptides at lipid-surfaces is to use a reverse micelle system. Reverse micelles are nanometer-sized droplets of an aqueous solution stabilized in an apolar solvent by surfactant molecules located at the interface. Peptides can be incorporated into the aqueous core of such a microdroplet. The main advantage of using the reverse micelles dissolved in a low viscosity solvent is that the correlation time of the reverse micelles and thus of the hosted peptides are much faster in low viscosity solvents than in water. Due to this fact conventional solution NMR spectroscopy can be used for high-resolution structure analysis of the extended β -sheets at surfactant-water interfaces.

To mimic the biological negatively charged membrane surface we used anionic charged surfactant molecules for preparation of the reverse micelles. The work demonstrates that encapsulated (KIGAKI)₃ and the Alzheimer peptide are adsorbed to the surfactant-water interface rather than dissolved in the water pool. It is shown by CD spectroscopy that all investigated peptides adopted a β -sheet structure at the surfactant-water interface comparable to their β -sheet structure found at negatively charged phospholipid membranes. NMR spectroscopy of encapsulated (KIGAKI)₃ peptides evidence the suitability of the reverse micelles system for future applications with isotopic labeled peptides.

6.2 – Manuscript: Structure analysis of encapsulated Peptide-Aggregates in reverse micelles

Introduction

Despite some progress over the last years^{1, 2}, high-resolution NMR structural information on membrane-associated peptides has remained sparse. Atom distances, dihedral angles and orientations relative to the lipid membrane are more difficult to obtain for peptides in β -sheet conformation at the membrane conformation than peptides in a helix conformation. For α -helical membrane-associated peptides, the most common approach is to measure the ^{15}N chemical shifts and ^{15}N - ^1H dipolar couplings by solid state NMR, when the peptides are bound to macroscopically oriented lipid membranes³. These two ^{15}N interaction tensors are approximately parallel to the helical axis and their frequencies reflect the orientation of the helical axis relative to the applied magnetic field, which is also the helix orientation relative to the bilayer normal. The fact that the N-H bonds in β -sheet peptides are perpendicular rather than parallel to the strand axis complicates the structural analysis^{4, 5}. Additionally, β -sheets have a strong tendency to twist^{6, 7}, and therefore more orientations of the N-H bond than the perpendicular one to the membrane normal can be expected. Another obstacle in analyzing β -sheet structures, formed by biological relevant peptides, i.e. amyloid peptides at membrane surfaces, is the fact that the β -sheets are formed intermolecular rather than intramolecular^{8, 9}. Therefore, in this case the structure of interest is a large aggregate and not a small peptide. In result, liquid-state NMR techniques, as for example with sodium dodecyl sulfate (SDS) micelles¹⁰, suffer from low resolution. Further, the β -sheet peptides avoid to adopt their β -sheet

structure in organic solvents such as trifluoroethanol or hexafluoroisopropanol, which are thought to mimic the membrane¹¹⁻¹³.

A new method to obtain structural information on β -sheet aggregated peptides at lipid-surfaces is to use a reverse micelle system¹⁴. Reverse micelles are nanometer-sized droplets of an aqueous solution stabilized in an unpolar solvent by surfactant molecules located at the interface¹⁵. Peptides can be incorporated into the aqueous core of such a microdroplet¹⁶. The benefit of the reverse micelles system is the low viscosity of the medium, in which the reverse micelles are formed. The correlation time, τ_c , of a spherical particle dissolved in a solvent of viscosity η can be described by the Stokes-Einstein relation

$$\tau_c = \frac{4\pi r^3 \eta}{3kT} \quad (1)$$

where k is the Boltzman constant, r is the hydrodynamic radius of the considered particle, and T is the absolute temperature. The NMR line width observed for the dissolved particle is determined by the transversal relaxation time, T_2 , which is governed by τ_c ¹⁷. Nonpolar solvents typically exhibit a lower viscosity than water¹⁸, which would result in decrease of τ_c , i.e. narrower lines for particles when dissolved in the low-viscosity solvent. It is important to note that the incorporation of a peptide into a reverse micelles results in an increased hydrodynamic radius, r , which means an increase of τ_c . The advantage of low-viscosity solvents is, therefore, abolished by the increase of r at least for smaller proteins. However, for larger peptide aggregates with a molecular weight exceeding circa 20 kDa, an improvement can be achieved¹⁹. It is also obvious that the size and the correlation time of reverse micelles are governed by the amount of water within the reverse micelles²⁰.

Following the common convention, the water content of the micellar solution is expressed by the ratio between the water concentration, $C_{\text{H}_2\text{O}}$, and the surfactant concentration, C_{AOT}

$$w_0 = \frac{C_{\text{H}_2\text{O}}}{C_{\text{AOT}}} \quad (2)$$

However, the correlation time advantage is only one aspect for using the reverse micelle system. Another benefit is the inverted lipid-water interface, which avoids unwanted aggregation of vesicles as it is often observed for SDS micelles and phospholipids vesicles after peptide binding.

Figure 1

Within this study we investigated the capability of the reverse micelles system for structural analysis of β -sheet aggregated peptides at membrane surfaces by circular dichroism- (CD) and nuclear magnetic resonance (NMR) spectroscopy. For this we encapsulated two peptides: KWGAKI-KIGAKI-KIGAKI-NH₂ (**1**) and KWG*aki*-KIG*aki*-KIG*aki*-NH₂ (**2**) (small italic letters denote for D-amino acids) into reverse micelles, composed of tetraethylglycol dodecyl ether (C₁₂E₄) and/or bis(2-ethylhexyl)sodium sulfosuccinate (AOT), dissolved in isooctane. Peptide **1** and **2** have shown to exhibit a random coil to β -sheet transition upon binding to negatively charged phospholipid surfaces. β -sheet formation of peptide **1** results in large, rigid peptide aggregates. In contrast, peptide **2** forms distinctively smaller aggregates as peptide **1** indicated by a reduced β -sheet content, and a high mobility at negatively charged phospholipid surfaces. Reduction of the aggregation size of peptide **2** at the membrane surface is explained by the substitution of two adjacent D-amino acids in all three KIGAKI segments. Double D

amino acid substitution leads to a local disturbance of the β -sheet structure. Figure 1 shows the envisaged encapsulation of peptides in a reverse micelle. Beside the (KIGAKI)₃ peptides we investigated the behavior of the amyloid peptide A β (1-40) within reverse micelles.

Material and Methods

Peptide **1** and **2** were synthesized using the Fmoc (N-(9-fluorenyl)methoxycarbonyl) chemistry on an Applied Biosystems model 433A peptide synthesizer. The crude peptides were purified by reverse phase high performance liquid chromatography (HPLC). TFA counterions of the KIGAKI peptides were exchanged by a lyophilization step with 10% acetic acid before use. Purity was proven by HPLC and mass spectrometry. The Alzheimer peptide (1-40) was purchased from rPeptide (Athens, USA).

Isooctane, bis(2-ethylhexyl)sodium sulfosuccinate (AOT), and tetraethyleneglycol dodecyl ether (C₄E₁₂) were purchased from Sigma-Aldrich (Switzerland). AOT and C₄E₁₂ were used without further purification. Approximately 11 mg of AOT, 28.5 μ L C₄E₁₂ and 1 mL of isooctane were added to a screw-cap to make a 100 mM surfactant solution. About 0.5 to 1 mg of peptide was hydrated in 40 μ L buffer solution. The buffer solution contained 20 mM HEPES pH 7.4 and 25 mM NaCl. The peptide solution was added to the surfactant solution and gently stirred over night. Peptides, which were not incorporated into reverse micelles, were removed from solution by short centrifugation. The concentration of the KIGAKI peptides in the reverse micelle phase was determined by absorbance at 280 nm ($\epsilon = 5500 \text{ M}^{-1} \text{ cm}^{-1}$ for Trp), whereas the A β concentration was estimated from the amount of

hydrated A β (see discussion). A control sample of reverse micelles was made without adding peptide.

CD data obtained for peptides **1** and **2** in presence of 1-palmitoyl-2-oleoyl-*sn*-glycero-3-phosphoethanolamine (POPE), 1-palmitoyl-2-oleoyl-*sn*-glycero-3-phosphoglycerol (POPG), and 1,2-dioleoyl-*sn*-glycero-3-phosphoethanolamine-N-[methoxy (polyethylene glycol)-2000] (mPEG 2000 POPE) small unilamellar vesicles (SUVs) are taken from reference²¹, whereas data for the A β (1-40) peptide in presence of or 1-palmitoyl-2-oleoyl-*sn*-glycero-3-phosphocholine and POPG from reference⁸.

¹H- and ¹⁵N-NMR experiments were performed on a Bruker 600 MHz spectrometer. Circular dichroism spectra measurements were performed on a Jasco J-720 spectropolarimeter. Spectra were recorded from 250 to 197 nm at room temperature, with resolution of 0.5 nm, response time of 2 s, bandwidth of 1 nm, scan speed of 20 nm/min and 6 accumulations. As a blank we used the reverse micelles sample without peptides. Peptide concentrations within the CD samples were about 50 μ M. CD and NMR measurements were performed at room temperature.

Results

Encapsulation of KIGAKI peptides in reverse micelles

Although there are many different surfactants capable of forming reverse micelles and hosting proteins, bis(2-ethylhexyl)sodium sulfosuccinate (AOT) is most often used for this purpose^{22, 23}. Furthermore, the negatively charged AOT provides a negative membrane surface potential at the water surfactant interface, which is important for binding and β -sheet formation of amyloid peptides, i.e. the KIGAKI- and Alzheimer peptides^{8, 24, 25}.

However, starting experiments with reverse micelles composed of only AOT have shown to suffer from low peptide encapsulation efficiency (~20% of the applied peptide). Therefore a surfactant mixture of the noncharged E₄C₁₂ and AOT has been used in a molar ratio of 75 to 25, respectively. The peptide encapsulation efficiency for this system is about 40% and 75% for peptide **1** and **2**, respectively. Encapsulation of peptide **1** and **2** in reverse micelles was evidenced by absorption at 280 nm. A control sample with **1** in pure isooctane showed that the KIGAKI peptides are insoluble in isooctane. Further, the A₂₈₀ value was used to determine the peptide concentration ($\epsilon_{280} = 5500 \text{ M}^{-1}\text{cm}^{-1}$). For this purpose the reverse micelles sample without peptide was used as blank. A final maximum peptide concentration of 70 μM and 180 μM could be obtained for peptide **1** and **2** respectively in an C₄E₁₂/AOT/water/isooctane reverse micelles system with a total surfactant concentration of 100 mM and a water content of $w_0=11$. Formation of a reverse micelles phase in all investigated samples could be evidenced by a characteristic ¹H-NMR spectrum²⁰. The apparent water content within the reverse micelle system is slightly lower ($w_0\sim 10$) than the theoretically calculated value ($w_0=11$). Apparent w_0 values are determined from the ratio of the ¹H-NMR integrals of H₂O (~4.4 ppm in reverse micelles) to the CH groups of AOT (~3.20 ppm). For carbon nomenclature of AOT see reference¹⁹.

CD spectroscopy of KIGAKI peptides in reverse micelles

CD spectroscopy has revealed that peptide **1** and **2** exhibit a mainly random coil conformation in aqueous solution, whereas at the surface of negatively charged phospholipid vesicles both peptides adopt a β -sheet conformation with different extent²¹.

Figure 2 shows the CD spectra of peptide **1** and **2** encapsulated into C₄E₁₂/AOT reverse micelles dissolved in isooctane (dotted lines) or in presence of negatively charged phospholipid SUVs composed of POPE/POPG/mPEG 2000 PE in a molar ratio of 45/50/5 (spectra are taken from reference²¹).

Figure 2

In both lipid environments the peptides show the characteristic CD spectrum of a β -sheet conformation as indicated with the CD absorption bands at 217 and 198 nm. For a comparison of the peptide structure at the water-surfactant and water-phospholipid surface, the CD spectra were simulated with a conventional CD deconvolution program²⁶. Table 1 summarizes the results of the simulation of all CD spectra shown in figure 2. It is obvious that the secondary structure of peptide **1** and **2** is in good agreement, when the peptides are encapsulated in C₄E₁₂/AOT reverse micelles, or bound to the surface of negatively charged phospholipid vesicles. The structural differences between **1** and **2** at both interfaces are caused by the structure breaking double D amino acid, substituted in peptide 2. For more details see reference²¹.

NMR spectroscopy of KIGAKI peptides in reverse micelles

To investigate the suitability of the reverse micelles system for aggregation studies by NMR we recorded ¹H-NMR spectra of peptide **1** and **2**, when encapsulated in AOT/C₄E₁₂ reverse micelle dissolved in isooctane. Figure 3 shows the ¹H-NMR spectrum of peptide **1** and **2** in the region between 6.5 and 10.5 ppm. As a control we recorded a ¹H-NMR spectrum of a reverse micelle phase without peptide under the same conditions. Despite

the large background signals from the solvent, surfactant, and buffer molecules amide proton resonances of the peptide backbone could be obtained in case of peptide **2**. In difference, for peptide **1** we could not detect any $^1\text{H-NMR}$ proton resonance. The absence of the proton resonances in case of peptides **1**, when encapsulated in $\text{C}_4\text{E}_{12}/\text{AOT}$ reverse micelles can be explained in two ways. Firstly, the concentration of peptide **1** is too low to observe natural abundance $^1\text{H-NMR}$ resonances or secondly the correlation time (τ_C) of peptide **1** is too slow. From solid state NMR experiments it is known that peptide **1** in the aggregated state has no internal motion at the surface of negatively charged phospholipid membranes. Additionally, isothermal titration calorimetry has evidenced that the apparent lipid binding constant of peptide **1** for negatively charged phospholipid membranes is about two orders of magnitude larger than for peptide **2**. The extremely rigid structure and strong lipid binding properties of peptide **1** lead to the conclusion that peptide **1** aggregates might adopt the correlation time of the reverse micelle, whereas peptide **2** exhibits a faster τ_C due to a higher degree of rotational freedom within the reverse micelles. The correlation time of a $\text{E}_4\text{C}_{12}/\text{AOT}$ (75/25 mol ratio) reverse micelle is about $2.3 \cdot 10^{-7}$ s (calculated from the hydrodynamic radius of the $\text{E}_4\text{C}_{12}/\text{AOT}$ reverse micelles, $r_H = 8 \pm 0.5$ nm, which was determined by dynamic light scattering), which is one order of magnitude too slow to obtain $^1\text{H-NMR}$ spectroscopic resolution.

A β (1-40) in reverse micelles

In an early study we encapsulated the A β (1-40) peptide in pure AOT reverse micelles. Encapsulation of A β (1-40) into AOT reverse micelles dissolved in isooctane can only be evidenced by CD spectroscopy since the absorption at 280 nm is too low due to the lack of

aromatic amino acids in the sequence of A β (1–40). In turn, the molar ellipticity given in figure 2b for A β (1–40) encapsulated in 50 mM pure AOT reverse micelles dissolved in isooctane (dotted line) was calculated from the applied amount of A β (1–40) and an encapsulation efficiency of 20 %. The encapsulation efficiency was estimated from previous experiments with (KIGAKI)₃ peptides in pure AOT reverse micelles. Therefore, the final concentration within the sample was about 10 μ M. Further, figure 2b shows a CD spectrum of A β bound to POPG/POPC SUVs. Secondary structure calculations for A β (1–40) in both media are given in table 1. NMR spectroscopy could not be performed due to the low peptide concentration.

Discussion

So far, the use of reverse micelle systems for protein structure determination has been only validated for ubiquitin¹⁴. Indeed numerous problems are encountered, especially i) low encapsulation efficiency and ii) denaturation of the native protein upon encapsulation²⁷. In view of the peptide encapsulation efficiency for KIGAKI peptides we found that pure AOT reverse micelles have a 10 to 15 fold lower encapsulation efficiency than reverse micelles composed of C₄E₁₂/AOT (75/25 molar ratio). Explained is this finding by former results on proteins. The efficiency to encapsulate proteins within reverse micelles tends to decrease with increasing ionic strength^{20, 28}. Thus it is most likely that the lower surface charge density in C₄E₁₂/AOT reverse micelles has the same effect on the encapsulation efficiency for peptides. However, the negatively surface charge is from importance for the encapsulation efficiency as it is demonstrated by using reverse micelles composed of only C₄E₁₂, where no peptide could be encapsulated.

Denaturation of proteins upon encapsulated in AOT reverse micelles is caused by adsorption of the protein to the surfactant-water interface. The adsorption process is driven by strong electrostatic interactions between the AOT polar head groups and the charged residues of the guest molecules^{29, 30}. This disadvantage for structure determination of proteins in reverse micelles can be turned into an advantage for membrane-associated peptides, since electrostatic adsorption to the interface is often required for the structural transition. The electrostatic attraction to the membrane surface is in particular of importance for the random coil to β -sheet transition of the (KIGAKI)₃ and A β (1-40) peptides.

The presented CD spectra of peptide **1** and **2** revealed that upon encapsulation in C₄E₁₂/AOT reverse micelles both peptides adopted a β -sheet structure. Thus it can be concluded that peptide **1** and **2** are bound to the reverse micelle membrane surface and are not dissolved in the water pool within the reverse micelle. Further we found that the secondary structure of peptide **1** and **2** is in good agreement with the secondary structure of the peptides at biological relevant phospholipid membranes. Although AOT exhibits a negatively charged sulfate head group instead of a phosphate head group, as it is found in the abundant biological negatively charged POPG, the influence on the peptide conformation at the membrane surface of peptide **1** and **2** is the same. Furthermore, it demonstrates that interaction of (KIGAKI)₃ with negatively charged lipid membranes is unspecific.

The first ¹H-NMR results of the C₄E₁₂/AOT reverse micelle phase with encapsulated KIGAKI peptides have shown the suitability of the reverse micelle system for future NMR applications on peptide aggregates. For peptide **2** we clearly observed natural abundance

proton resonances of the β -sheet aggregated form, when encapsulated in reverse micelles. For the larger or more extended β -sheet aggregates of peptide **1**, the reverse micelles system has to be improved. At the current stage NMR spectroscopic resolution for peptide **1** is properly lost due the slow tumbling rate of the reverse micelles and still a low peptide encapsulation efficiency. In an ongoing study we are trying to reduce the reverse micelles size (lower water content) and labeling isotopic the peptide to increase the NMR sensitivity.

Apart of the artificial KIGAKI peptides we could show that it is possible to encapsulate the $A\beta(1-40)$ peptide in pure AOT reverse micelles. Similar to the KIGAKI peptides adopted $A\beta(1-40)$ a β -sheet structure within the reverse micelles. However, the β -sheet structure of $A\beta(1-40)$ within the reverse micelles is more complicated to explain as for the KIGAKI peptides. $A\beta(1-40)$ can adopt a β -sheet conformation upon binding to negatively charged lipid membranes⁸ or upon self-aggregation. Self-aggregation starts in water at $A\beta(1-40)$ concentrations above 25 μM and low salt conditions³¹. Therefore, it is not clear if $A\beta(1-40)$ adopted its β -sheet structure upon adsorption to the AOT-water interface or by self-aggregation due to the high local $A\beta$ concentration within the reverse micelles. Nevertheless, the secondary structure of $A\beta$ within the AOT reverse micelles resembles the structure determined for $A\beta(1-40)$ at POPC/POPG (75/25 mol/mol) membrane surfaces at a lipid to peptide ratio of 20:1. α -helical structure elements observed at POPG/POPC lipid membranes at lipid to peptide ratios of 50:1 are not observed in AOT reverse micelles.

Conclusion

Our results show the suitability of the NMR technique to investigate peptide aggregates in reverse micelles. The (KIGAKI)₃ and Alzheimer peptide(1-40) adopt a β -sheet structure upon encapsulation in AOT reverse micelles, which is comparable to the aggregated bound form of the peptides at the surface of phospholipid membranes. With this we demonstrated that the negatively charged surfactant (AOT)-water interface of reverse micelles is a biologically relevant environment for peptide aggregation. The presented CD and NMR data of all encapsulated peptides in reverse micelles are promising results for future NMR studies, to gain high-resolution structure information of peptide aggregates in a membrane environment.

References

1. Opella, S. J., Ma, C. & Marassi, F. M. Nuclear magnetic resonance of membrane-associated peptides and proteins. *Methods Enzymol* 339, 285-313 (2001).
2. Bechinger, B. The structure, dynamics and orientation of antimicrobial peptides in membranes by multidimensional solid-state NMR spectroscopy. *Biochim Biophys Acta* 1462, 157-83 (1999).
3. Opella, S. J., Nevzorov, A., Mesleb, M. F. & Marassi, F. M. Structure determination of membrane proteins by NMR spectroscopy. *Biochem Cell Biol* 80, 597-604 (2002).
4. Marassi, F. M. A simple approach to membrane protein secondary structure and topology based on NMR spectroscopy. *Biophys J* 80, 994-1003 (2001).
5. Tang, M., Waring, A. J., Lehrer, R. I. & Hong, M. Orientation of a beta-hairpin antimicrobial peptide in lipid bilayers from two-dimensional dipolar chemical-shift correlation NMR. *Biophys J* 90, 3616-24 (2006).
6. Chothia, C. Conformation of twisted beta-pleated sheets in proteins. *J Mol Biol* 75, 295-302 (1973).
7. Ramachandran, G. N. & Sasisekharan, V. Conformation of polypeptides and proteins. *Adv Protein Chem* 23, 283-438 (1968).
8. Terzi, E., Holzemann, G. & Seelig, J. Interaction of Alzheimer beta-amyloid peptide(1-40) with lipid membranes. *Biochemistry* 36, 14845-52 (1997).
9. Knight, J. D. & Miranker, A. D. Phospholipid catalysis of diabetic amyloid assembly. *J Mol Biol* 341, 1175-87 (2004).
10. Arora, A. & Tamm, L. K. Biophysical approaches to membrane protein structure determination. *Curr Opin Struct Biol* 11, 540-7 (2001).
11. Buck, M. Trifluoroethanol and colleagues: cosolvents come of age. Recent studies with peptides and proteins. *Q Rev Biophys* 31, 297-355 (1998).
12. Barrow, C. J. & Zagorski, M. G. Solution structures of beta peptide and its constituent fragments: relation to amyloid deposition. *Science* 253, 179-82 (1991).
13. Satheeshkumar, K. S. & Jayakumar, R. Conformational polymorphism of the amyloidogenic peptide homologous to residues 113-127 of the prion protein. *Biophys J* 85, 473-83 (2003).
14. Wand, A. J., Ehrhardt, M. R. & Flynn, P. F. High-resolution NMR of encapsulated proteins dissolved in low-viscosity fluids. *Proc Natl Acad Sci U S A* 95, 15299-302 (1998).
15. Ekwall, P. Two types of micelle formation in organic solvents. *Journal of Colloid and Interface Science* 29, 16-26 (1969).
16. Pier Luigi, L. Enzymes Hosted in Reverse Micelles in Hydrocarbon Solution. *Angewandte Chemie International Edition in English* 24, 439-450 (1985).
17. Abragam, A. *The Principles of Nuclear Magnetism* (eds. Marshall, W. C. & Wilkinson, D. H.) (Oxford University Press, London, 1961).
18. Lide, D. R. *Handbook of Chemistry and Physics* (CRC Press, 2005).
19. Meier, M., Fink, A. & Brunner, E. Reverse micelles dissolved in supercritical xenon: an NMR spectroscopic study. *J Phys Chem B Condens Matter Mater Surf Interfaces Biophys* 109, 3494-8 (2005).
20. Babu, C. R., Flynn, P. F. & Wand, A. J. Preparation, characterization, and NMR spectroscopy of encapsulated proteins dissolved in low viscosity fluids. *J Biomol NMR* 25, 313-23 (2003).

21. Meier, M. & Seelig, J. Thermodynamics of the Coil to Beta-Sheet Transition in a Membrane Environment. in prep. (2006).
22. Flynn, P. F. Multidimensional multinuclear solution NMR studies of encapsulated macromolecules. *Progress in Nuclear Magnetic Resonance Spectroscopy* 45, 31-51 (2004).
23. Masahiro Goto, T. O. F. N. T. A. H. Design of surfactants suitable for protein extraction by reversed micelles. *Biotechnology and Bioengineering* 54, 26-32 (1997).
24. Kazlauskaitė, J., Sanghera, N., Sylvester, I., Venien-Bryan, C. & Pinheiro, T. J. Structural changes of the prion protein in lipid membranes leading to aggregation and fibrillization. *Biochemistry* 42, 3295-304 (2003).
25. Blazyk, J. et al. A novel linear amphipathic beta-sheet cationic antimicrobial peptide with enhanced selectivity for bacterial lipids. *J Biol Chem* 276, 27899-906 (2001).
26. Reed, J. & Reed, T. A. A Set of Constructed Type Spectra for the Practical Estimation of Peptide Secondary Structure from Circular Dichroism. *Analytical Biochemistry* 254, 36-40 (1997).
27. Doussin, S., Birlirakis, N., Georgin, D., Taran, F. & Berthault, P. Novel zwitterionic reverse micelles for encapsulation of proteins in low-viscosity media. *Chemistry* 12, 4170-5 (2006).
28. Adachi, M., Shibata, K., Shioi, A., Harada, M. & Katoh, S. Selective separation of trypsin from pancreatin using bioaffinity in reverse micellar system composed of a nonionic surfactant. *Biotechnol Bioeng* 58, 649-53 (1998).
29. Pinero, J., Bhuiyan, L. B. & Bratko, D. Electrostatic interactions of charged dipolar proteins in reverse micelles. *J Chem Phys* 120, 11941-7 (2004).
30. Shi, Z., Peterson, R. W. & Wand, A. J. New reverse micelle surfactant systems optimized for high-resolution NMR spectroscopy of encapsulated proteins. *Langmuir* 21, 10632-7 (2005).
31. Harper, J. D. & Lansbury, P. T., Jr. Models of amyloid seeding in Alzheimer's disease and scrapie: mechanistic truths and physiological consequences of the time-dependent solubility of amyloid proteins. *Annu Rev Biochem* 66, 385-407 (1997).

Figure Captions

Figure 1. AOT Reverse micelle with encapsulated peptide.

Figure 2. A) CD spectra of peptide **1** and **2** bound to SUV (solid lines) and incorporated in reverse micelles (dashed dotted lines). The SUVs contained POPE/POPG/mPEG-2000-PE in a molar ratio of 45/50/5 and the molar ratio of peptide to lipid is 1:50. The reverse micelles are formed out of 100 mM surfactant C₄E₁₂/AOT in a molar ratio of 75/25 in isooctane with $w_0 \sim 10$. The final peptide concentration in both media was about 50 μ M. B) CD spectra of A β bound to small unilamellar phospholipid SUVs (solid line) and incorporated in pure AOT reverse micelles (dashed dotted lines). The SUVs contained POPC/POPG in a molar ratio of 75/25 at a peptide to lipid ratio is 1:20. AOT reverse micelles were formed out of 50 mM AOT in isooctane with a $w_0 \sim 12$. For buffer conditions see material and methods.

Figure 3. A and B shows the ¹H-NMR spectrum of peptide **1** and **2** encapsulated in reverse micelles formed by 100 mM C₄E₁₂/AOT in a molar ratio of 75/25 in isooctane at 298 K and $w_0 = 10$, respectively. The aqueous solution used for the sample preparation contained 20 mM HEPES pH 7.2, 25 mM NaCl. The final peptide concentration for peptide **1** and **2** was 70 and 180 μ M, respectively. Figure 3C shows a control sample of reverse micelles under the same conditions without encapsulated peptides. Spectra are plotted with an offset of 0.2 ppm.

Tables

Table.1 Secondary structure comparison between peptide 1, 2 and A β (1-40) encapsulated in AOT reverse micelles and bound to phospholipids vesicles.

	Phospholipid vesicles			AOT reverse micelles		
	random coil	β -sheet	β -turn	random coil	β -sheet	β -turn
Peptide 1	0.02*	0.98*	-	0.06	0.94	-
Peptide 2	0.36*	0.64*	-	0.33	0.77	-
A β (1-40)	0.44**	0.34**	0.22**	0.39	0.41	0.19

*values are taken from reference²¹.

** values are determined from the CD spectra measured within reference⁸

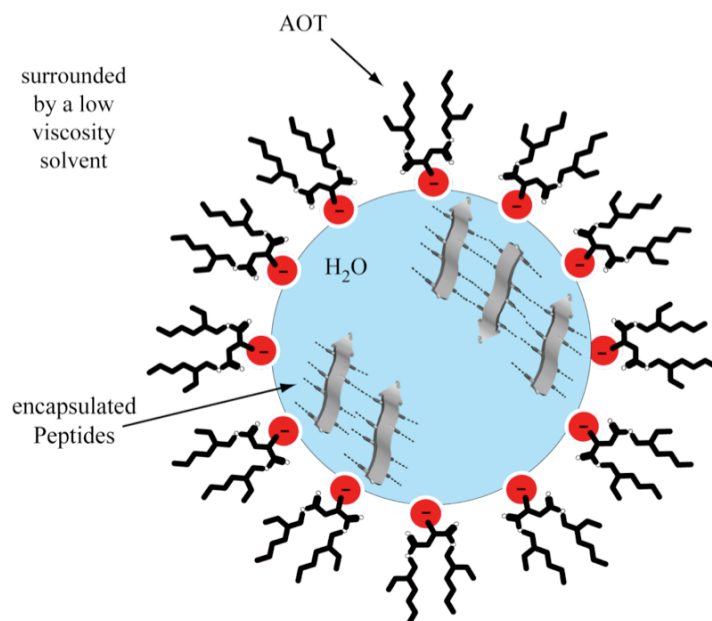
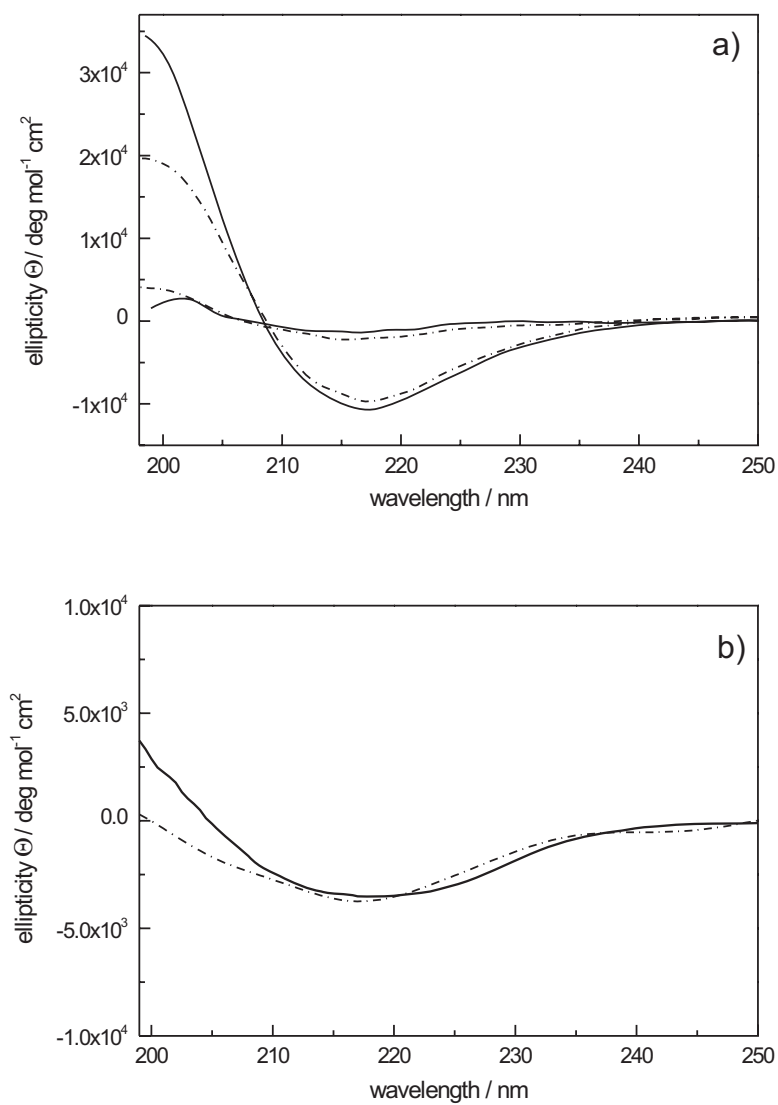


Figure 1

**Figure 2**

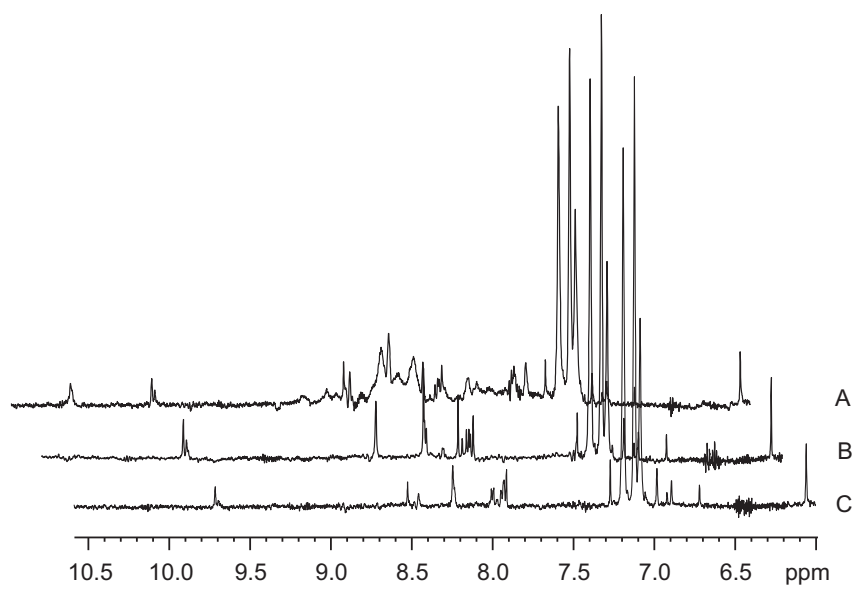


Figure 3

7. Interaction between xenon and phospholipid membranes studied by $^{129}\text{Xe}/^2\text{H}$ NMR

M. Meier, and J. Seelig

Department of Biophysical Chemistry, Biozentrum, University of Basel,

Klingelbergstrasse 50/70, CH-4056 Basel, Switzerland

Tel: +41-61-267 2190, Fax: +41-61-267 2189, e-mail: joachim.seelig@unibas.ch

7.1 – Summary: Interaction between Xenon and Phospholipid Membranes studied by $^{129}\text{Xe}/^2\text{H}$ -NMR

The most pronounced pharmacological property of the inert noble gas xenon is its ability to induce general anesthesia. It is a long lasting question if direct xenon-lipid interactions are involved in the mechanism of inducing general anesthesia. The question arose from the correlation between the potency of general anesthetics and their solubility in organic solvents (Meyer-Overton rule). It has been proposed that such correlation is founded on either an interaction of the anesthetic with the lipid bilayer of neuronal membranes or with the hydrophobic region of a protein contained in the membrane, so that partitioning of the anesthetic component into the lipid membrane is regarded as a pivotal step in mediating general anesthesia. In contrast to the commonly used anesthetics xenon is of special interest because of its small size and neutral charge. Further the chemical shift of the isotope ^{129}Xe is governed by its environment and can thus be exploited for monitoring lipid partitioning directly by NMR. We describe a fast method to obtain xenon gas/lipid partition coefficients based on the chemical shift properties of ^{129}Xe . The presented method can be applied to biological membrane samples, like tissue and blood samples. Furthermore, the results lead to a full thermodynamic characterization of the partitioning process of xenon in 1-palmitoyl-2-oleoyl-*sn*-glycero-3-phosphocholine (POPC), the major lipid component of neuronal membranes.

With respect to the anesthetic mechanism, we revealed that xenon is not altering the structural properties of lipid bilayers upon partitioning. Therefore we labeled phospholipid molecules at specific segments with deuterium and determined their order parameters. The resultant unchanged deuterium order parameter profile is unique among general anesthetics and suggests that structural changes of the lipid molecules are not necessary to mediate anesthesia. Although structural changes of the lipid molecules are not observed, interactions between xenon and the lipid molecules are evidenced by depression of the phase transition temperatures of 1,2-dipalmitoyl-*sn*-glycero-3-phosphocholine (DPPC) lipid bilayers.

7.2 – Manuscript: Interaction between Xenon and Phospholipid Membranes studied by $^{129}\text{Xe}/^2\text{H}$ -NMR

Introduction

The most pronounced pharmacological property of the inert noble gas xenon is its ability to induce general anesthesia¹. Although it has been revealed that xenon inhibits directly the excitatory NMDA (N-methyl-D-aspartate) membrane receptor channel², it is still a matter of debate if direct xenon-lipid interactions are involved in the mechanism of inducing general anesthesia. In this view, the classical argument for assuming hydrophobic interactions to be involved in the mechanism of general anesthesia is based on the correlation between the potency of general anesthetics and their solubility in organic solvents³ (Meyer-Overton rule). Such correlations arise either from an interaction with the lipid bilayer region of neuronal membranes or with the hydrophobic region of a protein contained in the membrane, so that partitioning of the anesthetic component into the lipid membrane is regarded as a pivotal step in mediating general anesthesia. In addition to the partitioning of the anesthetic molecule into the membrane, structural and dynamical changes of the lipids in the membrane are most likely involved in the anesthetic response. Here, structural data of lipid molecules upon membrane partitioning of xenon are unknown, but are of importance, because xenon differs distinctively in size and in its dipole moment from other general anesthetics.

It is also indispensable to gain knowledge of xenon-lipid interactions, because of the broad application range of xenon in medicine. Apart from its use as anesthetic, it serves as

nuclear magnetic resonance probe for tissue and blood, as contrast agent in magnetic resonance imaging, and in its polarized state as NMR signal enhancer (for a review see⁴).

So far, only a few studies report on the xenon-lipid interactions⁵⁻⁷. For example, water-lipid partition coefficients of xenon have been determined by volumetric experiments for phosphatidylcholine vesicles^{8, 9}. Ostwald's solubility coefficients of xenon were also determined for olive oil by radioactivity measurements¹⁰. Early NMR spectroscopic studies reported chemical shifts of ^{129}Xe in dimeristoyl lecithin, egg lecithin/cholesterol mixture, and biological membranes isolated from *T.californica*¹¹.

Within the present work, we provide a simple and fast method to determine lipid partition coefficients of xenon by exploiting its very sensitive chemical shift dispersion. For this purpose, the chemical shift of ^{129}Xe was measured in pure buffer, hydrated lipid POPC bilayers and in POPC suspensions at various concentrations. By monitoring the chemical shift of ^{129}Xe in dependence of the lipid concentration, a partition coefficient could be determined for the temperature range between 280 and 325 K. The results lead to a full thermodynamic characterization of the xenon partitioning in lipid bilayers composed of 1-palmitoyl-2-oleoyl-*sn*-glycero-3-phosphocholine (POPC), which is the major lipid component of neuronal membranes. Further we demonstrate by deuterium and phosphorus NMR that hydrated POPC bilayer conserve their structural properties upon partitioning of xenon. Although structural changes of the lipid molecules are not observed, interactions between xenon and the lipid molecules are evidenced by depression of the phase transition temperatures of 1,2-dipalmitoyl-*sn*-glycero-3-phosphocholine (DPPC) lipid bilayers.

Materials and Methods

1,2-dipalmitoyl-*sn*-glycero-3-phosphocholine (DPPC) and 1-palmitoyl-2-oleoyl-*sn*-glycero-3-phosphocholine (POPC) were purchased from Avanti Polar Lipids (Alabaster, AL). Deuterated lipids were synthesised as described previously^{12, 13}. Deuterium labels were attached separately either at the headgroup of α - or β -choline (-POC $_{\alpha}$ H $_2$ C $_{\beta}$ H $_2$ N-) of DPPC and POPC, or at the *cis*-double bond segment of the oleic acyl chain (carbon atoms C-9', C-10') of POPC. For preparing multilamellar vesicles (MLV), defined amounts of lipid were dissolved in chloroform and then dried with a stream of N $_2$ and then over night at high vacuum. Subsequently, buffer solution was added to the lipid film, and the mixture was vortexed extensively. Small unilamellar vesicles (SUVs) were prepared from MLV suspensions by sonication. All experiments were performed in 25 mM sodium phosphate (pH 7.4) buffer containing 100 mM NaCl.

¹²⁹Xe NMR

Xenon was purchased from Carbagas (Switzerland). Experiments were carried out using a sapphire high pressure NMR tube (Saphicon). Details of the tube are given elsewhere¹⁴. The xenon pressure within the NMR tube was always adjusted to 0.9 MPa using the reducing valve of the gas tank. Observed resonance frequencies were referenced to a sample of pure xenon gas at 0.9 MPa. The chemical shifts are reported in ppm downfield of the frequency of the pure gas phase at ambient pressure¹⁵. Chemical shift measurements were generally performed with a 30° pulse (9 μ s) and a repetition time of 2 s, with the exception of figure 1 (repetition time of 150 s). The T_1 relaxation time of ¹²⁹Xe was determined with the inversion recovery experiment in the temperature range between 280

and 320 K. In buffered solution and under the given conditions, the T_1 relaxation time of xenon was found to follow the equation $\ln(T_1 / s) = -1.16 \cdot (1000 / (T / K)) + 7.79$ and in 50 mM POPC SUV solution $\ln(T_1 / s) = -1.79 \cdot (1000 / (T / K)) + 9.35$, where T is the temperature in K. All ^{129}Xe experiments were performed on a Bruker Avance 400 MHz wide bore DRX spectrometer. Temperature correction of the chemical shift data was achieved by measuring glycerol contained within the sapphire tube. The absolute error in temperature was estimated to be ± 0.2 °C.

^2H NMR

Solid-state NMR tubes (O.D. 0.5 mm) were filled with ~50 to 100 mg of dry lipid and buffer was added to a final 1:2 wt ratio. Next, the samples were extensively vortexed and subjected to several freeze-thaw cycles to produce MLVs. The NMR-tubes were sealed with a rubber septum and evacuated before being pressurized by xenon or nitrogen. The Xe pressure was always adjusted to 0.6 MPa using the reducing valve of the gas tank. All ^2H -NMR experiments were performed on a Bruker Avance 400 MHz spectrometer. ^2H -NMR spectra were recorded with a quadrupole echo sequence $(90_x - \tau - 90_y - \tau)^{16}$ with a echo time of $\tau = 60$ μs , a $\pi/2$ pulse length of 4.6 μs and a recycling time of 200 ms. Typically, 8-K data FIDs were accumulated. The absolute error in temperature was estimated to be ± 0.5 °C.

Differential Scanning Calorimetry

DSC measurements were made with a VP-DSC calorimeter (MicroCal; Northampton, USA) equipped with a pressure perturbation unit that was used to regulate the xenon

pressure. MLV samples were degassed and incubated for 24 hours under a xenon pressure of 0.4 MPa and then filled into in the calorimeter cell. To provide a pure xenon atmosphere above the sample, the calorimeter cell was flooded several times with xenon before the xenon pressure was increased to 0.4 MPa. The DSC measurements were started after an equilibration period of 30 minutes. Reference samples were degassed and measured under a 0.4 MPa nitrogen atmosphere. All samples were measured with two different scan rates, 0.7 K/min and 1 K/min.

Theory of lipid partitioning

The affinity of xenon for the lipid membrane will be quantified in terms of a partition coefficient,

$$K_{Xe} = \frac{n_{Xe}^L \cdot V^{W+Xe}}{n_{Xe}^W \cdot V^{L+Xe}} \approx \frac{n_{Xe}^L \cdot V^W}{n_{Xe}^W \cdot V^L} \quad (1)$$

where K_{Xe} is the partition coefficient, n_{Xe}^W and n_{Xe}^L are the moles of xenon in the water and in the lipid membrane phase, respectively. The total volume of the water phase, V^{W+Xe} , and the lipid phase, V^{L+Xe} , which is the volume of the solvents plus the volume of xenon, was approximated by the volume of the pure solvent only, V^W and V^L . The volume of the lipid membrane phase was calculated with the help of the specific volume of the lipid molecule, v_L (for POPC 0.996 ml/g¹⁷), the molar amount of lipids in the membrane phase, n_L , and the molecular weight of the lipid, M_L

$$K_{Xe} = \frac{n_{Xe}^L \cdot V^W}{n_{Xe}^W \cdot n_L \cdot v_L \cdot M_L} \quad (2)$$

Substitution of n_L by the lipid concentration, c_L , leads to

$$K_{Xe} = \frac{n_{Xe}^L}{n_{Xe}^W} \cdot \frac{1}{c_L \cdot v_L \cdot M_L} = \frac{n_{Xe}^L}{n_{Xe}^W} \cdot \frac{1}{\Phi} \quad (3)$$

where Φ is the lipid volume fraction. Quantitative knowledge of the partition coefficient, K_{Xe} , is gained from the chemical shift of xenon, which is governed by the xenon environment only¹⁸. The observable chemical shift of xenon in lipid suspension, δ_{Xe}^{obs} , can be described by

$$\delta_{Xe}^{obs} = X^W \cdot \delta_{Xe}^W + X^L \cdot \delta_{Xe}^L \quad (4)$$

where δ_{Xe}^W , δ_{Xe}^L are the chemical shifts and X^W , X^L the mole fractions of xenon in the water and lipid phase, respectively. The model is valid under the conditions of fast chemical exchange of the xenon atoms between the water and lipid phase in the lipid suspension which has been shown previously¹¹. X^L is given by the mass conservation

$$\delta_{Xe}^{obs} = X^W \cdot \delta_{Xe}^W + (1 - X^W) \cdot \delta_{Xe}^L \quad (5)$$

Deriving X^W from equation 3 leads to the expression

$$X^W = \frac{1}{K_{Xe} \cdot \Phi + 1} \quad (6)$$

which can be substituted in equation 5 and leads to the fit function of the observable chemical shift of ^{129}Xe , δ_{Xe}^{obs} ,

$$\delta_{Xe}^{obs} = \frac{1}{K_{Xe} \Phi + 1} \cdot \delta_{Xe}^W + \frac{K_{Xe} \Phi}{K_{Xe} \Phi + 1} \cdot \delta_{Xe}^L \quad (7)$$

A van't Hoff analysis of the partitioning constant yielded from equation 7 was carried out to determine the thermodynamic partitioning parameters of xenon to POPC membranes. Therefore the partitioning data were fitted to

$$\ln K_{Xe} = -\frac{\Delta H^0}{R} \left(\frac{1}{T} - \frac{1}{T^0} \right) + \frac{\Delta C_p T^0}{R} \left(\frac{1}{T} - \frac{1}{T^0} \right) + \frac{\Delta C_p}{R} \ln \left(\frac{T}{T^0} \right) + \ln K_{Xe}^0 \quad (8)$$

where R is the gas constant, T^0 is the reference temperature (297 K) in degrees Kelvin; K_{Xe}^0 and ΔH^0 are binding constant and enthalpy change at the reference temperature, respectively, and ΔC_p is the heat capacity change of the partitioning reaction.

Results

Determination of the xenon-lipid partition coefficient from the ^{129}Xe chemical shift

For lipid suspensions, ^{129}Xe spectra were recorded as a function of the POPC concentration and temperature at a xenon pressure of 0.9 MPa. A single resonance line (line width ≤ 8 Hz) was observed for all POPC concentrations below 100 mM. Figure 1 shows ^{129}Xe -NMR spectra recorded for various POPC suspensions at 321 K.

Figure 1

Additionally, a single broad ^{129}Xe resonance signal (line width ~ 500 Hz) was found for more concentrated POPC lipid bilayers (water to lipid ratio 2:1) at 0.6 MPa (top spectrum in figure 1). It is obvious that the chemical shift of ^{129}Xe changes upon increasing the lipid concentration.

Beside of this, the chemical shift of ^{129}Xe changes also with temperature. Figure 2 shows the obtained chemical shifts of ^{129}Xe for buffered aqueous solution, POPC suspensions (representative for 15 and 50 mM POPC) and hydrated POPC bilayer for the temperature range between 280 and 325 K.

Figure 2

In buffered aqueous solution (25 mM NaPO₄, 100 mM NaCl, pH 7.4), the chemical shift of ¹²⁹Xe was found to describe a hyperbolic progression in the investigated temperature range with a maximum at 318 K, which is consistent with an earlier report¹⁹. Minor changes of the chemical shift of ¹²⁹Xe in pure water and buffer are due to the presence of buffer ions²⁰. For hydrated lipid bilayers the chemical shift of ¹²⁹Xe showed a linear temperature dependency close to reported¹¹ chemical shift values of ¹²⁹Xe in olive oil (figure 2).

The change of the chemical shift in dependence of the POPC concentration and temperature can be used to determine the partition coefficients of xenon for POPC membranes. This is because the chemical shift of ¹²⁹Xe is governed by its environment only and therefore reflects the xenon distribution between the lipid and aqueous phase in the POPC suspension. By assuming the chemical exchange rate of xenon between the two phases is fast and independent of the POPC concentration, it is possible to describe the chemical shift of ¹²⁹Xe by equation 7. For this the chemical shift of ¹²⁹Xe in pure POPC lipid membranes is approximated by the chemical shift of ¹²⁹Xe in hydrated POPC bilayers. In figure 3 we plotted the chemical shift of ¹²⁹Xe in dependence of the POPC concentration for three temperatures.

Figure 3

The solid lines are the best theoretical fit to equation 7. For the characteristic temperatures of 298 K and 310 K, we determined partition coefficients of 12.1 and 25.5 respectively. Figure 4 shows the resulting xenon/POPC partition coefficients in dependence of the temperature.

Figure 4

A van't Hoff analysis of the partitioning coefficient was carried out to determine the thermodynamic partitioning parameters of xenon. The solid line in figure 4 corresponds to the best theoretical fit (equation 8) to the experimental data. The calculated enthalpy, heat capacity and standard free energy of xenon partitioning from the aqueous to the POPC bilayer was found to be $\Delta H_{Xe}^0 = -3.75$ kcal/mol, $\Delta C_p = -95 \pm 12$ cal/molK, and $\Delta G_{Xe}^0 = -4.2$ kcal/mol at 298 K, respectively. ΔG_{Xe}^0 was calculated as $\Delta G_0 = -RT \ln(K \cdot 55.5M)$, where RT is the thermal energy and the factor 55.5 is the molar concentration of water and corrects for the cratic contribution.

A different behaviour of the chemical shift of ^{129}Xe was found for POPC suspensions above 120 mM. Figure 5 shows the ^{129}Xe NMR spectra for a POPC suspension of 150 mM, recorded in the temperature range between 300 K and 325 K.

Figure 5

At 301 to 305 K, a line broadening of the ^{129}Xe signal was observed. Above that temperature, the broadening of the ^{129}Xe resonance got more pronounced and a splitting of the resonance line occurred. The line broadening and splitting of the ^{129}Xe resonance can

only be explained by a decrease of the rate constant of the chemical exchange between the water and lipid phase. By comparison of the chemical shift of the arising ^{129}Xe peak at the high field site with the above determined chemical shift values, we assigned the signal to xenon dissolved in water. As judged from the partition coefficient, the downfield peak corresponds to xenon dissolved in the POPC membrane. Direct determination of the xenon-lipid partitioning coefficient from the intensities of the ^{129}Xe spectra at POPC concentrations higher than 100 mM and temperatures above 305 K are not possible, due to inadequate resolution of the resonance signals for line fitting.

Structural changes of the lipid bilayer upon partitioning of xenon as monitored by deuterium and phosphorus NMR

^2H -NMR spectra were obtained with hydrated POPC bilayers (water to lipid ratio 2:1) composed of POPC, deuterated at the α -segment of the choline moiety or carbon double bond segment of the oleic acyl chain and measured at 310 K and 0.6 MPa xenon pressure. The xenon concentration within such an hydrated lipid bilayer sample can be approximated by taking the Ostwald solubility coefficient of xenon in olive oil (1.8 at 310 K)⁹, that is the ratio of the volume of gas absorbed to the volume of the absorbing liquid measured at the same temperature, and the xenon density of 31 kg/m³ at 310 K. As a result, we approximate a xenon concentration of 25-30 mol% with respect to the POPC molecules.

The quadrupole splittings of the deuterons at the head group and double bond segment were not changed upon the partitioning of xenon (0.6 MPa) for the temperature range between 280 and 330 K. As a reference for the splitting, we used the same lipid sample

under 0.6 MPa N₂ pressure. All deuterons showed a single quadrupole splitting in the NMR spectra. To test if a higher xenon concentration within the POPC bilayer perturbs the POPC structure, we saturated a POPC bilayer sample (water to lipid ratio 4:1) at ambient pressure for 4 h with xenon and measured the quadrupole splitting again at the head and tail position under a xenon pressure of 0.6 MPa. In this experiment, the quadrupole splitting was identical to the first experiment. Apparently, the mobility of xenon in the POPC membrane is fast, and the residence time of xenon at an individual lipid segment must be shorter than the time scale of a deuterium NMR experiment (10⁻⁵s). Phosphorus-31 NMR spectra of the POPC bilayer were recorded, to confirm an intact POPC bilayer structure upon xenon partitioning (0.6 MPa) at 280 and 325 K. All phosphorus-31 NMR spectra were similar, showing the typical signature of the bilayer phase¹² with a chemical shielding anisotropy of 47 ppm (spectra not shown).

To generalize these results, we measured ²H-NMR spectra of deuterium labelled DPPC hydrated bilayer (water to lipid ratio 2:1) under a xenon pressure of 0.6 MPa. DPPC was labelled separately at the α - and β -segment of the choline moiety. In contrast to the POPC bilayer, the DPPC bilayer displays a phase transition at 41 °C. Figure 6A shows the quadrupole splittings, $\Delta\nu_Q$, of the α - and β -deuterons in dependence of the temperature under 0.6 MPa xenon and nitrogen pressure. The influence of xenon on the pre ($T_p=37^\circ\text{C}$) and main ($T_m=41^\circ\text{C}$) phase transition temperatures of DPPC is obvious. In general, in going through the phase transition from the gel to the liquid crystalline phase the conformational motion of DPPC molecules become less restricted.

Figure 6

This leads to an observable reduction of the quadrupole splitting at the phase transition temperatures^{13, 21} as compared to POPC bilayers. The reduction of quadrupole splittings of the α - and β -deuterons attached to DPPC due to the phase transition is considerably different between the reference sample (0.6 MPa N₂ pressure) and xenon pressurized sample (0.6 MPa). T_m of the DPPC bilayer in presence of xenon is reduced by 1 ± 0.5 °C from 41°C to 40°C, whereas T_p is reduced by 1.5 ± 0.5 °C from 36.5 to 35 °C. T_p was only evaluated for the β -deuterons, because the α -deuterons of DPPC are less sensitive and are not responding to the pre transition¹³. The quadrupole splittings of the choline head group deuterons of DPPC above and below the phase transition temperature are not changed due to the presence of the xenon atoms. We also measured the phase transition temperatures of DPPC under xenon saturated conditions, where T_p and T_m are reduced by 3 ± 0.5 and 2.5 ± 0.5 °C.

To confirm these results, we recorded DSC thermograms of a 10 mM DPPC MLV solution under 0.4 MPa xenon and 0.4 MPa nitrogen pressure (shown in Figure 5b). Xenon decreased the T_m of DPPC by 0.5 °C and increased the T_p by 0.3 °C. A quantitative evaluation of the DSC experiment is not possible since mixing, transfer, and equilibration of the DSC samples with xenon proved to vary throughout our experiments. Nevertheless, deuterium NMR and DSC experiments reveal both a reduction of the main phase transition of DPPC in presence of xenon. Differences in DSC and NMR samples such as the higher xenon pressure and vesicle form explain differences in the strength of the temperature depression. We also monitored the chemical shift and T_1 relaxation times of ¹²⁹Xe in DPPC suspension. Both parameters were insensitive to the phase transition of DPPC.

Discussion

Thermodynamics of xenon partitioning

The presented work reports a full thermodynamic characterization of the xenon partitioning into POPC lipid bilayers. Lipid-water partition coefficients of xenon varied from 12 to 24.2 in the temperature range of 280 to 325 K. In comparison to literature values of lipid-water partition coefficients of xenon determined by volumetric and radioactivity methods, we find excellent agreement, with a faster and more quantitative method. For example, Smith et al. reported for phosphatidylcholine vesicle suspensions K_{Xe} values of 13 and 15.1 at 283 K and 298 K respectively. For olive oil K_{Xe} values of 14.6, 19.3, 22.5, and 23.9 at 277, 293, 300, and 310 K were determined, respectively (all K_{Xe} values are translated from Oswald's solubility coefficients).

The free energy, enthalpy and the heat capacity changes for the partitioning process of xenon from the water to the lipid phase were -4.2 kcal/mol (at 298 K), -3.75 ± 0.5 kcal/mol and -95 ± 12 cal/molK, respectively. It has been shown that the heat capacity change ΔC_p can be empirically related to the change in hydrophobic and hydrophilic solvation²². Therefore, ΔC_p can be assumed to reflect changes in the exposure of hydrophobic surface of xenon to water. Taking into account a water accessible apolar surface area (ASA_{ap}) of 156 \AA^2 for xenon²³, and a change in heat capacity of $-0.45 \text{ cal/Kmol\AA}^2$ ²², a theoretical ΔC_p of -70 cal/molK is calculated. The experimental error and uncertainties in the ASA_{ap} value of xenon might explain the difference of 25 cal/molK between the experimental and theoretical ΔC_p value. Additional contributions to ΔC_p , as for example changes in the water accessibility of the lipid surface, cannot be ruled out, but

are small in comparison to the contribution of the burial of water-accessible apolar surface from xenon.

NMR spectroscopic behaviour of ^{129}Xe in lipid suspension

The systematic determination of the temperature and lipid concentration dependency of the chemical shift of ^{129}Xe in phospholipid suspensions exemplifies for the first time some general behaviour of ^{129}Xe in lipid solution. A linear temperature dependence of the ^{129}Xe chemical shift is mostly found for xenon dissolved in organic solvents²⁴, which is in line with the findings of ^{129}Xe dissolved in hydrated lipid bilayer. For POPC SUVs we observed that the chemical shifts of ^{129}Xe were in the range of ^{129}Xe resonances found in buffered aqueous solution and in hydrated POPC bilayer. Additionally, the appearance of only one resonance signal for ^{129}Xe dissolved in POPC suspension below 100 mM leads to the conclusion that xenon is in fast chemical exchange between the lipid and water phase. As a result, the exchange rate of xenon k_{Xe} between the two phases must be faster than $(\nu_{\text{Xe}}^M - \nu_{\text{Xe}}^W) / 2\pi\sqrt{2}$ ²⁵, where ν_{Xe}^W and ν_{Xe}^M are the resonance frequencies of ^{129}Xe in buffered aqueous solution and in hydrated POPC membrane, respectively. At higher POPC (>100 mM) concentration and temperatures above 305 K, we observed a line broadening of the ^{129}Xe resonance, which can be interpreted as a decrease of the exchange rate below 40 s^{-1} . In analogy, Miller et al. observed for ~130 mM DMPC at 308 K a clear peak separation between the lipid and water resonances of ^{129}Xe , whereas one broad ^{129}Xe resonance was yet again observed at 325 K. The merged lipid and water ^{129}Xe resonance with increasing temperature was taken to reflect an increasing exchange rate of xenon in the lipid suspension with temperature. In contrast, present work suggests that the chemical

shift of ^{129}Xe decreases concomitantly with increasing temperature. Therefore, the appearance of one broad xenon signal at higher temperature is more likely caused by the overlap of the ^{129}Xe water and lipid signals rather than due to a fast chemical exchange. The increase of the residence time of xenon in the lipid bilayer at higher POPC concentration and temperature, and thus the line broadening, could be explained the formation of multilamellar vesicles. Accordingly, the chemical exchange by with multilamellar bilayers would increase the exchange rate. As a consequence, the exchange of xenon in hydrated lipid bilayer is slow and must lead to a splitting of the ^{129}Xe resonances. However, this was not observed experimentally due to the limited resolution in the solid state NMR samples.

The structural behaviour of the lipid membrane upon xenon partitioning

Xenon has shown not to alter the structure and dynamics of the POPC molecules upon partitioning into POPC lipid bilayers under the observed conditions. This property distinguishes xenon from other gaseous anesthetics as halothane, enflurane and isoflurane. For these anesthetics, an increase of the order parameter for POPC segments near the interface and a decrease of order for those POPC segments within the hydrophobic region of the membrane at anesthetic concentrations of 25 mol% has been reported²⁶. In these experiments, however, the anesthetic concentration greatly exceeded those used clinically. Likewise, the xenon concentration in present investigation exceeded the clinically relevant xenon concentration; but even at such saturation conditions of xenon in the POPC lipid membrane, no changes in the lipid structure and dynamics of the POPC bilayer could be observed. The absence of structural perturbation of the membrane upon xenon partitioning

can be explained by the three to five time smaller accessible surface area of xenon compared to gaseous anesthetics as halothane or enflurane. Additionally, xenon exhibits only a residence in the millisecond range in the membrane, where the time scale of a deuterium NMR experiment cannot resolve smaller differences.

The distribution of the anaesthetic component within the lipid membrane is closely related to the order parameter profile of the membrane. Here conflicting results were reported. For example, Xu et al. revealed for xenon a preferential location at the head group region of phosphatidylcholine lipid bilayers by measuring site-selective intermolecular $^{129}\text{Xe}\{-^1\text{H}\}$ nuclear Overhauser effects between xenon and head group protons of phosphatidylcholine in sonicated unilamellar vesicles at 298 K⁶. The opposite result was found in molecular dynamic simulation of the xenon partitioning process in a DPPC bilayer²⁷. Therein it was postulated that xenon is directed more to the hydrophobic core of the bilayer than to the head group region. Present results cannot clarify this dispute, but the unchanged quadrupole splittings of the deuterium labels attached to both the head group and double bond segment within the hydrophobic core of the POPC and DPPC bilayer arguments against a strong local preference of the xenon atoms in the phosphatidylcholine bilayer. This is also supported by considering that xenon exhibits no dipole moment, which could align with the dipole of the POPC molecules in the bilayer. In particular, present findings cannot support the MD simulation, because they predicted changes of the averaged order parameter of the DPPC molecules of about 0.003 (translates into a change of the quadrupole splitting constant of 0.4 kHz) upon xenon partitioning of 25 mol% in the DPPC bilayer which was not observed in present results.

Even though xenon molecules obviously do not perturb the structure of the lipid molecules of the bilayer, we found evidence that xenon interacts with the lipid molecules of the bilayer. Accordingly, xenon affected the thermotropic behaviour of DPPC multilamellar vesicles. In detail, xenon decreased the T_m and T_p of the DPPC bilayer under the presented conditions of about 1 and 0.5 °C, respectively. The reduction of the phase transition temperature was found to be dependent on the amount of added anesthetic molecules²⁸. In comparison, halothane and enflurane reduced T_m of DPPC by about 6.4 ° and 3.3 °C respectively under a partial pressure of 0.15 atm²⁹. Only under xenon saturation conditions we observed phase transition temperatures of DPPC in the same order as for halothane and enflurane, which is reasonable since both have higher partition coefficients and smaller maximum alveolar concentrations (MAC value) required for anesthesia compared to xenon. Many suggestions have been made to explain the depression of the phase transition temperature of DPPC due to anesthetic partitioning, but the mechanism is still not clear, but present results demonstrate for the first time that lipid structural changes cannot account for the depression of the phase transition.

Conclusion

A new method for the rapid measurement of the xenon partition coefficients was presented exploiting the sensitive chemical shift of ^{129}Xe . The main advantage of measuring the partition coefficient of xenon by ^{129}Xe -NMR is its simplicity as compared to volumetric and radioactivity methods. Furthermore, the ^{129}Xe -NMR characterization of the partitioning process of xenon provides important insights into the behaviour of xenon in lipid suspensions, which is of importance for its medical applications. With respect to the

anesthetic mechanism, we revealed that xenon is not altering the deuterium order profile of the lipid membrane under conditions used for anesthesia. This suggests that structural changes of the lipid molecules are not necessary to mediate anesthesia.

Acknowledgement

We thank Dr. Daniel Häusinger for providing the high-pressure NMR tube. Further we thank Dr. André Ziegler for proofreading the manuscript and discussion.

References

1. Cullen, S. C. & Gross, E. G. The anesthetic properties of xenon in animals and human beings, with additional observations on krypton. *Science* 113, 580-2 (1951).
2. Franks, N. P., Dickinson, R., de Sousa, S. L., Hall, A. C. & Lieb, W. R. How does xenon produce anaesthesia? *Nature* 396, 324 (1998).
3. Overton, C. E. Studien ueber Narkose, zugleich ein Beitrag zur allgemeinen Pharmakologie (Fischer, Jena, 1901).
4. Goodson, B. M. Nuclear magnetic resonance of laser-polarized noble gases in molecules, materials, and organisms. *J Magn Reson* 155, 157-216 (2002).
5. McKim, S. & Hinton, J. F. Evidence of xenon transport through the gramicidin channel: a ^{129}Xe -NMR study. *Biochimica et Biophysica Acta (BBA) - Biomembranes* 1193, 186-198 (1994).
6. Xu, Y. & Tang, P. Amphiphilic sites for general anesthetic action? Evidence from ^{129}Xe -[^1H] intermolecular nuclear Overhauser effects. *Biochim Biophys Acta* 1323, 154-62 (1997).
7. Li, X. et al. Interactions between xenon and phospholipid bicelles studied by $^2\text{H}/^{129}\text{Xe}/^{131}\text{Xe}$ NMR and optical pumping of nuclear spins. *Chemical Physics Letters* 419, 233-239 (2006).
8. Smith, R. A., Porter, E. G. & Miller, K. W. The solubility of anesthetic gases in lipid bilayers. *Biochimica et Biophysica Acta (BBA) - Biomembranes* 645, 327-338 (1981).
9. Clever, H. Solubility data series. (Pergamon Press, Oxford, 1979).
10. Chen, R. Y. et al. Tissue-blood partition coefficient for xenon: temperature and hematocrit dependence. *J Appl Physiol* 49, 178-83 (1980).
11. Miller, K. W. et al. Xenon NMR: Chemical Shifts of a General Anesthetic in Common Solvents, Proteins, and Membranes. *PNAS* 78, 4946-4949 (1981).
12. Seelig, J. & Waespe-Sarcevic, N. Molecular order in cis and trans unsaturated phospholipid bilayers. *Biochemistry* 17, 3310-5 (1978).
13. Gally, H. U., Niederberger, W. & Seelig, J. Conformation and motion of the choline head group in bilayers of dipalmitoyl-3-sn-phosphatidylcholine. *Biochemistry* 14, 3647-52 (1975).
14. Roe, D. C. *J Magn Reson* 63, 388 (1985).
15. Jameson, C. J., Jameson, A. K. & Chohen, S. M. Temperature and density dependence of ^{129}Xe chemical shift in xenon gas. *J Chem Phys* 59, 4540-4539 (1973).
16. Davis, J. H., Jeffrey, K. R., Bloom, M., Valic, M. I. & Higgs, T. P. Quadrupolar echo deuteron magnetic resonance spectroscopy in ordered hydrocarbon chains. *Chemical Physics Letters* 42, 390-394 (1976).
17. Greenwood, A. I., Tristram-Nagle, S. & Nagle, J. F. Partial molecular volumes of lipids and cholesterol. *Chem Phys Lipids* 143, 1-10 (2006).
18. Fraissard, J. & Ito, T. Xenon- ^{129}NMR study of adsorbed xenon: a new method for studying zeolites and metal-zeolites. *Zeolites* 8, 350-61 (1988).
19. Mazitov, R. K., Enikeev, K. M. & Ilyasov, A. V. NMR of inert gases in aqueous solutions. *Interact. Water Ionic Nonionic Hydrates, Proc. Symp.*, 137-40 (1987).
20. McKim, S. & Hinton, J. F. Xenon- ^{129}NMR spectroscopic investigation of the interaction of xenon with ions in aqueous solution. *Journal of Magnetic Resonance, Series A* 104, 268-72 (1993).

21. Davis, J. H. Deuterium magnetic resonance study of the gel and liquid crystalline phases of dipalmitoyl phosphatidylcholine. *Biophys J* 27, 339-58 (1979).
22. Baker, B. M. & Murphy, K. P. Prediction of binding energetics from structure using empirical parameterization. *Methods in enzymology* 295, 294-315 (1998).
23. Scharlin, P., Battino, R., Silla, E., Tunon, I. & Pascual-Ahuir, J. L. Solubility of gases in water: Correlation between solubility and the number of water molecules in the first solvation shell. *Pure and Applied Chemistry* 70, 1895-1904 (1998).
24. Saunavaara, J. & Jokisaari, J. Determination of sample temperature and temperature stability with ^{129}Xe NMR. *J Magn Reson* 180, 58-62 (2006).
25. Carrington, A. & McLachlan, A. D. *Introduction to Magnetic Resonance* (Harper and Row, New York, 1967).
26. Baber, J., Ellena, J. F. & Cafiso, D. S. Distribution of general anesthetics in phospholipid bilayers determined using ^2H NMR and ^1H - ^1H NOE spectroscopy. *Biochemistry* 34, 6533-9 (1995).
27. Stimson, L. M., Vattulainen, I., Rog, T. & Karttunen, M. Exploring the effect of xenon on biomembranes. *Cell Mol Biol Lett* 10, 563-9 (2005).
28. Hata, T., Matsuki, H. & Kaneshina, S. Effect of local anesthetics on the bilayer membrane of dipalmitoylphosphatidylcholine: interdigitation of lipid bilayer and vesicle-micelle transition. *Biophysical Chemistry* 87, 25-36 (2000).
29. Mountcastle, D. B., Biltonen, R. L. & Halsey, M. J. Effect of anesthetics and pressure on the thermotropic behavior of multilamellar dipalmitoylphosphatidylcholine liposomes. *Proc Natl Acad Sci U S A* 75, 4906-10 (1978).

Figure Captions

Figure 1. ^{129}Xe -NMR spectra of various POPC SUV solutions at 321 K. Top spectrum corresponds to xenon dissolved in hydrated POPC bilayer (lipid to water ratio 1:2) at 321 K. The two ^{129}Xe resonances in the top spectrum are assigned to xenon dissolved in the lipid bilayer (193.05 ppm) and xenon in the gas phase above the bilayer (3.1 ppm). The xenon pressure in the lipid solution was adjusted to 0.9 MPa and in the hydrated lipid bilayer sample to 0.6 MPa.

Figure 2. Upper panel: Chemical shift of ^{129}Xe in buffered solution (●), in POPC SUV suspension with 15 (○), 50 (▽) mM and in hydrated POPC bilayer (◇) (lipid to water ratio 1:2) as function of the temperature. Additionally, the chemical shift of ^{129}Xe in olive oil (■) is shown. Lower panel: To illustrate the effect of the lipid POPC phase on the chemical shift of ^{129}Xe , we referenced the chemical shift of ^{129}Xe to the chemical shift of ^{129}Xe in water. The labels denote for the same solution as in (A).

Figure 3. Chemical shift of ^{129}Xe as function of the POPC concentration at 321 K (○), 313 (□), and 297 K (△). The solid lines correspond to the best fit of the experimental data to equation 7.

Figure 4. Partition coefficient of xenon into POPC SUV vesicles in dependence of the temperature. The solid line corresponds to the best fit of the experimental data to the van't Hoff equation (equation 8).

Figure 5. NMR spectra of ^{129}Xe dissolved in 100 mM POPC SUV solutions (25 mM Tris, pH 7.4, 0.1 M NaCl) in dependence of the temperature. The applied xenon pressure was 0.9 MPa. Numbers above the xenon resonances assign for the temperature in K.

Figure 6. Upper panel: Quadrupole splittings, $\Delta\nu_Q$, of deuterium atoms attached to DPPC at the α - (squares) and β - (circles) segment of the choline head group in dependence of the temperature. The coarsed liposomes of DPPC (water to lipid ratio 1:2) were pressurized either with 0.6 MPa xenon (closed symbols) or with 0.6 MPa nitrogen (open

symbols). Lower panel: DSC heating thermograms of 10 mM DPPC MLV suspension under 0.4 MPa Xe (red line) and 0.4 MPa N₂ (black line) pressure.

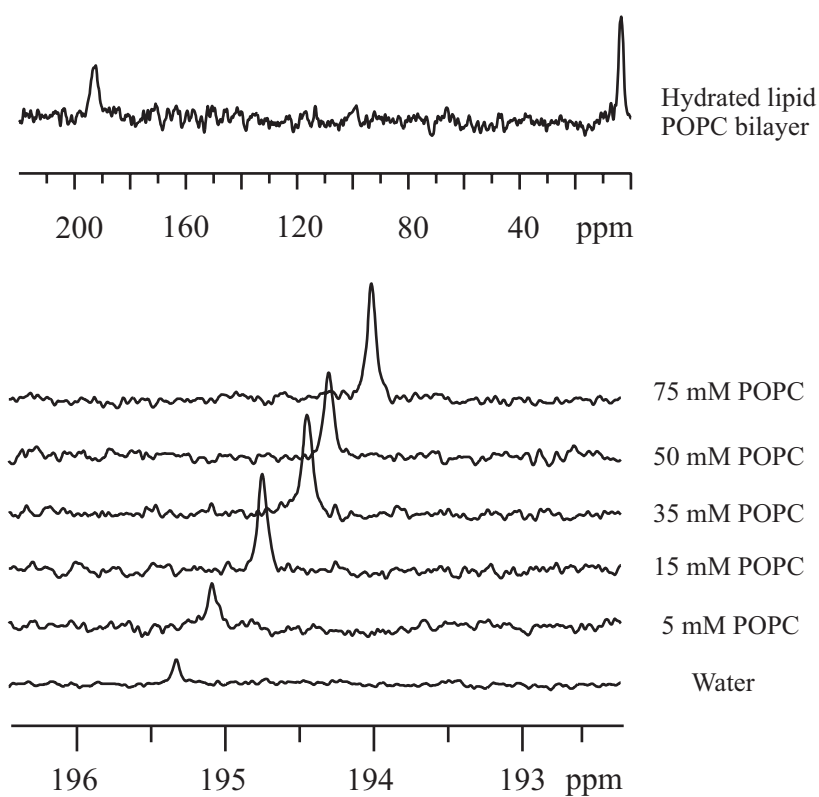
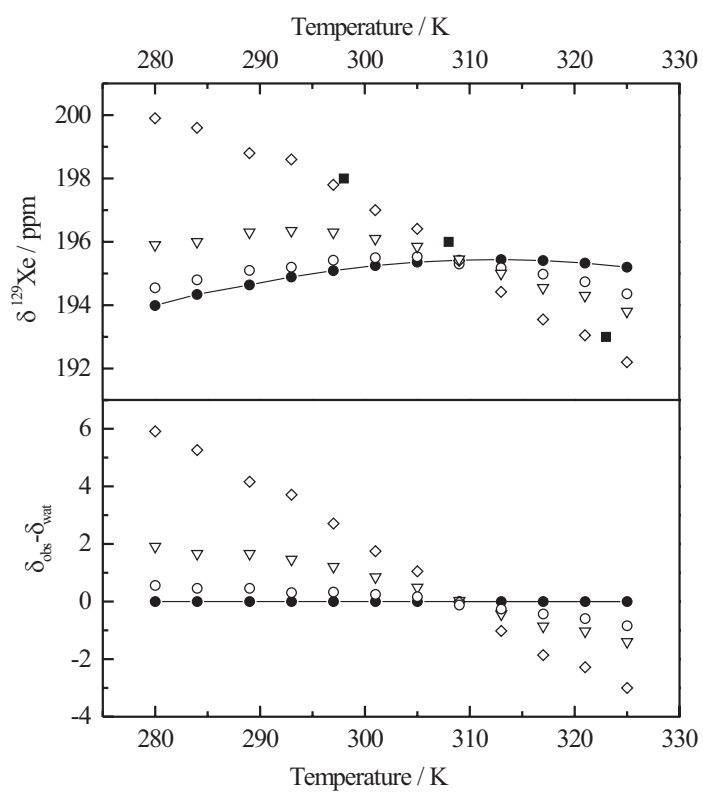
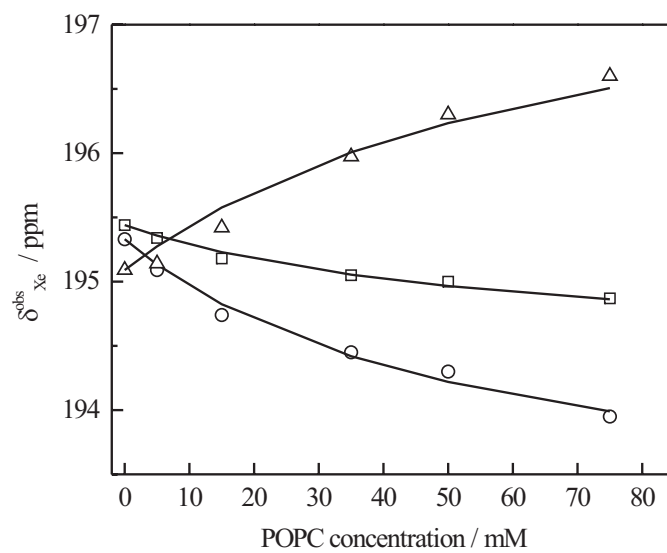
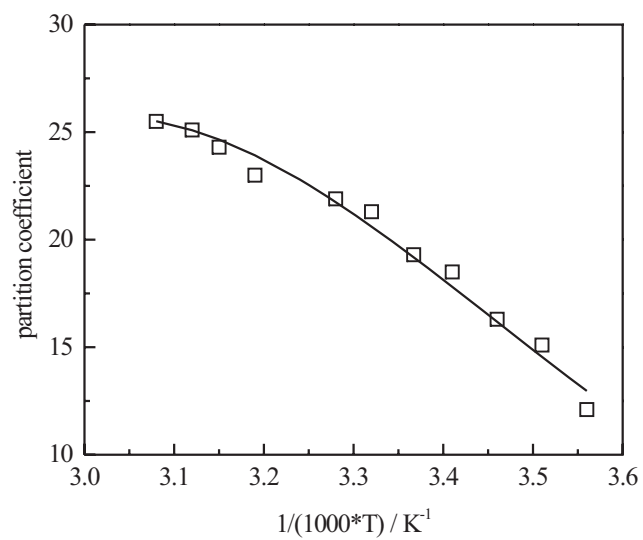
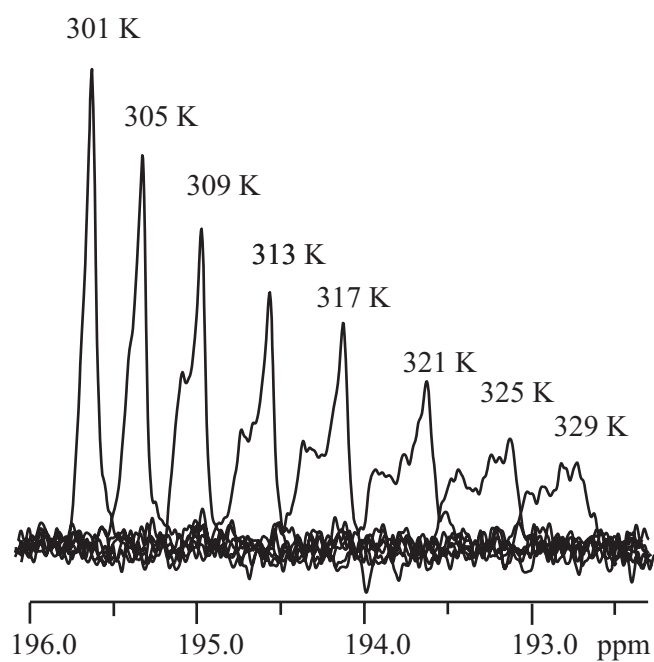
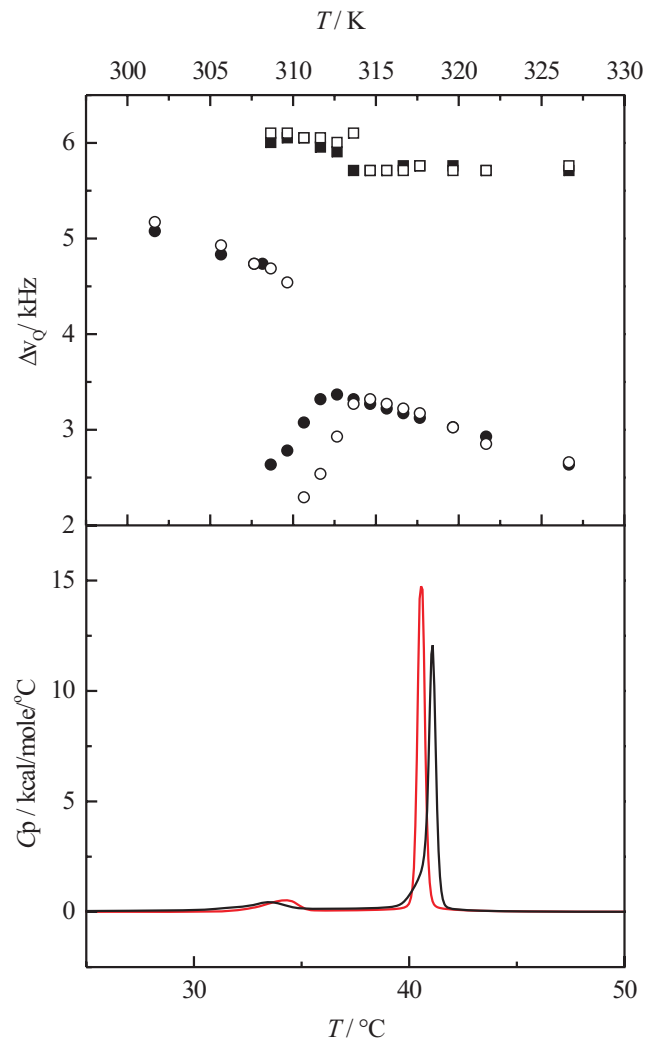


Figure 1

**Figure 2****Figure 3**

**Figure 4****Figure 5**

**Figure 6.**

8. Summary

This thesis aimed at improving our understanding of the thermodynamic and structural aspects of peptide aggregation processes at membrane surfaces. For this purpose we investigated a class of model peptides, which form a β -sheet structure upon binding to membrane surfaces. Binding of peptides with the repeating sequence of KIGAKI to anionic membrane surfaces was chosen as model system to characterize the transition from a random coil to β -sheet structure. Evidence is brought that the process of intermolecular β -sheets formation by the KIGAKI peptides is a suitable model system for a peptide aggregation process at membrane surfaces.

In order to understand this aggregation process, thermodynamic parameters of (KIGAKI)₃ binding to lipid membranes were determined directly by isothermal titration calorimetry. For a description of the peptide binding data a theoretical binding model was developed and evaluated with the drug verapamil. It is shown that the binding model, which is based on the Gouy-Chapman theory, can be used in a general way to describe electrostatic attraction and repulsion of charged molecules to lipid membranes under a variety of environmental conditions. Nevertheless, binding of peptides to lipid membranes is more complex as simply considering electrostatic attraction of the peptide to the membrane. Thermodynamic binding parameters of (KIGAKI)₃ to lipid membranes, obtained by ITC, combines mainly two reactions, the intrinsic binding and β -sheet folding process. Separation of both subprocesses from the overall thermodynamic binding process could be achieved by varying the extent of β -sheet formation due to substitution of two adjacent D amino acids within the peptide sequence. Double D amino acid substitution leads to a local disturbance of the β -sheet structure, where the extent of the β -sheet formation is dependent on the number and position of the double D amino acid substitution. With this approach it was possible to determine for the first time a full thermodynamic profile of the random coil to β -sheet transition for a peptide in a membrane environment and concomitantly these parameters are the first clearly defined parameters of a peptide aggregation reaction.

Beta sheet folds in proteins tend to be distinctively smaller than current models predict for β -sheets in protein and peptide aggregates. To reveal differences between the β -sheet folding reaction in a native and aggregated protein, we extended the study and determined

the length dependence of the β -sheet folding reaction. Thermodynamic parameters of the β -sheet folding reaction for KIGAKI peptide with different lengths were determined in analogy to (KIGAKI)₃. A linear length stabilization effect could be demonstrated for KIGAKI β -sheet structure. Furthermore, for β -sheets shorter than 10 residues the folding reaction is driven by entropy, whereas for longer β -sheets the folding reaction is driven by enthalpy. Underlying length dependence of the thermodynamic driving forces of β -sheet folding reaction is therefore the most important finding of this work since it reveals an important difference in the folding reaction between native and aggregating β -sheets. Furthermore, the double D amino acid substitution strategy opens a new way to systematically resolve the characteristic β -sheet-aggregation at membrane surfaces, as for example for the Alzheimer peptide.

Beside thermodynamics of the β -sheet folding process we also studied the dynamics and size of the extended β -sheet structure of KIGAKI at the membrane surface by deuterium solid state NMR. It is revealed that the β -sheet structure formed by the (KIGAKI)₃ peptide is large and rigid and therefore inevitably extended at the membrane surface. Perturbation of the membrane integrity, due to peptide binding and β -sheet formation are not observed. In turn, these findings weaken the theories that peptide aggregates at the membrane surface mediating cell death by disrupting the cell membrane.

As a new approach to study extended β -sheet structures at membrane surfaces, the (KIGAKI)₃ and Alzheimer peptide were encapsulated in reverse micelles and dissolved in a low viscosity solvent. Within the reverse micelles KIGAKI peptides adopted their characteristic β -sheet structure. Promising NMR results show that the reverse micelles technique is an interesting alternative for the structure analysis of membrane peptide and protein aggregates.

The last part of this thesis dealt with the partitioning process of xenon in lipid membranes. NMR spectroscopic analysis of the chemical shift behavior of ¹²⁹Xe in lipid suspension offered a new method to determine partitioning coefficients of xenon in lipid membrane samples, like blood and tissue samples, which are of particular interest for various medical applications of xenon. Additionally, our data provide new aspects of the anesthetic properties of xenon. In particular, we demonstrated that lipid molecules maintained their structure upon xenon partitioning, which suggests that structural changes of the lipid molecules are not necessary to mediate anesthesia.

9. Acknowledgement

This work was carried out from the April 2004 until October 2006 in the laboratory of Prof. Dr. Seelig in the Department of Biophysical Chemistry at the Biozentrum of the University of Basel.

At first I would like to express my sincere gratitude to my supervisor, Professor Joachim Seelig. His wide knowledge and his logical way of thinking have been a great value for me. I am also very grateful for his encouragements and advices, which have provided the basis for the presented thesis.

I warmly thank Dr. Anna Seelig, who gave me the opportunity to work with her in the field of membrane biophysics in connection with pharmaceutical science. Her guidance in the beginning of my thesis has been a great help.

I wish also to express my thanks to Dr. Sebastian Meier, Dr. André Ziegler and Dr. Heiko Heerklotz for their constant support and time for discussion. Especially thanks to Sebastian, who played two and half years the academic beat-box. I also appreciate the work of Prof. Dagmar Klostermeier as referee of this thesis.

Many thanks are due to my lab and floor mates, in particular Andreas Reiner, Xiaochun Li Blatter, and Andreas Möglich, who directed me in practical work. Further, I experienced great support from Hans Vogt, Leo Faletti, Gernot Hänisch and Simon Saner of the technical workshop, when things went seriously wrong. I also want to thank Susanna Notz, Gabriela Klocek, Peter Gantz, Götz Kohler, Paivi Aanismaa, Renate Reiter, Stephan Langheld, Beat Fierz, Marillo Crespo, Sonja Lorenz, Daniel Häusinger, Pernille Jensen and Christoph Bodenreider for the friendly working environment.

I owe my loving thanks to my family and friends.

10. Curriculum Vitae

Personal details

Name and address: Matthias Meier
Biozentrum der Universität Basel
Abteilung Biophysikalische Chemie
Klingelbergstrasse 70
4056 Basel, Switzerland
Tel.: 0041-(0)61-2672191

Date and place of birth: April 14th 1977
Hamburg, Germany

Nationality: german

Marital status: single

Education

04/2004 - 11/2006 Biozentrum der Universität Basel, Switzerland
Graduate (Ph. D.) studies in Biophysics
Thesis supervisor: Prof. Dr. Joachim Seelig
Thesis title: Thermodynamics and Structure of Peptide-Aggregates at membrane surfaces

04/2003 - 01/2004 Universität Regensburg, Germany
Diploma thesis in Biochemistry
Diploma supervisor: Prof. Dr. Eike Brunner
Thesis title: Reverse Micelles dissolved in Supercritical Xenon: an NMR spectroscopic study

- 10/1998 - 01/2004 Universität Regensburg, Germany
Diploma studies in Biochemistry
- 08/2001 - 05/2002 University of Kent, Canterbury, England
Exchange studies
Research supervisor: Prof. Dr. Gullick
- 09/1994 - 06/1997 Katholische Schule, Hamburg Bergedorf, Germany
Abitur

11. Declaration

I declare that I wrote this thesis “Thermodynamics and Structure of Peptide-Aggregates at Membrane Surfaces” with help indicated and only handed it in to the faculty of science of the University of Basel and to no other faculty and no other university.

Basel, 6th of November